AMERICAN UNIVERSITY OF BEIRUT

UNSTRUCTURED CENTRAL FINITE VOLUME SCHEMES FOR HYPERBOLIC CONSERVATION LAWS

by
GHINA IBRAHIM EL-JANNOUN

A thesis
submitted in partial fulfillment of the requirements
for the degree of Master of Science
to the Computational Sciences
Program of the Faculty of Arts and Sciences
at the American University of Beirut

Beirut, Lebanon
August 2010

AMERICAN UNIVERSITY OF BEIRUT

UNSTRUCTURED CENTRAL FINITE VOLUME SCHEMES FOR HYPERBOLIC CONSERVATION LAWS

by

GHINA IBRAHIM EL-JANNOUN

Approved by:

Dr. Friedemann Brock, Associate Professor Mathematics	Advisor
Dr. Nabil Nassif, Professor Mathematics	Member of Committee
Dr. Rony Touma, Assistant Professor Mathematics, LAU	Member of Committee

Date of thesis defense: August 10, 2010

AMERICAN UNIVERSITY OF BEIRUT

THESIS RELEASE FORM

I, Ghina Ibrahim El-Jannoun

☐ authorize the American University of Beirut to supply copies of my thesis to libraries or individuals upon request.

☐ do not authorize the American University of Beirut to supply copies of my thesis to libraries or individuals for a period of two years starting with the date of the thesis defense.

_____

Signature

_____

Date

ACKNOWLEDGEMENTS

This thesis arose out of a year of hard working. All throughout that time, I have been helped from a number of people whose contribution deserves special mention.

At first place, I gratefully acknowledge my advisor Prof. Friedmann Brock. His scientific intuition inspired and enriched my growth as a scientist; he provided me with constructive comments throughout the course of my thesis.
Furthermore, I would like to record my most sincere gratitude to my co-advisor Prof. Rony Touma. Without his valuable supervision, advice and guidance from the very early stage this thesis would not have been possible. I deeply appreciate his remarks and encouragement, and thank him for offering me this interesting thesis problem as well as the opportunity to be self dependent and develop as a researcher.
In addition, my special thanks go to my chairperson Prof. Nabil Nassif who established the backbones of my development as a student, starting from the basic undergraduate courses all the way through the most challenging graduate tasks. He has nourished my intellectual maturity that I will benefit from, for a long time.

I have truly been blessed with friends all over this long journey. I would especially like to thank Sarah Khankan for the great memories we have built together, for sharing various thoughts and giving me valuable opinions. Sarah I was fortunate to have you by my side. Lama Saneh thank you for the moral support, for the joy you planted in me during the few moments we spent together this year. To Farah Hariri who gave me words of comfort all through this long journey I would like to express my deepest gratitude. I would also like to acknowledge Sarah and Rouba Awadi, Dania Sheaib, Loa awde and Nour Fatairi; it was fun and inspiring to be around with you guys.

Words fail me to express my appreciation to Yousef Daher whose support, dedication and persistent confidence in me, has taken the load off my shoulder. You have been the source of fuel that kept me going on. Thanks for the humor, motivation and moral support, and for bearing with my mood swings after long days of hard work. Thanks for always being there, no matter what. Yousef I would have never done it without you.

My parents deserve special mention for their inseparable support and prayers. My brother, Said, you have been a protective shelter and a driving force through the best and worst of times. My Father, the person who showed me the joy of intellectual pursuit ever since I was a child; I am greatly indebted to you for everything you have done for me. My Mother, the one who sincerely raised me with her caring and gentle love, thanks for your unwavering faith, trust and mostly patience; thanks for being my mom. GrandMa I don't have words to thank you for your prayers; I love you so much.
Family, if I am to be anything in this world, it is because of you.

AN ABSTRACT OF THE THESIS OF

Ghina Ibrahim El-Jannoun for Master of Science
Major: Computational Sciences

Title: Unstructured Central Finite Volume Schemes for Hyperbolic Conservation Laws

We propose a new class of central finite volume schemes on unstructured triangular grids to approximate the solution of general two-dimensional hyperbolic systems of conservation laws. The proposed methods are extensions of the first-order accurate Lax-Friedrichs scheme and the non-oscillatory second-order accurate Nessyahu-Tadmor scheme, and evolve the numerical solution on an original unstructured triangular grid and on a staggered dual one. The control cells of the original grid are the triangles of a conformal finite element triangulation, while the staggered dual cells are the quadrilaterals obtained by joining the centers of two adjacent triangular cells to the endpoints of their common side. The cell-centered numerical solution alternates between the original grid (triangular cells) at even time steps and the dual staggered grid (quadrilateral cells) at odd time steps. Thanks to this staggering process the time consuming resolution of the Riemann problems arising at the cell interfaces is bypassed, and the resulting scheme is numerically stable under an appropriate CFL condition. In contrast with the extension of the Lax-Friedrichs scheme that evolves a piecewise constant numerical solution, our extension of the Nessyahu-Tadmor scheme evolves a piecewise linear numerical solution defined at the cell centers and thus ensures second-order of accuracy in space; the flux integral is approximated using the midpoint quadrature rule and ensures the second-order accuracy in time. Furthermore, oscillations are avoided thanks to limited numerical gradients. We validate the developed scheme and solve classical two-dimensional problems arising in gas dynamics. The quality of the obtained numerical results confirms the efficiency and robustness of our proposed schemes.

CONTENTS

LIST OF FIGURES

LIST OF TABLES

CHAPTER 1

INTRODUCTION

Hyperbolic systems of partial differential equations can be used to model a wide variety of phenomena that involve wave motion or the advective transport of substances (a substance being carried along with fluid motion). The derivation of the principal equations of fluid dynamics is based on the fact that the dynamical behavior of a fluid is determined by the conservation of mass, energy and momentum over time. The conservation of a certain flow quantity means that its total variation inside an arbitrary volume can be expressed as the net effect of the amount of the quantity being transported across the boundary, any internal forces and sources, and external forces acting on the volume [10].

Most commonly used numerical schemes for approximating the solution of conservation laws are finite difference, finite element and finite volume schemes. In this thesis, we are concerned with the finite volume methods on unstructured grids.

In 1959, S. Godunov [20] presented a one-dimensional finite volume method for approximating the solution of nonlinear hyperbolic systems of conservation laws. Godunov's method relies on a piecewise constant reconstruction of the numerical solution at each time step, is of first-order accuracy in space and time, and preserves the monotonicity of the numerical solution. Its main disadvantage relies in the necessity of solving locally, and for each interface the Riemann problem:

$$\begin{cases} \dfrac{\partial}{\partial t} + \dfrac{\partial}{\partial x} f(u) = 0 & \text{for } t^n \le t \le t^{n+1} \text{ and} \\ u(x, t^n) = \begin{cases} u_i^n & x < x_{i+1/2} \\ u_{i+1}^n & x \ge x_{i+1/2} \end{cases} \end{cases}$$

Usually, its hard and time consuming to compute the exact/approximate solution of the Riemann problem due to the necessity of identifying the nature and properties of the characteristics of the left and right going waves. That's why schemes that do not rely on the resolution of the Riemann problems are preferred. Furthermore, it is important to reduce the computing time and to improve the order of accuracy whenever real life problems are solved and solutions are required in real time.

Important progress was achieved by Boris and Book [11], Van Leer [38; 39; 40], Roe [49], Osher [46], and Harten [24; 22; 23]. Van Leer proposed replacing the piecewise constant reconstruction by a piecewise linear numerical solution. On the other hand, Roe and Osher proposed replacing the exact solution of the Riemann problems by an approximate solution based on local linearization. They introduced Riemann Solvers.

Other approaches like Richtmyer-Von Neumann [45] and Richtmyer-Morton [48] used an artificial viscosity in order to stabilize the solution near the discontinuities. This method has its merits but it would require detailed adjustments depending on the particular problem [51]. The Riemann solvers (whether computing the exact solution or an approximate one) all have the same major disadvantage which is that the Riemann problems arising at the cell interfaces were solved in the direction normal to the interface, and thus the multi-dimensional aspect of the problem ends up approximating one-dimensional problems in the directions normal to the cell interfaces [51]. In addition, fractional time step methods suffer from the same problem which is the grid orientation [51].

The robustness of the central schemes (Lax-Friedrichs (1954) [37] and Nessyahu-Tadmor (1990) [44] schemes) lies in the fact that unlike the upwind schemes, the integration is over the entire Riemann fan taking into account both left and right directed waves and they avoid the resolution of Riemann problems arising at the cell interfaces by evolving the numerical solution on an original grid and on a staggered

dual one at consecutive time steps. This is achieved by using a staggering process and an appropriate CFL condition.

The prototype central scheme is the Lax-Friedrichs scheme which is of first-order of accuracy in both space and time. A second-order non-oscillatory extension of the Lax-Friedrichs (LF) scheme was introduced by Nessyahu and Tadmor (NT) [44]. The second-order of accuracy is obtained using a piecewise linear numerical solution defined on the computational cells and by using second-order quadrature rules for the time integrals at intermediate time steps. Furthermore, the oscillation-free numerical solution resides upon the choice of the slope limiting of the numerical gradients used while reconstructing the piecewise linear interpolants from the piecewise constant data.

Over the last two decades, the NT scheme has lead to a significant amount of research on the topic of non-oscillatory central schemes. Some of the recent work on central schemes includes extensions to multiple spatial dimensions on Cartesian [3; 6; 26; 27; 42], unstructured [2; 14; 35], and unstaggered [52; 53] grids.

Structured grids have been the most used meshes in finite volume methods for several reasons. One of the reasons for this use is that the finite volume methods have deeply inherited from finite difference schemes. The great advantage of a scheme based on structured grids is that it is much easier to implement since it can be formed with well organized loops and it is also highly vectorizable. The main disadvantage is that such meshes are restricted to simple computational domains which are simply connexed. The application to complex geometries which are multiply connexed is very difficult.

On the other hand, unstructured grids involve triangles and tetrahedra in 2D and 3D, respectively. The latter have been used for a long time in finite element methods but they were recently introduced into finite volume schemes. The use of unstruc-

tured grids is motivated by the fact that they can be used to discretize most of the irregular domains without any gap [19]. Another feature of unstructured grids is the ability to apply local mesh refinements.

In [2; 14; 35] two-dimensional finite volume generalizations of the one-dimensional Lax-Friedrichs [37] and Nessyahu-Tadmor [44] finite volume schemes for hyperbolic conservation laws to unstructured grid were developed, while in [3; 4; 6; 26; 27; 42] corresponding extensions in the case of two-dimensional Cartesian grids were constructed and were used to solve problems in aerodynamics, gas dynamics, hydrodynamics and magnetohydrodynamics. Unstaggered central schemes that evolve the numerical solution on a single grid were developed in [52; 53] and were successfully used to solve ideal and shallow water magnetohydrodynamic problems.

In this thesis, we present new finite volume extensions of the one-dimensional LF and NT schemes to the two-dimensional case on unstructured finite volume grids. The simplicity of the domain discretization is the main advantage of our schemes over the other developed schemes on unstructured grids. The 2D extension of the Lax-Friedrichs scheme is first-order accurate in space and time and is somehow diffusive at the locations of discontinuities. To compensate for this numerical diffusion we adopt the same procedure used in the derivation of the one-dimensional Nessyahu-Tadmor scheme, i.e. by replacing the piecewise constant numerical solution of the Lax-Friedrichs scheme by a piecewise linear one with the help of gradient approximations and slope limiting approaches to prevent spurious oscillations from appearing at the cell interfaces.

As the previously developed central schemes, our unstructured extensions of the NT and LF schemes bypass the resolution of the Riemann problems arising at the cell

interfaces by evolving the numerical solution on two staggered grids at consecutive time steps.

The thesis is divided into 7 chapters: In chapter 2 by study the existence of weak solutions as well as the existence and uniqueness of the entropy solution for the hyperbolic systems of conservation laws in both one and two space dimensions. Then, we present in chapter 3 an overview of the one-dimensional Lax-Friedrichs and Nessyahu-Tadmor schemes. We then present in chapters 4, 5, 6 and 7 our finite volume extensions of these schemes to the two-dimensional space on unstructured grids. In chapter 4, we introduce a new domain discretization based on finite element triangulations, we also define the control cells (both original and staggered) used in both newly developed schemes. In chapter 5, we present our extension of the Lax-Friedrichs scheme to the case of 2D unstructured grids and in chapter 6, we discuss our 2D extension of the Nessyahu and Tadmor to the case of unstructured grids. Finally, in chapter 7, we validate the developed numerical methods, we verify their accuracy and stability, and then we solve classical problems arising in gas dynamics.

CHAPTER 2

THEORETICAL BACKGROUND

In this chapter we present the theoretical background that is necessary to go through the corresponding numerical analysis. We start with some basic definitions and principles for the nonlinear hyperbolic equations, then we show that in general classical solutions cannot exist, and we define weak solutions and the entropy condition, which guarantees uniqueness.

Consider the following one-dimensional system of equations:

$$\frac{\partial u}{\partial t} + \frac{\partial}{\partial x} f(u) = 0 \,, \tag{2.1}$$

where (x, t) lies in the upper half plane $\mathbb{R}^2_+ := (-\infty, +\infty) \times [0, +\infty)$.

The unknown vector field is u: $\mathbb{R}^2_+ \to \mathbb{R}^d$ and f: $\mathbb{R}^d \to \mathbb{R}^d$ is a given function assumed to be sufficiently smooth, usually at least $C^2(D)$, for some open set $D \subseteq \mathbb{R}^d$.

A scalar conservation law in one space dimension is a first order partial differential equation of form (2.1) where u is called *the conserved quantity* and f is called *the flux*.

Integrating (2.1) over a given interval [a,b] one obtains:

$$\begin{aligned} \frac{\partial}{\partial t} \int_a^b u(x,t)\, dx &= \int_a^b u_t(x,t)\, dx \\ &= -\int_a^b \frac{\partial}{\partial x} f(u(x,t))\, dx \\ &= f(u(a,t)) - f(u(b,t)) \\ &= \text{[inflow at a]-[outflow at b]} \,. \end{aligned}$$

In other words, the total amount u contained inside any given interval [a,b] can change with time only due to the flow of $f(u)$ across the boundary points.
Consider the initial condition associated with the system of equations (2.1):

$$u(x,t) = u_0(x) \qquad \text{for } x \in \mathbb{R}\,,\ t = 0.$$

The existence of an exact solution for the nonlinear hyperbolic system (2.1) associated with certain initial condition remains a very complex problem that we will not tackle in this thesis.
The interested reader can consult the references [18; 25; 29].
It can be shown that even a scalar one-dimensional conservation law, and for a finite time interval, can lead to discontinuous solutions, even when the initial condition is in C^∞. Thus the existence of a solution in the classical sense can rarely be observed. We need therefore to define weak solutions for the problem which are made of piecewise classical solutions, separated by a finite number of discontinuities.

2.1 Weak solutions and Entropy condition for 1.D hyperbolic systems

2.1.1 Basic Definitions and hypotheses

Definition 1 *A system of the form (2.1) is called* ***quasilinear****. It is called* ***hyperbolic*** *if* $\forall\ u \in \mathbb{R}^d$ *the Jacobian matrix* $A = \nabla_u f(u)$ *has real eigenvalues and its eigenvectors span* $\mathbb{R}^d$.

Definition 2 *A system of the form (2.1) is* ***linear*** *if the Jacobian matrix* $A = \nabla_u f(u)$ *does not depend on u.*

Linear hyperbolic systems are much easier to study. For these systems, the initial value problem is well-posed and the solution maintains the regularity of the initial data for any time.
Such systems of the form $u_t + Au_x = 0$ can be diagonalized and therefore can be

reduced into d linear scalar equations.

The situation is more complex for quasi-linear systems for which the initial value problem is well-posed locally in time.

Definition 3 *Let $f : \mathcal{X} \mapsto \mathbb{R}^d$ with $\mathcal{X}$ be a metric space.*

The closure of the set $\{(x,t) \in \mathbb{R}^2_+ : f(x,t) \neq 0\}$ is called the support of f, and is denoted by supp(f).

Definition 4 *Let $U \in \mathbb{R}^n$.*

$L^\infty(U) := \{u : U \to \mathbb{R} |$ *u is Lebesgue measurable on U, and* ess $\sup_{\mathrm{u}} |\mathrm{u}| < \infty\}$.

Definition 5 *Let U be an open set in $\mathbb{R}^n$.*

Then define $C_0^\infty(U)$:= $\{f : U \mapsto \mathbb{R}$: $\partial^\alpha f$ is continuous and has compact support in U, for every multi-index $\alpha\}$.

Every function $f \in C_0^\infty(U)$ is called a ***test function****. We write $\mathcal{D}(\mathcal{U}) := C_0^\infty(U)$.*

We also define $C_0^k(U)$:= $\{f : U \mapsto \mathbb{R}$: $\partial^\alpha f$ is continuous and has compact support in U, for every multi-index α with $|\alpha| \leq k\}$.

In general, the solution loses the regularity of the initial data after a finite time.

Even for the case of single scalar equation ($d = 1$) the strong solution fails to exist and it is necessary to consider weak solutions.

Definition 6 *A* ***weak solution*** *of the non linear hyperbolic system of conservation law is a function u: $\mathbb{R}^2_+ \to \mathbb{R}^d$ such that:*

$$\int_0^{+\infty} \int_{-\infty}^{+\infty} [u(x,t)\varphi_t(x,t) + f(u(x,t))\varphi_x(x,t)]\, dx\, dt + \int_{-\infty}^{+\infty} u_0(x)\varphi(x,0)\, dx = 0\,, \tag{2.2}$$

for every test function $\varphi \in C_0^1(\mathbb{R}^2_+)$.

Notice: $C_0^1(\mathbb{R}^2_+) := \{\varphi \in C^1(\mathbb{R}^2_+)$ such that: $\exists r > 0$ with $supp(\varphi) \subset B_r(0,0) \cap \mathbb{R}^2_+\}$

Theorem 2.1.1 *Suppose $u \in C^1(\mathbb{R}^2_+)$ is a classical solution of (2.1), then u is also a weak solution of (2.1).*

After defining weak solutions, our aim now is to define necessary conditions for a discontinuous weak solution.

Theorem 2.1.2 ***Rankine Hugoniot Condition***

Let $\mathcal{N}$ be an open neighborhood in the open upper half plane, and suppose a curve $\mathcal{C}$ represented parametrically as $\mathcal{C} := \{(x,t)\,|x = \overline{x}(t)\}$ divides $\mathcal{N}$ into two pieces, $\mathcal{N}^l$ and $\mathcal{N}^r$ lying to the left and right of the curve, respectively.

Let u be a weak solution of (2.1) such that:

- *u is a classical (smooth) solution of (2.1) in both $\mathcal{N}^l$ and $\mathcal{N}^r$*
- *u undergoes a jump discontinuity $[[u]]$ at the curve $\mathcal{C}$, and*
- *The jump $[[u]]$ is continuous along $\mathcal{C}$*
- *Denote by u^l and u^r the limits of u. on $\mathcal{C}$ when approaching from $\mathcal{N}^l$ and $\mathcal{N}^r$ respectively.*

For any p= $(x_0, t_0) \in \mathcal{C}$, let s:=$\overline{x}'(p)$ be the slope of $\mathcal{C}$ at p.

Then the following relation holds between the curve and the jumps:

$$s\,[[u]] = [[f(u)]]\ .$$

Notation 1

$$\begin{aligned} [[u]] &= u^r - u^l = \text{jump in u across the curve } \mathcal{C} \\ [[f(u)]] &= f(u^r) - f(u^l) = \text{jump in f(u) across the curve } \mathcal{C} \\ s &= \text{speed of the curve } \mathcal{C} \end{aligned}$$

Proof: Consider equation (2.2),

$$\int_0^{+\infty}\int_{-\infty}^{+\infty}\left[u(x,t)\varphi_t(x,t)+f(u(x,t))\varphi_x(x,t)\right]\,dx\,dt+\int_{-\infty}^{+\infty}u_0(x)\varphi(x,0)\,dx=0\,.$$

First choose a test function φ with compact support in $\mathcal{N}^l$. Then (2.2) becomes:

$$\int_0^{+\infty}\int_{-\infty}^{+\infty}\left[u(x,t)\varphi_t(x,t)+f(u(x,t))\varphi_x(x,t)\right]\,dx\,dt=0\,,$$

since φ vanishes outside of $\mathcal{N}^l$.

Since u is in C^1 in $\mathcal{N}^l$ and φ vanishes near the boundary of $\mathcal{N}^l$ we can then apply the integration by parts:

$$\begin{aligned}&\int_0^{\infty}\int_{-\infty}^{\infty}\left(u_t(x,t)+\frac{\partial}{\partial x}f(u)\right)\varphi\,dx\,dt\\ &\quad=\;-\int_0^{+\infty}\int_{-\infty}^{+\infty}\left[u(x,t)\varphi_t(x,t)+f(u(x,t))\varphi_x(x,t)\right]\,dx\,dt\\ &\qquad-\int_{-\infty}^{+\infty}u_0(x)\varphi(x,0)\,dx\,,\end{aligned}$$

with supp(φ)$\in\mathcal{N}^l$, hence

$$\begin{aligned}&\int_0^{\infty}\int_{-\infty}^{\infty}\left(u_t(x,t)+\frac{\partial}{\partial x}f(u)\right)\varphi\,dx\,dt\\ &\quad=\;-\int_0^{+\infty}\int_{-\infty}^{+\infty}\left[u(x,t)\varphi_t(x,t)+f(u(x,t))\varphi_x(x,t)\right]\,dx\,dt\,.\end{aligned}$$

Thus,

$$\int_0^{\infty}\int_{-\infty}^{\infty}\left(u_t(x,t)+\frac{\partial}{\partial x}f(u)\right)\varphi\,dx\,dt=0\,.$$

This identity holds for every test function φ with compact support in $\mathcal{N}^l$ therefore

$$u_t+\frac{\partial}{\partial x}f(u)=0\qquad\text{in }\mathcal{N}^l\,.$$

Similarly, choose a test function φ with compact support in $\mathcal{N}^r$ one gets

$$\int_0^\infty \int_{-\infty}^\infty \left(u_t(x,t) + \frac{\partial}{\partial x} f(u) \right) \varphi \, dx \, dt = 0 \, .$$

This identity holds for every test function φ with compact support in $\mathcal{N}^r$ therefore:

$$u_t + \frac{\partial}{\partial x} f(u) = 0 \qquad \text{in } \mathcal{N}^r \, .$$

Consider now the general case, let φ be a test function with compact support in $\mathcal{N}$(φ need not vanish along the curve $\mathcal{C}$).

Note that:

$$\int_0^\infty \int_{-\infty}^\infty \left(u_t(x,t) + \frac{\partial}{\partial x} f(u) \right) \varphi \, dx \, dt = 0 \qquad \text{in } \mathcal{N}^l$$

and,

$$\int_0^\infty \int_{-\infty}^\infty \left(u_t(x,t) + \frac{\partial}{\partial x} f(u) \right) \varphi \, dx \, dt = 0 \qquad \text{in } \mathcal{N}^r$$

Therefore

$$\begin{aligned} 0 &= -\int_0^{+\infty} \int_{-\infty}^{+\infty} \left[u(x,t)\varphi_t(x,t) + f(u(x,t))\varphi_x(x,t) \right] \, dx \, dt \\ &\quad -\int_{-\infty}^{+\infty} u_0(x)\varphi(x,0) \, dx \\ &= \int\int_{\mathcal{N}^l} u\varphi_t + f(u)\varphi_x \, dx \, dt + \int_{\mathcal{N}^r} u\varphi_t + f(u)\varphi_x \, dx \, dt \, . \end{aligned}$$

Since φ has compact support within $\mathcal{N}$, we have

$$\begin{aligned} &\int\int_{\mathcal{N}^l} u\varphi_t + f(u)\varphi_x \, dx \, dt \\ &= \underbrace{-\int\int_{\mathcal{N}^l} \left(u_t + \frac{\partial}{\partial x} f(u) \right) \varphi \, dx \, dt}_{=0} + \int_{\mathcal{C}} \left(u^l \mu^1 + f(u^l)\mu^2 \right) \varphi \, dl \\ &= \int_{\mathcal{C}} \left(u^l \mu^1 + f(u^l)\mu^2 \right) \varphi \, dl \, , \end{aligned}$$

with $\mu = \left(\mu^1, \mu^2\right)$ is the unit normal to the curve $\mathcal{C}$ pointing out of $\mathcal{N}^l$ i.e. from $\mathcal{N}^l$ to $\mathcal{N}^r$. Similarly,

$$\begin{aligned}
&\int\int_{\mathcal{N}^r} u\varphi_t + f(u)\varphi_x \, dx \, dt \\
&\quad = \underbrace{-\int\int_{\mathcal{N}^r} \left(u_t + \frac{\partial}{\partial x} f(u)\right) \varphi \, dx \, dt}_{=0} + \int_{\mathcal{C}} \left(u^r(-\mu^1) + f(u^r)(-\mu^2)\right) \varphi \, dl \\
&\quad = -\int_{\mathcal{C}} \left(u^r \mu^1 + f(u^r)\mu^2\right) \varphi \, dl \, ,
\end{aligned}$$

with $\left(-\mu^1, -\mu^2\right)$ is the unit normal to the curve $\mathcal{C}$ pointing out of $\mathcal{N}^r$ i.e. from $\mathcal{N}^r$ to $\mathcal{N}^l$. Then,

$$\begin{aligned}
0 &= \int\int_{\mathcal{N}^l} u\varphi_t + f(u)\varphi_x \, dx \, dt + \int\int_{\mathcal{N}^r} u\varphi_t + f(u)\varphi_x \, dx \, dt \\
&= \int_{\mathcal{C}} \left(u^l \mu^1 + f(u^l)\mu^2\right) \varphi \, dl - \int_{\mathcal{C}} \left(u^r \mu^1 + f(u^r)\mu^2\right) \varphi \, dl \\
&= \int_{\mathcal{C}} \left(\left(u^l - u^r\right) \mu^1 + \left(f(u^l) - f(u^r)\right) \mu^2\right) \varphi \, dl \, .
\end{aligned}$$

This equality holds for all test functions φ in $\mathcal{N}$. Therefore

$$\left(u^l - u^r\right) \mu^1 + \left(f(u^l) - f(u^r)\right) \mu^2 = 0 \qquad \text{along } \mathcal{C} \, .$$

Recall that $\mathcal{C}$:= $\{(x,t) \, | x = \overline{x}(t)\}$ and s:=$\overline{x}'$ is the slope of $\mathcal{C}$. $\mathcal{C}$ is given implicitly,

$$\mathcal{C} : x = \overline{x}(t) \qquad \text{where } \overline{x} \in C^1\left((t_0 - \epsilon, t_0 + \epsilon)\right) \, .$$

Hence,

$$\mu = \frac{\left(1, -\overline{x}'(t)\right)}{\sqrt{1 + \overline{x}'(t)^2}} \, .$$

Thus,

$$[[f(u)]] \, \mu^1 + [[u]] \, \mu^2 = 0 \qquad \text{on } \mathcal{C}.$$

Therefore,

$$f(u^l) - f(u^r) = s\left(u^l - u^r\right) ,$$

with s:=$\overline{x}'$ being the slope of $\mathcal{C}$.

Assume u is smooth in $V \subset [0, +\infty)\text{x}\mathbb{R}$. Since our equation is quasilinear then u is constant along any straight segment C with $C \subset V$.

Every such C is called a ***characteristic line.***

It is possible to construct weak solutions of (2.1) containing characteristic lines that emerge from a shock curve. But those solutions are physically not relevant. To avoid such ***nonphysical shocks***, we require that characteristic lines may only end in but are not allowed to emerge from a shock, if we move forward in time. In the following we will express this requirement in mathematical terms.

Assume $\mathcal{N}^l$, $\mathcal{N}^r$, u^l, u^r and $\mathcal{C}$ are as before and that two characteristic lines $\mathcal{S}^l$, $\mathcal{S}^r$ (with $\mathcal{S}^l \subset \mathcal{N}^l$ and $\mathcal{S}^r \subset \mathcal{N}^r$) hit $\mathcal{C}$ at a point $(x_0, y_0) \in \mathcal{C}$.

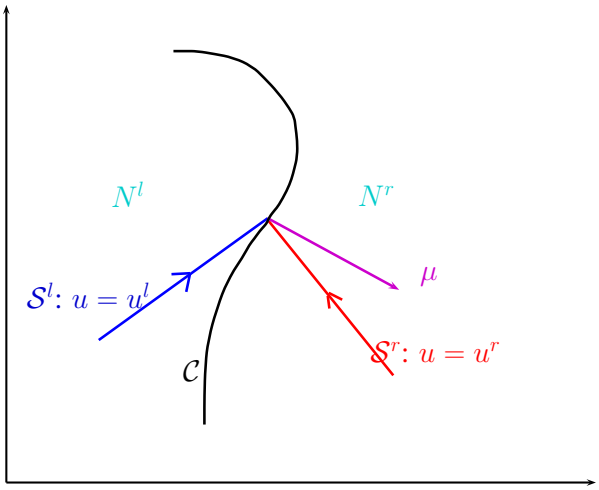

$\mathcal{S}^l$ and $\mathcal{S}^r$ have representations as follows:

$$\begin{aligned} \mathcal{S}^l : x &= x_0 + f'(u^l)(t - t_0), \qquad \text{and} \\ \mathcal{S}^r : x &= x_0 + f'(u^r)(t - t_0) . \end{aligned}$$

with $t_0 - \epsilon \leq t \leq t_0$, $\epsilon > 0$, ϵ small.

$\mathcal{S}^l$ and $\mathcal{S}^r$ have tangent vectors $T^l = \Big(f'(u^l), 1\Big)$ and $T^r = \big(f'(u^r), 1\big)$ respectively. If μ denote unit normal to $\mathcal{C}$ at (x_0, t_0) pointing into $\mathcal{N}^r$, then the above condition reads as $T^l\mu > 0 > T^r\mu$ that is

$$\Big(f'(u^l), 1\Big)\,\mu > 0 > \big(f'(u^r), 1\big)\,\mu \qquad \text{at } (x_0, t_0)\,.$$

i.e.
$$f'(u^l) \;>\; 0 > f'(u^r) \qquad \text{at } (x_0, t_0)$$
and
$$f'(u^l) - s \;>\; 0 > f'(u^r) - s\,.$$

These inequalities are called the ***entropy condition*** (a rough analogy with thermodynamics principle that physical entropy cannot decrease as time goes forward).

Definition 7 *A curve of discontinuity for u is called a **shock** provided both the Rankine Hugoniot condition and the entropy conditions hold.*

Let us now go further and interpret the entropy condition in the case when f is $\in C^2$ and is strictly convex, i.e. $f''(u) > 0\,\forall\, u \in \mathbb{R}$

Example 1 *Burger's equation:*

$$u_t + \left(\frac{u^2}{2}\right)_x = 0,$$

f is strictly convex since $f(u) = \left(\frac{u^2}{2}\right)$ then $f''(u) = 1 \;> 0$.

Let u, $v \in \mathbb{R}$ with $v > u$. Using a taylor series expansion around u one gets:

$$f(v) = f(u) + f'(u)(v-u)f''\left(u + \theta(v-u)\right)\frac{(v-u)^2}{2}\,.$$

then,

$$f(v) > f(u) + f'(u)(v-u)$$

i.e.
$$f(v) - f(u) > f'(u)(v-u)\,.$$

Similarly, $f(v) - f(u) < f'(v)(v-u)$ if $v > u$. In other words,

$$f'(u) < \frac{f(v)-f(u)}{v-u} < f'(v) \qquad \text{if } v > u\,. \tag{2.3}$$

But the Rankine Hugoniot gives: $[[f(u)]] = s\,[[u]]$ i.e $s = \frac{[[f(u)]]}{[[u]]}$ with the entropy condition given by:

$$f'(u^l) > s > f'(u^r) \quad \Rightarrow \quad f'(u^l) > \frac{[[f(u)]]}{[[u]]} > f'(u^r)\,.$$

In view of (2.3) this is equivalent to $u^l > u^r$.

Therefore, the ***entropy condition in the case of convex function f*** is given by: $u^l > u^r$.

Remark 1 *In the two dimensional case with u=u(x,y,t) it is not easy to simplify the entropy condition as in the last analysis.*

Definition 8 *An entropy/entropy-flux pair is a pair of functions* $(U, F) : \mathbb{R}^n \mapsto \mathbb{R}^2$ *satisfying*

$$\nabla F = \nabla U \times \nabla f.$$

Let $(U, F) : \mathbb{R}^n \mapsto \mathbb{R}^2$ be an entropy flux pair and assume that u is a classical solution of (2.1) then

$$\begin{aligned}
\frac{\partial}{\partial t}U(u) + \frac{\partial}{\partial x}F(u) &= \frac{\partial U}{\partial u}\frac{\partial u}{\partial t} + \frac{\partial F}{\partial u}\frac{\partial u}{\partial x} && \text{using the chain rule}\\
&= \frac{\partial U}{\partial u}\frac{\partial u}{\partial t} + \left(\frac{\partial U}{\partial u}\frac{\partial f}{\partial u}\right)\frac{\partial u}{\partial x} && \text{from the definition of entropy pair}\\
&= \frac{\partial U}{\partial u}\left(\frac{\partial u}{\partial t} + \frac{\partial f}{\partial u}\frac{\partial u}{\partial x}\right)\\
&= \frac{\partial U}{\partial u} \times 0\\
&= 0.
\end{aligned}$$

Note that a weak solution need not necessarily satisfy this identity.

Definition 9 *A weak solution of (2.1) is said to satisfy the entropy condition if there exists an entropy/entropy flux pair with $u \mapsto U(u)$ convex such that*

$$-\int\int \left(U(u)\varphi_t + F(u)\varphi_x\right)\, dx\, dt \leq 0\,, \tag{2.4}$$

for every non negative C^1 test function φ with compact support in the open upper half-plane.

Assume (U, F) is an entropy pair satisfying the following inequality

$$\frac{\partial}{\partial t}U(u) + \frac{\partial}{\partial x}F(u) \leq 0\,. \tag{2.5}$$

Multiplying (2.5) by a nonnegative test function we get

$$\frac{\partial}{\partial t}U(u)\varphi + \frac{\partial}{\partial x}F(u)\varphi \leq 0\,. \tag{2.6}$$

Integrating (2.6) in the plane, we obtain

$$\int_0^\infty \int_{\mathbb{R}} \frac{\partial}{\partial t}U(u)\varphi + \frac{\partial}{\partial x}F(u)\varphi\, dx\, dt \leq 0\,.$$

Using Green's formula

$$\begin{aligned}\int_0^\infty \int_{\mathbb{R}} \frac{\partial}{\partial t}U(u)\varphi + \frac{\partial}{\partial x}F(u)\varphi\, dx\, dt \;&=\; \oint \left(\nu \frac{\partial}{\partial t}U(u)\right)\varphi - \int\int U(u)\varphi_t\, dx\, dt \\ &\quad + \oint \left(\mu \frac{\partial}{\partial x}F(u)\right)\varphi - \int\int F(u)\varphi_t\, dx\, dt\,.\end{aligned}$$

But φ is a test function hence

$$\oint \left(\nu \frac{\partial}{\partial t}U(u)\right)\varphi = \oint \left(\mu \frac{\partial}{\partial x}F(u)\right)\varphi = 0\,.$$

Then,

$$\int_0^\infty \int_{\mathbb{R}} \frac{\partial}{\partial t} U(u)\varphi + \frac{\partial}{\partial x} F(u)\varphi \, dx \, dt = -\int \int U(u)\varphi_t + F(u)\varphi_x \, dx \, dt \, .$$

Recall that

$$\int_0^\infty \int_{\mathbb{R}} \frac{\partial}{\partial t} U(u)\varphi + \frac{\partial}{\partial x} F(u)\varphi \, dx \, dt \leq 0 \, ,$$

then

$$-\int \int U(u)\varphi_t + F(u)\varphi_x \, dx \, dt \leq 0 \, .$$

Therefore an entropy/entropy flux pair satisfying (2.5) also satisfies the entropy condition (2.4) in the sense of distributions i.e.

$$\int_{\mathbb{R}_+} \int_{\mathbb{R}} U(u)\varphi_t + F(u)\varphi_x \geq 0 \qquad \forall \varphi \in C_0^\infty(\mathbb{R} \times \mathbb{R}_+), \text{with } \varphi \geq 0 \, .$$

Our aim now is to specify U and F.

Set $U(u) = |u - k|$, ($k \in \mathbb{R}$, fixed). Then Kruzkov's entropy condition follows, that is

$$\int_{\mathbb{R}^2} \int_{\mathbb{R}^+} \{\partial_t \varphi \ |u - k| + \partial_x \varphi \ sign(u - k) \, [f(u) - f(k)]\} \geq 0 \, .$$

Definition 10 ***Kruzkov's Entropy Condition in 1D***

A weak solution of (2.1) is called an entropy solution if we have for all $\varphi \in C_0^\infty(\mathbb{R}^+ \times \mathbb{R})$, $\varphi \geq 0$, *and for any constant* $k \in \mathbb{R}$

$$\int_{\mathbb{R}^2} \int_{\mathbb{R}^+} \{\partial_t \varphi \ |u - k| + \partial_x \varphi \ sign(u - k) \, [f(u) - f(k)]\} \geq 0 \, ,$$

where sign(x) $= \begin{cases} 1 & \text{if } x > 0 \\ -1 & \text{if } x < 0 \end{cases}$

Note that another way of obtaining Kruzkov's inequality from (2.5) is presented in the proof of theorem 2.1.16 the book of Kroner [29].

Definition 11 ***A Riemann problem*** *consists of a conservation law together with piecewise constant data having a single discontinuity i.e.*

$$\begin{cases} u_t + f_x(u) = 0 \\ u(x,0) = \begin{cases} u_L & \text{if } x < x_i \\ u_R & \text{if } x \geq x_i \end{cases} \end{cases}$$

2.2 Weak solutions and Entropy condition for 2.D hyperbolic systems

Consider the following two dimensional system of equations:

$$\frac{\partial u}{\partial t} + \frac{\partial}{\partial x} f(u) + \frac{\partial}{\partial y} g(u) = 0 \,, \tag{2.7}$$

where (x, y, t) lies in the upper half plane $(-\infty, +\infty)^2$x[0,$+\infty$).

Definition 12 ***Weak Solution in 2D***

A bounded, measurable function u: $\mathbb{R}^+ \times \mathbb{R}^2 \mapsto \mathbb{R}$ *is said to be a weak solution to the initial value problem consisting of (2.7) with initial data* $u(x, y, 0) = u_0(x, y)$ *if*

$$\int_{\mathbb{R}^+} \int_{\mathbb{R}^2} u \frac{\partial}{\partial t}\varphi + f(u)\frac{\partial}{\partial x}\varphi + g(u)\frac{\partial}{\partial y}\varphi \, dx \, dy \, dt = 0 \,,$$

for every test function $\varphi \in C_0^\infty(\mathbb{R}^+ \times \mathbb{R}^2)$*, and if* $u(.,.,t) \mapsto u_0 \in L^1_{loc}$ *as* $t \mapsto 0$

As in the one dimensional case, the weak solution is not uniquely defined. Therefore we need an entropy condition in order to select a solution that has a physical meaning.

Consider the following system:

$$u_t + f(u)u_x + g(u)u_y = 0 \,. \tag{2.8}$$

Let U be Lipschitz continuous and define a Lipschitz continuous vector function $F = (F_1, F_2)$ by

$$(F_1)'(u) = U'(u)f(u)$$

and

$$(F_2)'(u) = U'(u)g(u)$$

for a.e. $u \in \mathbb{R}$.

(That is, $F_1(u) = \int_0^u U'(s)f(s)ds$, and $F_2(u) = \int_0^u U'(s)f(s)ds$ for every $u \in \mathbb{R}$).

The pair $(U, F) = (U, F_1, F_2)$ is called an entropy pair for equation (2.8).

Then, an entropy solution of (2.8) is any weak solution of (2.8) that additionally satisfies for every $\varphi \in C_0^\infty(\mathbb{R}^2 \times \mathbb{R}_+)$ with $\varphi \geq 0$, and for every entropy pair (U, F), with U convex:

$$\int_{\mathbb{R}^2 \times \mathbb{R}_+} (U(u)\varphi_t + F_1(u)\varphi_x + F_2(u)\varphi_y)dxdydt \geq 0\,.$$

From this, one obtains Kruzkov's condition of an entropy solution, by choosing $U(u) := |u - k|$, $(k \in \mathbb{R})$.

Definition 13 ***Kruzkov's Entropy Condition in 2D***

A weak solution of (2.7) is called an entropy solution if we have for all $\varphi \in C_0^\infty(\mathbb{R}^+ \times \mathbb{R}^2)$, $\varphi \geq 0$, *and for any constant* $k \in \mathbb{R}$

$$\int_{\mathbb{R}^2}\int_{\mathbb{R}^+} \{\partial_t\varphi\ |u-k| + \partial_x\varphi\ sign(u-k)\,[f(u)-f(k)] + \partial_y\varphi\ sign(u-k)\,[g(u)-g(k)]\,\} \geq 0\,.$$

The derivation of this entropy condition is similar to the one presented in the one-dimensional case and it can be found in [31].

Remark 2 *This condition is also known as the Kruzkov entropy condition. Kruzkov [31] has shown that every entropy solution can be considered as a viscosity limit, that is as a limit of a family of associated parabolic problems.*

Theorem 2.2.1 ***Existence and uniqueness of entropy solution in 2D***

Let $u_0 \in L^1(\mathbb{R}^2) \cap L^\infty(\mathbb{R}^2)$. Then there exists one and only one entropy solution u of (2.7) and $u \in C^0([0,T], L^1(\mathbb{R}^2)) \cap L^\infty([0,T] \times \mathbb{R}^2)$.

We omit the details of the proof and refer to Kruzkov [31].

The definition of entropy condition implies two conditions on the discontinuities of the solution.

- **Rankine Hugoniot condition**

  At any point p of a surface of discontinuity S of the solution u, if

  - $\mathbf{n}$ is a unit normal vector to S at p,
  - $u^+ = \lim_{\epsilon \mapsto 0^+} u(p + \epsilon \mathbf{n})$,
  - $u^- = \lim_{\epsilon \mapsto 0^+} u(p - \epsilon \mathbf{n})$,

  then,

$$\mathbf{n}\left(u^+ - u^-, f(u^+) - f(u^-), g(u^+) - g(u^-)\right) = 0\,.$$

- **Entropy condition**

  Orient $\mathbf{n}$ so that $u^+ \geq u^-$. If k is any constant such that $u^- \leq k \leq u^+$, then

$$\mathbf{n}\left(k - u^+, f(k) - f(u^+), g(k) - g(u^+)\right) \geq 0\,,$$

  which is equivalent to,

$$\mathbf{n}\left(k - u^-, f(k) - f(u^-), g(k) - g(u^-)\right) \geq 0\,.$$

  One may further check that if a function u is a piecewise classical solution, except for smooth surfaces of discontinuity where the 2 conditions hold, then u is a weak solution satisfying the entropy condition.

CHAPTER 3

ONE-DIMENSIONAL CENTRAL FINITE VOLUME SCHEMES FOR HYPERBOLIC CONSERVATION LAWS

Several motivations have lead to the development of shock capturing schemes for numerical approximation of the solution of conservation laws [13]. In fact, the solution of a conservation law may develop jump discontinuities in finite time and thus developing a classical solution is non trivial (as discussed in chapter 1).
Another motivation for developing high-order numerical schemes for approximating the solution of conservation laws is the wide range of applications in hydrodynamics, magnetohydrodynamics and aerodynamics [41].
In this chapter we shall briefly present the Lax-Friedrichs and the Nessyahu-Tadmor schemes for approximating the solutions of systems of conservation laws.

3.1 Statement of the Problem and Notations

Consider the following one-dimensional scalar conservation law:

$$u_t + f_x(u) = 0 \qquad \text{for} \qquad t \geq 0 \quad , \qquad x \in [a, b] \tag{3.1}$$

where $u : \mathbb{R} \times [0, \infty) \to \mathbb{R}$ is a function of x and t, with initial condition given by:

$$u(x, 0) = u_0(x)$$

Without loss of generality, assume that we have a uniform discretization in space, with a constant grid spacing h such that $x_k = x_0 + kh$ and $x_0 = a$. Let

$$u_i(t) := \frac{1}{\Delta x} \int_{x_{i-1/2}}^{x_{i+1/2}} u(x, t)\, dx$$

be the average value of u at time t over the cell $C_i := [x_{i-1/2}, x_{i+1/2}]$.

A staggered central scheme is a two-step method that evolves the numerical solution on two staggered dual grids at consecutive time steps in order to bypass the time consuming resolution of the Riemann problems arising at the cell interfaces.

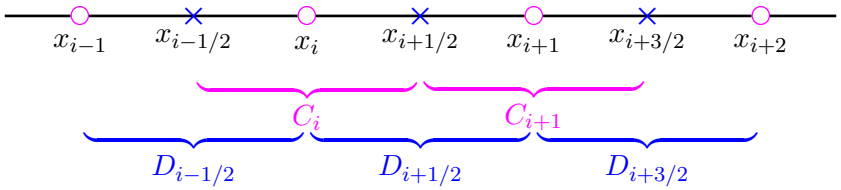

Figure 3.1: Original control volumes C_i's and staggered control volumes $D_{i+1/2}$'s.

The control cells C_i are the intervals $[x_{i-1/2}, x_{i+1/2}]$ and the solution is defined at the centers x_i of C_i at time $t = t^n$ for $n = 0, 2, 4, ...$
On the other hand, the dual control cells $D_{i+1/2}$ are the intervals $[x_i, x_{i+1}]$ and the solution is defined at the centers $x_{i+1/2}$ of $D_{i+1/2}$ at time $t = t^{2n+1}$, for $n = 0, 1, 2, ...$
More details are provided in [44].

3.2 Central schemes vs Riemann solvers

In the first step of a Godunov type scheme [20] we assume that the numerical solution is defined on the original cells C_i at time t^n and the goal is to compute the solution on these cells C_i at time t^{n+1}. Integrating the conservation law over the volume $R_i^n = C_i \times [t^n, t^{n+1}]$ and applying Green's formula we obtain

$$\oint_{\partial R_i^n} (u\,dx - f(u)\,dt) = 0\,.$$

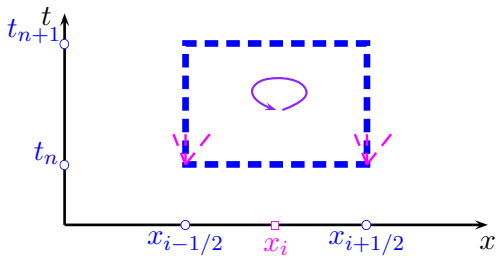

Figure 3.2: Rectangle $R_i^n = [x_{i-1/2}, x_{i+1/2}] \times [t^n, t^{n+1}]$

Expanding the integral one gets

$$\int_{x_{i-1/2}}^{x_{i+1/2}} u(x, t^{n+1})\, dx = \int_{x_{i-1/2}}^{x_{i+1/2}} u(x, t^n)\, dx - \left(\int_{t^n}^{t^{n+1}} f(u(x_{i+1/2}, t))\, dt - \int_{t^n}^{t^{n+1}} f(u(x_{i-1/2}, t))\, dt \right) .$$

The integrals of the flux function require the solutions at the points $x_{i-1/2}$ and $x_{i+1/2}$ along the interval $[t^n, t^{n+1}]$ which are the solutions of the Riemann problems that arise at these points. The resolution of these Riemann problems requires a characteristic decomposition and thus alot of computations.

Central schemes avoid the resolution of these problems by using a staggering process i.e. by alternating between an original grid and a staggered dual one. As in the Godunov type schemes, in the first step of a central scheme we assume that the numerical solution is defined on the original cells C_i at time t^n. Integrating the conservation law over the volume $R_{i+1/2}^n = D_{i+1/2} \times [t^n, t^{n+1}]$ and applying Green's formula we obtain

$$\oint_{\partial R_{i+1/2}^n} (u\, dx - f(u)\, dt) = 0 .$$

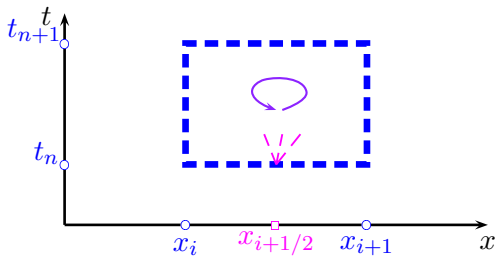

Figure 3.3: Rectangle $R^n_{i+1/2} = [x_i, x_{i+1}] \times [t^n, t^{n+1}]$

Expanding the integrals one gets,

$$\begin{aligned}\int_{x_i}^{x_{i+1}} u(x, t^{n+1})\, dx \;&=\; \int_{x_i}^{x_{i+1}} u(x, t^n)\, dx \\ &\quad - \left(\int_{t^n}^{t^{n+1}} f(u(x_{i+1}, t))\, dt - \int_{t^n}^{t^{n+1}} f(u(x_i, t))\, dt \right) .\end{aligned}$$

Unlike the Godunov type schemes the integrals of the flux do not require the solution of the Riemann problems arising at the cell interfaces $x_{i-1/2}$ and $x_{i+1/2}$ along the interval $[t^n, t^{n+1}]$ since the required values of the solution at the points x_i and x_{i+1} can be computed all over the interval $[t^n, t^{n+1}]$. The time integrals are approximated using the midpoint quadrature rule and the solution at the intermediate time step can be easily obtained using Taylor expansions.

3.3 One-dimensional Lax-Friedrichs Central Scheme

We assume a piecewise constant numerical solution u_i^n defined at the center x_i of the cell C_i at time $t = t^n$. The solution $u_{i+1/2}^{n+1}$ at the next time step t^{n+1} is calculated at the center $x_{i+1/2}$ of the dual cell $D_{i+1/2}$.

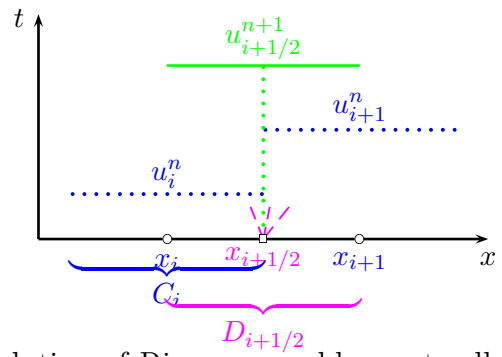

Figure 3.4: The resolution of Riemann problems at cell interfaces is avoided when alternating from original to staggered grid

Integrating the hyperbolic conservation law (3.1) over the rectangle $R^n_{i+1/2} = D_{i+1/2} \times [t^n, t^{n+1}]$ and applying Green's formula, we obtain

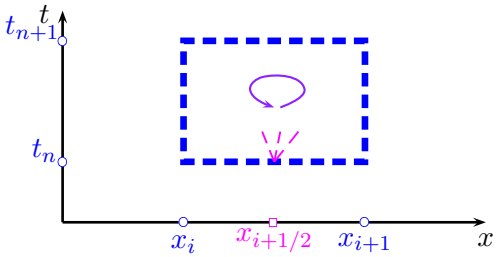

Figure 3.5: Integrating over the rectangle $R^n_{i+1/2} = [x_i, x_{i+1}] \times [t^n, t^{n+1}]$

$$\oint_{\partial R^n_{i+1/2}} (u\,dx - f(u)\,dt) = 0\,.$$

Expanding this integral and rearranging the terms one gets,

$$\begin{aligned} \Delta x.u^{n+1}_{i+1/2} \;=\; & \int_{x_i}^{x_{i+1/2}} u(x,t^n)\,dx + \int_{x_{i+1/2}}^{x_{i+1}} u(x,t^n)\,dx \\ & - \left(\int_{t^n}^{t^{n+1}} f(u(x_{i+1},t))\,dt - \int_{t^n}^{t^{n+1}} f(u(x_i,t))\,dt \right)\,. \end{aligned} \tag{3.2}$$

The first two integrands on the right hand side of equation (3.2) can be computed in the same way since u^n_i and u^n_{i+1} are known constant values. The time intergrands are

approximated; they cannot be determined exactly since we don't know the variations of the flux function over time.

Substituting the integrals $\int_{x_i}^{x_{i+1/2}} u(x,t^n)\,dx = \frac{\Delta x}{2}\, u_i^n$ and $\int_{x_{i+1/2}}^{x_{i+1}} u(x,t^n)\,dx = \frac{\Delta x}{2}\, u_{i+1}^n$ by their values in equation (3.2) we get:

$$\begin{aligned} u_{i+1/2}^{n+1} &= \frac{1}{\Delta x}\frac{\Delta x}{2}\left(u_i^n + u_{i+1}^n\right) - \frac{1}{\Delta x}\left(\int_{t^n}^{t^{n+1}} f(u(x_{i+1},t))\,dt - \int_{t^n}^{t^{n+1}} f(u(x_i,t))\,dt\right) \\ &= \frac{1}{2}\left(u_i^n + u_{i+1}^n\right) - \frac{1}{\Delta x}\left(\int_{t^n}^{t^{n+1}} f(u(x_{i+1},t))\,dt - \int_{t^n}^{t^{n+1}} f(u(x_i,t))\,dt\right) . \quad (3.3) \end{aligned}$$

The flux integrals are approximated using first-order quadrature rule as follows: $\int_{t^n}^{t^{n+1}} f(u(x_{i+1},t))\,dt \simeq \Delta t f(u_{i+1}^n)$. Therefore, the numerical solution of the hyperbolic system at time t^{n+1}(odd time step) is given by:

$$u_{i+1/2}^{n+1} = \frac{1}{2}\left(u_i^n + u_{i+1}^n\right) - \frac{\Delta t}{\Delta x}\left(f(u_{i+1}^n) - f(u_i^n)\right)$$

In a similar approach, the numerical solution at even time steps will be computed on the cells C_i of the original grid as follows:

$$u_i^{n+2} = \frac{1}{2}\left(u_{i-1/2}^{n+1} + u_{i+1/2}^{n+1}\right) - \frac{\Delta t}{\Delta x}\left(f(u_{i+1/2}^{n+1}) - f(u_{i-1/2}^{n+1})\right) . \quad (3.4)$$

The time step Δt is computed dynamically at the beginning of each iteration according to the following CFL condition:

$$\frac{\Delta t}{\Delta x} \max_{x_j \le x \le x_{j+1}} \rho\left(A\left(u\left(x,t\right)\right)\right) < \frac{1}{2}\,, \quad (3.5)$$

where $\rho(A) = \max_{1\le i\le d} |\lambda_i(A)|$ is the spectral radius of the Jacobian matrix A=$\frac{\partial f}{\partial u}$, with λ_i denoting the i^{th} eigenvalue.

3.4 One-dimensional Nessyahu and Tadmor Central Scheme

In order to improve the spatial accuracy and based on the LF scheme, the NT scheme evolves piecewise linear cell interpolants.

Starting with the same control cells as the LF scheme $C_i = [x_{i-1/2}, x_{i+1/2}]$ and $D_{i+1/2} = [x_i, x_{i+1}]$, and assuming that the solution is known at the cell centers, we use a Taylor series expansion about x_i and define the linear interpolant $L_i(x, t^n)$ on the cell C_i:

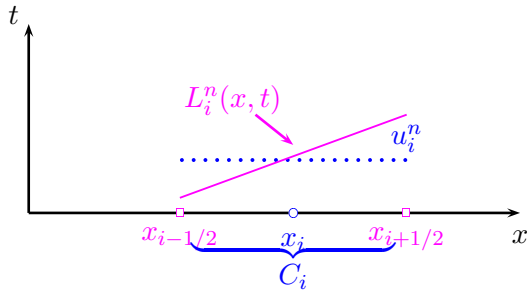

Figure 3.6: $L(x, t^n)$ is the piecewise linear approximation of $u(x, t^n)$ on C_i at $t = t^n$

$$L_i(x, t^n) \quad = \quad u_i^n + (x - x_i)\frac{\delta_i^n}{\Delta x} \qquad \text{on } [x_{i-1/2}, x_{i+1/2}]\,. \tag{3.6}$$

where $\frac{\delta_i^n}{\Delta x}$ approximates the numerical derivative of $u(x, t^n)$ at the point x_i and it will be discussed in section 3.4.1.

Thus the value of the numerical solution at any point in the cell C_i is determined according to the linear interpolant.

Assume the solution at time t^n is known at the centers of the cells C_i, the solution on the staggered cells $D_{i+1/2}$ at time t^{n+1} is calculated as follows:

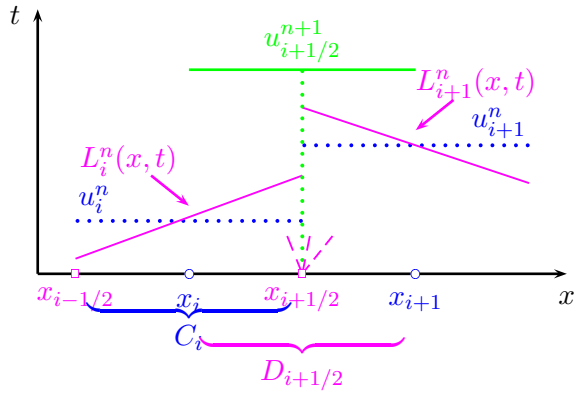

Figure 3.7: The resolution of Riemann problems at cell interfaces is avoided when alternating from original to staggered grid

Integrating the hyperbolic equation (3.1) over the rectangle $R^n_{i+1/2} = D_{i+1/2} \times [t^n, t^{n+1}]$ and applying Green's formula, we obtain

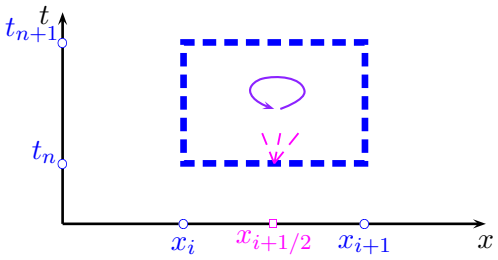

Figure 3.8: Integrating over the rectangle $R^n_{i+1/2} = [x_i, x_{i+1}] \times [t^n, t^{n+1}]$

$$\oint_{\partial R^n_{i+1/2}} (u\,dx - f(u)\,dt) = 0\,. \tag{3.7}$$

Expanding the integral and rearranging the terms one gets,

$$\begin{aligned} \Delta x\, u^{n+1}_{i+1/2} \;=\; & \int_{x_i}^{x_{i+1/2}} L_i(x,t^n)\,dx + \int_{x_{i+1/2}}^{x_{i+1}} L_{i+1}(x,t^n)\,dx \\ & - \left(\int_{t^n}^{t^{n+1}} f(u(x_{i+1},t))\,dt - \int_{t^n}^{t^{n+1}} f(u(x_i,t))\,dt \right)\,. \end{aligned} \tag{3.8}$$

The first two integrals on the right hand side of equation (3.8) can be computed exactly since $L_i(x,t^n)$ and $L_{i+1}(x,t^n)$ are defined in (3.6). The flux intergrals will be estimated with second-order of accuracy using the midpoint quadrature rule. Using the mean value theorem, we obtain:

$$\int_{x_i}^{x_{i+1/2}} L_i(x,t^n)\,dx = \frac{\Delta x}{2} L_i\left(x_{i+\frac{1}{4}}, t^n\right) = \left(u_i^n + \frac{\delta_i^n}{4}\right)\frac{\Delta x}{2}\,.$$

Substituting $\int_{x_i}^{x_{i+1/2}} L_i(x,t^n)\,dx$ and $\int_{x_{i+1/2}}^{x_{i+1}} L_{i+1}(x,t^n)\,dx$ by their values in equation (3.8) one gets:

$$\begin{aligned} u_{i+1/2}^{n+1} &= \frac{1}{\Delta x}\left(u_i^n + \frac{\delta_i^n}{4}\right)\frac{\Delta x}{2} + \frac{1}{\Delta x}\left(u_{i+1}^n - \frac{\delta_{i+1}^n}{4}\right)\frac{\Delta x}{2} \\ &\quad -\frac{1}{\Delta x}\left(\int_{t^n}^{t^{n+1}} f(u(x_{i+1},t))\,dt - \int_{t^n}^{t^{n+1}} f(u(x_i,t))\,dt\right) \\ &= \frac{1}{2}\left(u_i^n + u_{i+1}^n\right) + \frac{1}{8}\left(\delta_i^n - \delta_{i+1}^n\right) \\ &\quad -\frac{1}{\Delta x}\left(\int_{t^n}^{t^{n+1}} f(u(x_{i+1},t))\,dt - \int_{t^n}^{t^{n+1}} f(u(x_i,t))\,dt\right)\,. \end{aligned} \tag{3.9}$$

Using the midpoint rule we get $\int_{t^n}^{t^{n+1}} f(u(x_i,t))\,dt \simeq \Delta t\, f(u_i^{n+1/2})$.
Therefore, the numerical solution of the hyperbolic conservation law at an odd time step is given by:

$$u_{i+1/2}^{n+1} = \frac{1}{2}\left(u_i^n + u_{i+1}^n\right) + \frac{1}{8}\left(\delta_i^n - \delta_{i+1}^n\right) - \frac{\Delta t}{\Delta x}\left(f(u_{i+1}^{n+1/2}) - f(u_i^{n+1/2})\right)\,,$$

where the solution at the intermediate time step $t^{n+1/2}$ is calculated using a first-order Taylor expansion and the conservation rule:

$$\begin{aligned} u_{i+1}^{n+1/2} &= u_{i+1}^n - \frac{1}{2}\frac{\Delta t}{\Delta x} f'(u_{i+1}^n)\ \delta_{i+1}^n \\ &= u_{i+1}^n - \frac{1}{2}\frac{\Delta t}{\Delta x} A_{i+1}^n\ \delta_{i+1}^n\,. \end{aligned} \tag{3.10}$$

and A^n_{i+1} is the Jacobian matrix of the flux function f at time t^n evaluated at the point x_{i+1}.

In a similar approach, the numerical solution at an even time step will be computed on the cells of the original grid as follows:

$$\begin{aligned} u_i^{n+2} &= \frac{1}{2}\left(u_{i-1/2}^{n+1} + u_{i+1/2}^{n+1}\right) + \frac{1}{8}\left(\delta_{i-1/2}^{n+1} - \delta_{i+1/2}^{n+1}\right) \\ &\quad -\frac{\Delta t}{\Delta x}\left(f(u_{i+1/2}^{n+3/2}) - f(u_{i-1/2}^{n+3/2})\right) , \end{aligned} \tag{3.11}$$

where

$$\begin{aligned} u_{i+1/2}^{n+3/2} &= u_{i+1/2}^{n+1} - \frac{1}{2}\frac{\Delta t}{\Delta x} f'(u_{i+1/2}^{n+1})\ \delta_{i+1/2}^{n+1} \\ &= u_{i+1/2}^{n+1} - \frac{1}{2}\frac{\Delta t}{\Delta x} A_{i+1/2}^{n+1}\ \delta_{i+1/2}^{n+1} , \end{aligned} \tag{3.12}$$

and $A^{n+1}_{i+1/2}$ is the Jacobian matrix of the flux function f at time t^{n+1} and evaluated at the point $x_{i+1/2}$.

As in the Lax-Friedrichs' case, the time step Δt is computed dynamically according to equation (3.5).

3.4.1 Computing the numerical derivatives

The approximate slope $\left\{(u_i^n)' = \frac{\delta_i^n}{\Delta x}\right\}$ of the piecewise linear reconstruction at the grid point x_i at time $t = t^n$ should be chosen in such a way to guarantee second-order of accuracy in space i.e.

$$\begin{aligned} (u_i^n)' &= \frac{\partial}{\partial x} u(x = x_i, t^n) + O(\Delta x) \\ &= \frac{\delta_i^n}{\Delta x} + O(\Delta x) \end{aligned}$$

The second-order of accuracy in time is ensured by the use of the midpoint quadrature rule for integration.

The numerical derivatives should be carefully chosen to avoid spurious oscillations

in the numerical solution. Many limiters can be used to estimate them. In this chapter we will consider two types of limiters: the minmod and the MC-θ limiters. The van Leer monotonized centered limiter (MC-θ) is given by:

$$(u_i^n)' = \text{minmod}\Big[\theta(u_i^n - u_{i-1}^n)\,,\, \frac{u_{i+1}^n - u_{i-1}^n}{2}\,,\, \theta(u_{i+1}^n - u_i^n)\Big]$$

where $1 \leq \theta \leq 2$

The minmod limiter is given by:

$$(u_i^n)' = \text{minmod}\Big[u_i^n - u_{i-1}^n\,,\, u_{i+1}^n - u_i^n\Big]$$

where minmod is define by:

$$\text{minmod}(a,b) = \begin{cases} \min(a,b) & \text{if a, b } > 0 \\ \max(a,b) & \text{if a, b } < 0 \\ 0 & \text{if a } \times \text{ b} < 0 \end{cases}$$

The numerical results obtained using the MC-θ slope limiter are sharper than those obtained using the MinMod limiter.

CHAPTER 4

OVERVIEW OF CENTRAL SCHEMES FOR TWO-DIMENSIONAL SYSTEMS OF CONSERVATION LAWS

In this chapter we present an overview of existing unstructured central schemes and we introduce some notations needed for the derivation of our schemes.

Several two-dimensional extensions of the Lax-Friedrichs and Nessyahu-Tadmor schemes on unstructured grid were previously developed. The extension presented in [2] is based on barycentric cells constructed around the nodes of a finite element triangulation, for even time steps, and staggered quadrilateral cells associated with this triangulation, for odd time steps.

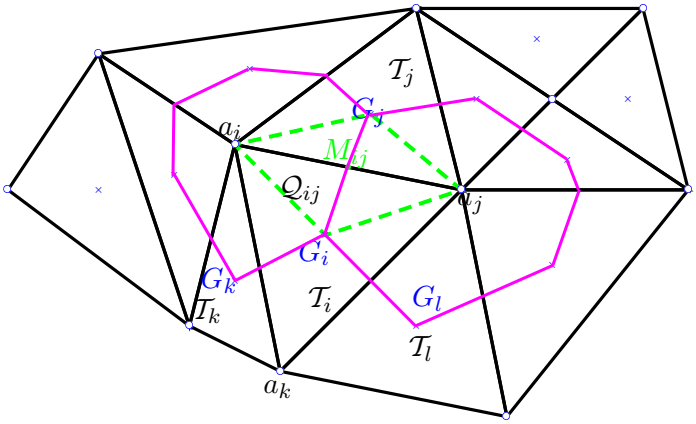

Figure 4.1: Two original cells for the solution at time t^n and a staggered dual cell for the solution at time t^{n+1}.

The method is then applied and used to solve problems arising in gas dynamics and aerodynamics. This method is highly efficient but it is very difficult to implement due to the complexity of its geometry.

Another two-dimensional extension of the Nessyahu-Tadmor scheme on unstructured grids was presented in [35; 14] in which the control cells are the triangles of a finite element triangulation at even time steps and some special cells, such that the elements of the staggered grid contain the Riemann fans emanating from the discontinuities in the piecewise linear solution, at odd time steps. The dual cells are constructed based on the idea that the solution discontinuities at time t^n from cell T_i cannot propagate into the sub-triangle Δ_i, whose vertices are located at $\frac{1}{3}$ of the distance from the vertices of T_i to its centroid, i.e. the dual cells S_i are constructed in a way to contain the discontinuities arising at the cell interfaces.

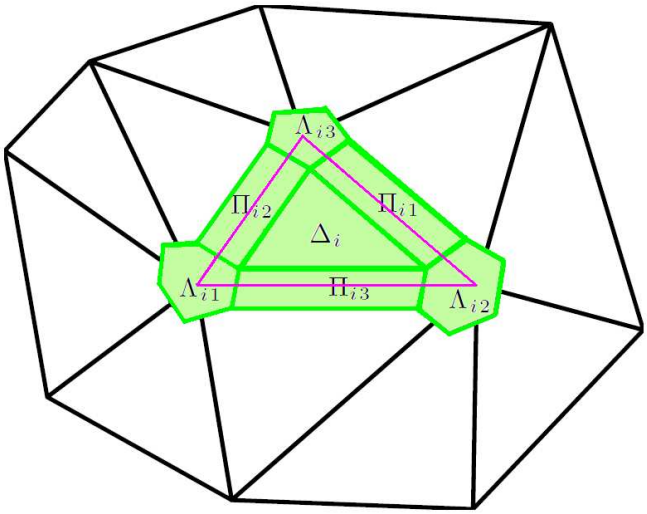

Figure 4.2: Original cell (triangles) and dual cell $S_i = \Lambda_{i_1} \cup \Pi_{i_2} \cup \Lambda_{i_3} \cup \Pi_{i_1} \cup \Lambda_{i_2}$

On the other hand, two-dimensional extensions on Cartesian grid with Cartesian or diamond shaped dual cells were developed in [6; 3; 26; 27]. These extensions were successfully used to solve problems arising in aerodynamics, hydrodynamics and magnetohydrodynamics. Three-dimensional extensions on cartesian cells with diamond dual cells were developed in [4] and adopted to Magnetohydrodynamics. Furthermore, unstaggered central schemes that evolve the numerical solution on a unique grid were developed in [52; 53] and used to solve problems in hydrodynamics and magnetohydrodynamics.

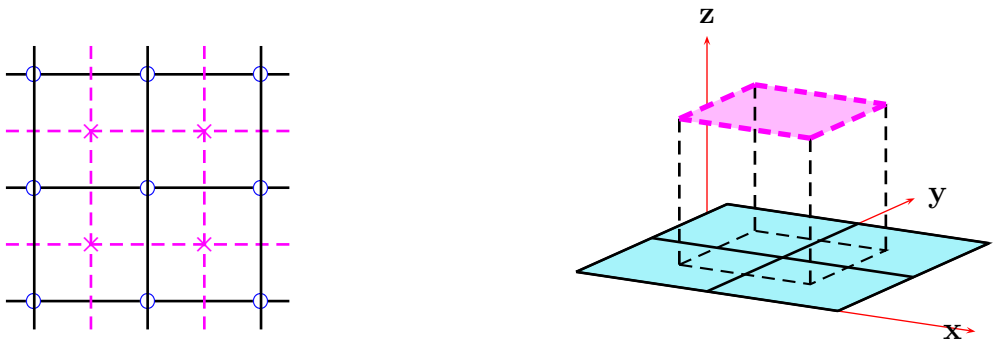

Figure 4.3: Four original cells (solid lines) for the solution at time t^n and a staggered dual cell (dashed lines) for the solution at time t^{n+1}.

4.1 Statement of the Problem and Notations

Consider the two-dimensional scalar conservation law

$$u_t + \frac{\partial}{\partial x} f(u) + \frac{\partial}{\partial y} g(u) = 0 \,, \tag{4.1}$$

with initial condition

$$u(x, y, 0) = u_0(x, y) \,.$$

We want to estimate the solution of the IVP on some region Ω of the xy-plane.

In the one-dimensional space, we have seen that the staggered forms of the Lax-Friedrichs and the Nessyahu-Tadmor schemes use two alternate grids with cells centered at $\{x_j\}$ and $\{x_{j+1/2}\}$ at the odd and even time steps, respectively. In two-dimensional space, we proceed in a similar way, starting from a conformal finite element triangular grid $\mathcal{T}_h$ such that the intersection of two triangles is either empty or consists of one common vertex or side i.e.

$$T \cap T' = \begin{cases} \phi \\ \text{one vertex} \\ \text{one side} \end{cases} \quad \text{for any } T,\, T' \in \mathcal{T}_h$$

Without loss of generality, let us consider the case of scalar conservation law. In the case of a system of conservation laws, we can apply the same procedure for each conservation equation of the system i.e. we adopt a componentwise approach for constructing the numerical solution of a system of conservation laws.

Each of the proposed methods is a two step scheme defined with the help of two dual, staggered grids at consecutive time steps in order to bypass the resolution of the Riemann problems arising at the cell interfaces.

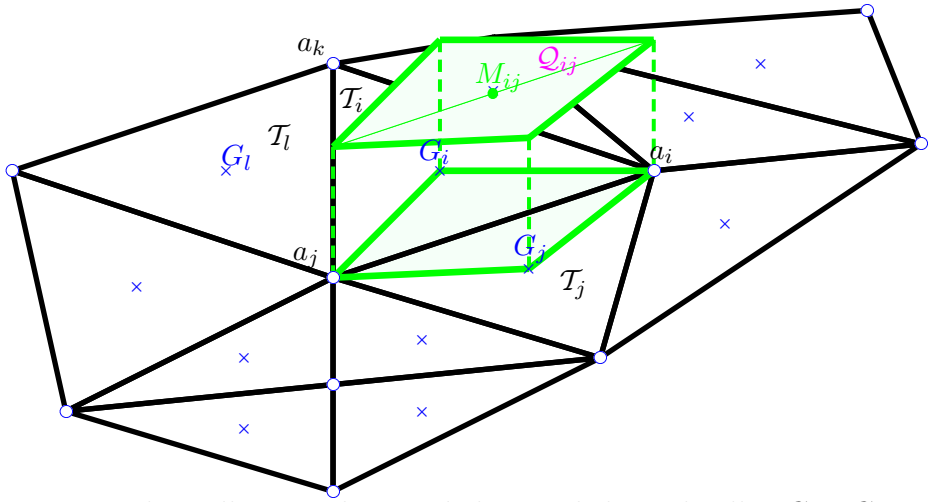

Figure 4.4: Triangular cells T_i and T_j and the quadrilateral cell $a_i G_i a_j G_j$.

The control cells of the original grid associated with our finite volume extensions of the Lax-Friedrichs and the Nessyahu-Tadmor schemes, are the triangles T_i of $\mathcal{T}_h$ and the cell average solution at even time steps will be defined at the centroids G_i of T_i, while the cells of the staggered dual grid are the quadrilaterals $Q_{ij} = a_i G_i a_j G_j$ (fig. 6.1). Q_{ij} is obtained by joining the centroids G_i and G_j of two adjacent triangles T_i and T_j to the endpoints of their common edge. The cell average solution at odd time steps will be defined at the midpoints M_{ij} of $a_i a_j$.

Let $u_i^n \simeq u\left(G_i, t^n\right)$ and $u_{ij}^{n+1} \simeq u\left(M_{ij}, t^{n+1}\right)$ denote the cell average values on the original and dual grids at time $t = t^n$ and $t = t^{n+1}$, respectively. (n is considered to be even).

Starting with the initial condition $u(x, y, 0)$, we define

$$u_i^0 = \frac{1}{\mathcal{A}(T_i)} \int_{T_i} u_0(x, y)\, d\mathcal{A}\,. \tag{4.2}$$

The solution $u(x, y, t)$ of the conservation law is approximated at each time step by a piecewise solution (a piecewise constant solution u_i^n, or u_{ij}^{n+1}, for the Lax-Friedrichs scheme or a piecewise linear solution L_i^n, or L_{ij}^{n+1}, for the Nessyahu-Tadmor scheme) on the control volumes T_i for even time steps and Q_{ij} for odd time steps.

Let ω_i^1, ω_i^2, and ω_i^3 be the outer unit normal vectors to the boundary ∂T_i of the cell T_i, and ν_{ij}^1, ν_{ij}^2, ν_{ij}^3 and ν_{ij}^4 be the outer unit normal vectors to the boundary ∂Q_{ij} of the cell Q_{ij} as shown in figure 4.5.

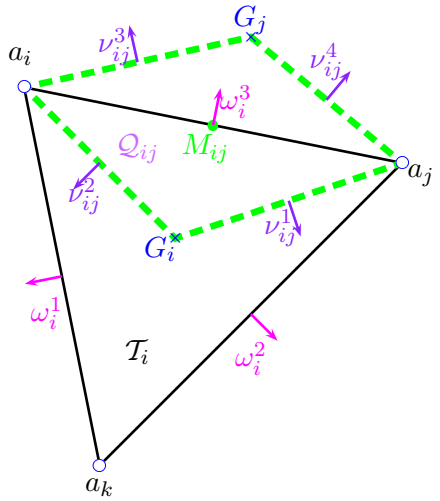

Figure 4.5: Triangular cell T_i and the quadrilateral cell $Q_{ij} = a_i G_i a_j G_j$ with the normal vectors to their sides.

We also define the following elementary flux vectors for the triangular cell T_i

$$\begin{aligned} \theta_i &= \int_{\Gamma_i = \partial T_i = a_k a_j \cup a_j a_i \cup a_i a_k} \omega\, d\sigma \\ &= \omega_i^1 |a_i a_k| + \omega_i^2 |a_k a_j| + \omega_i^3 |a_i a_j|\,, \end{aligned}$$

and for the quadrilateral cell Q_{ij}

$$\begin{aligned} \eta_{ij} &= \int_{\Gamma_{ij} = \partial Q_{ij} = a_i G_i \cup G_i a_j \cup a_j G_j \cup G_j a_i} \nu\, d\sigma \\ &= \nu_{ij}^1 |a_i G_i| + \nu_{ij}^2 |G_i a_j| + \nu_{ij}^3 |a_j G_j| + \nu_{ij}^4 |G_j a_i|\,. \end{aligned}$$

Definition 14 *The volume of a cylindrical solid in 2D is the product of the area of its base with the depth b of this solid.*

Definition 15 (Gauss's formula: Area of a triangle) *[10]*

The area of a triangle T with vertices (x_1, y_1), (x_2, y_2) and (x_3, y_3) labeled in the counter-clockwise direction is given by:

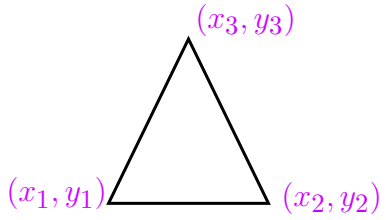

$$\mathcal{A}(T) = \frac{1}{2}\left[(x_1 - x_2)(y_1 + y_2) + (x_2 - x_3)(y_2 + y_3) + (x_3 - x_1)(y_3 + y_1)\right] . \quad (4.3)$$

Definition 16 (Gauss's formula: Area of a quadrilateral) *[10]*

The area of a quadrilateral Q with vertices (x_1, y_1), (x_2, y_2), (x_3, y_3) and (x_4, y_4) labeled in the counter-clockwise direction is given by:

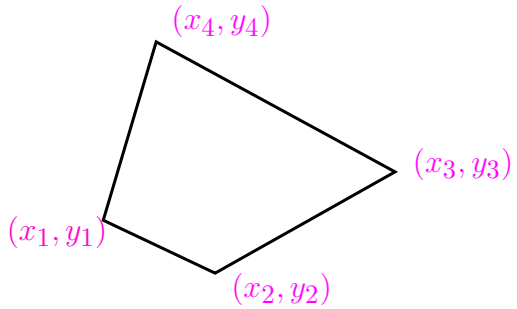

$$\mathcal{A}(Q) = \frac{1}{2}\left[(x_1 - x_3)(y_2 - y_4) + (x_4 - x_2)(y_1 - y_3)\right] . \quad (4.4)$$

CHAPTER 5

A LAX-FRIEDRICHS TYPE SCHEME ON UNSTRUCTURED GRIDS

In this chapter we present a finite volume extension of the Lax-Friedrichs on unstructured triangular grids. The proposed extension evolves the numerical solution on triangular cells at even time steps and on staggered quadrilateral dual cells at odd time steps, and thus bypasses the resolution of the Riemann problems arising at the cell interfaces.

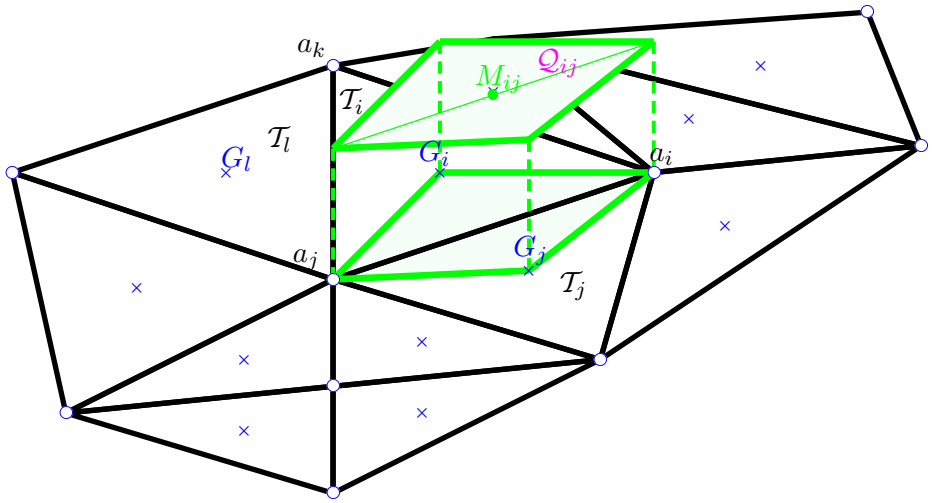

Figure 5.1: Triangular cells T_i and T_j and the quadrilateral cell $a_iG_ia_jG_j$.

Let the domain Ω in $\mathbb{R}^2$, and let $\mathcal{T}_h$ be a finite element triangulation of Ω. The control cells of the original grid associated with our finite volume extension of the Lax-Friedrichs scheme are the triangles T_i of $\mathcal{T}_h$ and the numerical solution at even time steps will be defined at the centroids G_i of T_i, while at odd time steps it will be defined at the midpoints M_{ij} of the sides a_ia_j of the triangulation. The cells of the staggered dual grid are the quadrilaterals Q_{ij} (obtained by joining the centroids of the triangles T_i and T_j to the endpoints of their common edge).

Let the two-dimensional scalar conservation law

$$u_t + \frac{\partial}{\partial x} f(u) + \frac{\partial}{\partial y} g(u) = 0 \,, \qquad \text{for } t > 0 \,,\ (x, y) \in \Omega \tag{5.1}$$

with initial condition

$$u(x, y, 0) = u_0(x, y) \,.$$

The first step of the two-dimensional finite volume extension of the Lax-Friedrichs scheme is defined by integrating equation (5.1) over the volume $Q_{ij} \times [t^n, t^{n+1}]$ and by assuming that the triangular cell values are known at time t^n:

$$\int_{t^n}^{t^{n+1}} \int_{Q_{ij}} \left(u_t + \frac{\partial}{\partial x} f(u) + \frac{\partial}{\partial y} g(u) \right) d\mathcal{A}\, dt = 0 \,, \tag{5.2}$$

where $d\mathcal{A}$ is an area element, and $t^{n+1} = t^n + \Delta t$.

Applying the divergence theorem to the spatial integral we get

$$\begin{aligned} \int_{Q_{ij}} u(x, y, t^{n+1})\, d\mathcal{A} \;\; - \;\; & \int_{Q_{ij}} u(x, y, t^n)\, d\mathcal{A} + \\ & \int_{t^n}^{t^{n+1}} \int_{\partial Q_{ij}} \big(f(u(x, y, t))\nu_x + g(u(x, y, t))\nu_y \big)\, d\sigma\, dt = 0 \,, \end{aligned} \tag{5.3}$$

where $\nu = (\nu_x, \nu_y)$ denotes the unit outer normal vector to the boundary of Q_{ij}. Since $Q_{ij} = (Q_{ij} \cap T_i) \cup (Q_{ij} \cap T_j)$ then,

$$\int_{Q_{ij}} u(x, y, t^n)\, d\mathcal{A} = \int_{Q_{ij} \cap T_i} u(x, y, t^n)\, d\mathcal{A} + \int_{Q_{ij} \cap T_j} u(x, y, t^n)\, d\mathcal{A} \,.$$

Therefore equation (5.3) becomes

$$\begin{aligned} \int_{Q_{ij}} u(x, y, t^{n+1})\, d\mathcal{A} \;\; = \;\; & \int_{Q_{ij} \cap T_i} u(x, y, t^n)\, d\mathcal{A} + \int_{Q_{ij} \cap T_j} u(x, y, t^n)\, d\mathcal{A} \\ & - \int_{t^n}^{t^{n+1}} \int_{\partial Q_{ij}} \big(f(u(x, y, t))\nu_x + g(u(x, y, t))\nu_y \big)\, d\sigma\, dt \,. \end{aligned} \tag{5.4}$$

Everything up to this point is exact.

Since the numerical solution at time $t = t^n$ is a piecewise constant function defined at the points M_{ij}, we thus obtain

$$\int_{Q_{ij}} u(x, y, t^{n+1})\, d\mathcal{A} = \mathcal{A}(Q_{ij}) u_{ij}^{n+1} \,, \tag{5.5}$$

where $\mathcal{A}(Q_{ij}) = \mathcal{A}$rea of the quadrilateral Q_{ij} is computed using Gauss's formula (4.4). Equation (5.4) becomes

$$\begin{aligned} \mathcal{A}(Q_{ij}) u_{ij}^{n+1} \;=\; & \int_{Q_{ij}\cap T_i} u(x, y, t^n)\, d\mathcal{A} + \int_{Q_{ij}\cap T_j} u(x, y, t^n)\, d\mathcal{A} \\ & - \int_{t^n}^{t^{n+1}} \int_{\partial Q_{ij}} \big(f(u(x, y, t))\nu_x + g(u(x, y, t))\nu_y \big)\, d\sigma\, dt \,. \end{aligned} \tag{5.6}$$

Using the same approach as in equation (5.5), we obtain

$$\int_{Q_{ij}\cap T_i} u(x, y, t^n)\, d\mathcal{A} = u_i^n \times \mathcal{A}rea(Q_{ij} \cap T_i) = u_i^n \times \mathcal{A}rea(a_i G_i a_j) \,, \tag{5.7}$$

and,

$$\int_{Q_{ij}\cap T_j} u(x, y, t^n)\, d\mathcal{A} = u_j^n \times \mathcal{A}rea(Q_{ij} \cap T_j) = u_j^n \times \mathcal{A}rea(a_i a_j G_j) \,, \tag{5.8}$$

where $\mathcal{A}rea(a_i G_i a_j)$ and $\mathcal{A}rea(a_i a_j G_j)$ are computed using Gauss's formula (4.3). Assuming an appropriate CFL condition so that the discontinuities in the solution do not leave the staggered cells during the current time step,

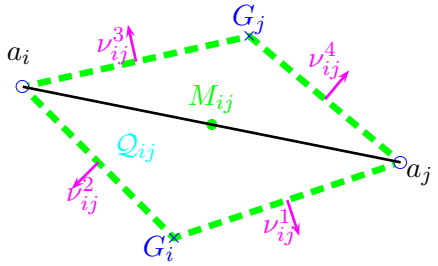

Figure 5.2: Quadrilateral cell $\mathcal{Q}_{ij} = a_i G_i a_j G_j$ with the normal vectors to its sides

The flux integral can be approximated as follows:

$$\int_{t^n}^{t^{n+1}} \int_{\partial Q_{ij}} \big(f(u(x,y,t))\nu_x + g(u(x,y,t))\nu_y\big)\, d\sigma\, dt \cong \Delta t \Big(f(u_i^n)\nu_{ij_x}^1 |a_j G_i| + f(u_i^n)\nu_{ij_x}^2 |a_i G_i| + g(u_i^n)\nu_{ij_y}^1 |a_j G_i| + g(u_i^n)\nu_{ij_y}^2 |a_i G_i| + f(u_j^n)\nu_{ij_x}^3 |a_i G_j| + f(u_j^n)\nu_{ij_x}^4 |a_j G_j| + g(u_j^n)\nu_{ij_y}^3 |a_i G_j| + g(u_j^n)\nu_{ij_y}^4 |a_j G_j| \Big) , \quad (5.9)$$

where $\nu_{ij}^k = \left(\nu_{ij_x}^k, \nu_{ij_y}^k\right)^{k=1,\dots,4}$ denote the normal vectors to the boundary ∂Q_{ij} of Q_{ij} pointing out of the cell as shown in figure 5.2.

Gathering equations (5.7), (5.8), (5.9) and dividing by $\mathcal{A}(Q_{ij})$ we obtain:

$$\begin{aligned} u_{ij}^{n+1} \;=\; & \frac{1}{\mathcal{A}(Q_{ij})} \Big(u_i^n \mathcal{A}(Q_{ij} \cap T_i) + u_j^n \mathcal{A}(Q_{ij} \cap T_j) \Big) \\ & - \frac{1}{\mathcal{A}(Q_{ij})} \Delta t \Big(f(u_i^n)\nu_{ij_x}^1 |a_j G_i| + f(u_i^n)\nu_{ij_x}^2 |a_i G_i| \\ & \qquad + g(u_i^n)\nu_{ij_y}^1 |a_j G_i| + g(u_i^n)\nu_{ij_y}^2 |a_i G_i| \\ & \qquad + f(u_j^n)\nu_{ij_x}^3 |a_i G_j| + f(u_j^n)\nu_{ij_x}^4 |a_j G_j| \\ & \qquad + g(u_j^n)\nu_{ij_y}^3 |a_i G_j| + g(u_j^n)\nu_{ij_y}^4 |a_j G_j| \Big) , \end{aligned}$$

The second step of the two-dimensional extension of the Lax-Friedrichs scheme is constructed by integrating equation (5.1) over the volume $T_i \times [t^{n+1}, t^{n+2}]$.

We assume that the numerical solution u_{ij}^{n+1} is known at time t^{n+1} on the quadrilateral cells Q_{ij} and is defined at the midpoint M_{ij} of $a_i a_j$. We proceed as previously, integrating over the volume $T_i \times [t^{n+1}, t^{n+2}]$ and applying the divergence theorem, we get

$$\begin{aligned} \int_{T_i} u(x,y,t^{n+2})\, d\mathcal{A} \;-\; & \int_{T_i} u(x,y,t^{n+1})\, d\mathcal{A} + \\ & \int_{t^{n+1}}^{t^{n+2}} \int_{\partial T_i} \big(f(u(x,y,t))\omega_x + g(u(x,y,t))\omega_y\big)\, d\sigma\, dt = 0 . \end{aligned}$$

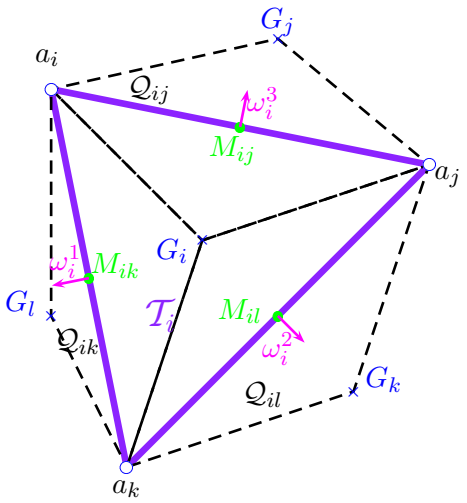

Figure 5.3: Triangular cell T_i and the quadrilateral cells $\mathcal{Q}_{ij}$, $\mathcal{Q}_{ik}$,and $\mathcal{Q}_{il}$ together with the normal vectors to the boundary ∂T_i of T_i.

Note that $T_i = (T_i \cap Q_{ij}) \cup (T_i \cap Q_{il}) \cup (T_i \cap Q_{ik})$ as shown in figure 5.3, we obtain

$$\int_{T_i} u(x,y,t^{n+2})\,d\mathcal{A} = \int_{T_i \cap Q_{ij}} u(x,y,t^{n+1})\,d\mathcal{A} + \int_{T_i \cap Q_{il}} u(x,y,t^{n+1})\,d\mathcal{A} + \tag{5.10}$$
$$\int_{T_i \cap Q_{ik}} u(x,y,t^{n+1})\,d\mathcal{A} - \int_{t^{n+1}}^{t^{n+2}} \int_{\partial T_i} \big(f(u(x,y,t))\omega_x + g(u(x,y,t))\omega_y\big)\,d\sigma\,dt\,.$$

Since the numerical solution is piecewise constant defined at the centers of the triangles T_i, we get

$$\int_{T_i} u(x,y,t^{n+2})\,d\mathcal{A} = \mathcal{A}(T_i)u_i^{n+2}\,.$$

Then equation (5.10) becomes

$$\begin{aligned}\mathcal{A}(T_i)u_i^{n+2} \;=\; & \int_{T_i \cap Q_{ij}} u(x,y,t^{n+1})\,d\mathcal{A} + \int_{T_i \cap Q_{il}} u(x,y,t^{n+1})\,d\mathcal{A} + \\ & \int_{T_i \cap Q_{ik}} u(x,y,t^{n+1})\,d\mathcal{A} - \int_{t^{n+1}}^{t^{n+2}} \int_{\partial T_i} \big(f(u(x,y,t))\omega_x + g(u(x,y,t))\omega_y\big)\,d\sigma\,dt\,.\end{aligned}$$

In addition,

$$\int_{T_i \cap Q_{ij}} u(x,y,t^{n+1})\,d\mathcal{A} = \mathcal{A}rea(T_i \cap Q_{ij})u_{ij}^{n+1} = \mathcal{A}rea(a_iG_ia_j)u_{ij}^{n+1}\,, \tag{5.11}$$

where $\mathcal{A}rea(a_iG_ia_j)$ is computed using Gauss's formula (4.3).

The integrals $\int_{T_i \cap Q_{ik}} u(x,y,t^{n+1})\, d\mathcal{A}$ and $\int_{T_i \cap Q_{il}} u(x,y,t^{n+1})\, d\mathcal{A}$ are computed similarly. We now approximate the flux integral with respect to time as follows

$$\begin{aligned} \int_{t^{n+1}}^{t^{n+2}} \int_{\partial T_i} \left(f(u(x,y,t))\omega_x + g(u(x,y,t))\omega_y \right) d\sigma\, dt \\ \cong \Delta t \int_{\partial T_i} \left(f(u(x,y,t^{n+1}))\omega_x + g(u(x,y,t^{n+1}))\omega_y \right) d\sigma\,, \end{aligned} \tag{5.12}$$

$$\text{where, } u(x,y,t^{n+1}) = \begin{cases} u_{ij}^{n+1} & \text{if (x,y)} \in Q_{ij} \\ u_{il}^{n+1} & \text{if (x,y)} \in Q_{il} \\ u_{ik}^{n+1} & \text{if (x,y)} \in Q_{ik} \end{cases}$$

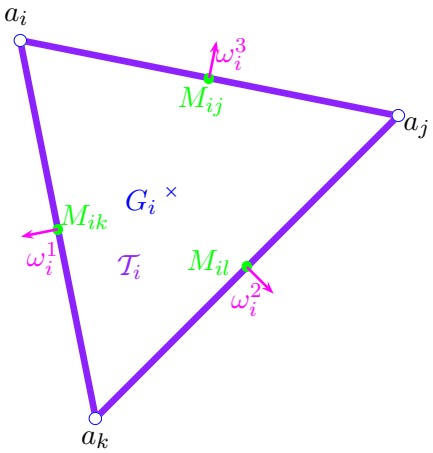

Figure 5.4: Triangular cell T_i with the unit normal vectors to ∂T_i pointing outward.

Evaluating the integral, we obtain

$$\begin{aligned} \int_{t^{n+1}}^{t^{n+2}} \int_{\partial T_i} \left(f(u(x,y,t))\omega_x + g(u(x,y,t))\omega_y \right) d\sigma\, dt \\ \cong \Delta t \Big(f(u_{ij}^{n+1})\omega_{ix}^3 |a_i a_j| + g(u_{ij}^{n+1})\omega_{iy}^3 |a_i a_j| \\ + f(u_{ik}^{n+1})\omega_{ix}^1 |a_i a_k| + g(u_{ik})^{n+1}\omega_{iy}^1 |a_i a_k| \\ + f(u_{il}^{n+1})\omega_{ix}^2 |a_j a_k| + g(u_{il}^{n+1})\omega_{iy}^2 |a_j a_k| \Big)\,, \end{aligned} \tag{5.13}$$

where ω_i^1, ω_i^2, and ω_i^3 are the normal vectors to the cell edges $a_i a_k, a_k a_j$, and $a_i a_j$ respectively pointing out of the triangular cell T_i.

Therefore, equation (5.11) becomes

$$
\begin{aligned}
u_i^{n+2} &= \frac{1}{\mathcal{A}(T_i)}\left(u_{ij}^{n+1}\mathcal{A}(T_i\cap Q_{ij}) + u_{il}^{n+1}\mathcal{A}(T_i\cap Q_{il}) + u_{ik}^{n+1}\mathcal{A}(T_i\cap Q_{ik})\right) \\
&\quad - \frac{1}{\mathcal{A}(T_i)}\Delta t\left(f(u_{ij}^{n+1})\omega_{ix}^3|a_ia_j| + g(u_i^{n+1})\omega_{iy}^3|a_ia_j| + f(u_{ik}^{n+1})\omega_{ix}^1|a_ia_k|\right. \\
&\qquad \left. + g(u_{ik})^{n+1}\omega_{iy}^1|a_ia_k| + f(u_{il}^{n+1})\omega_{ix}^2|a_ja_k| + g(u_{il}^{n+1})\omega_{iy}^2|a_ja_k|\right) ,
\end{aligned}
$$

which is the numerical solution at time t^{n+2} on the centroids of the triangular cells. Since our 2D extension of the LF scheme evolves a piecewise constant numerical solution then the solution at the cell T_i at time t^{n+2} is equal to u_i^{n+2}.

CHAPTER 6

A NESSYAHU-TADMOR TYPE SCHEME ON UNSTRUCTURED GRIDS

In chapter 4 we presented a two-dimensional extension of the Lax-Friedrichs scheme on unstructured grids that evolves a piecewise constant numerical solution on two staggered grids. In this chapter, we present a new non-oscillatory, second-order accurate central scheme. The proposed method is an extension of the central, non-oscillatory, one-dimensional finite volume method of Nessyahu and Tadmor [44]. It avoids the resolution of the Riemann problems arising at the cell interfaces by evolving the numerical solution on triangular cells at even time steps and on staggered quadrilateral dual cells at odd time steps.

We have adopted two types of piecewise linear cell interpolants. The first one is based on the minimum angle plane reconstruction MAPR [14] founded on a selection of an interpolation stencil yielding a linear reconstruction of the solution on a certain cell, given the values on the centers of this cell and the centers of its neighboring cells. The second is based on least squares gradients combined with a slope limiting procedure. We have tested three different slope limiters: the van Leer slope limiter [2], Barth and Jespersen slope limiter [43; 9] and the Venkatakrishnan slope limiter [43]. Piecewise linear reconstructions ensure spatial second-order of accuracy. Temporal second-order of accuracy is ensured using the midpoint quadrature rule.

This chapter is organized as follows: First, the derivation of the numerical scheme is described. Then, we explain how we computed the limited gradients.

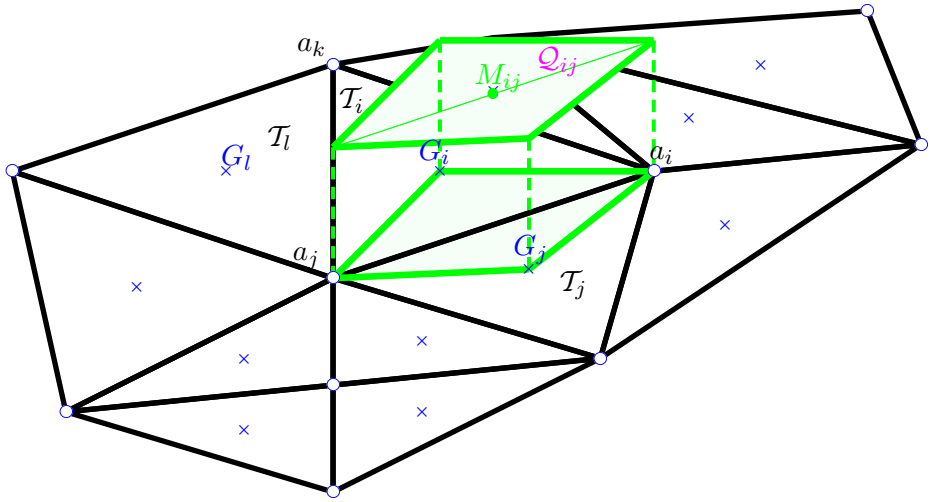

Figure 6.1: Triangular cells T_i and T_j and the quadrilateral cell $a_i G_i a_j G_j$.

As in chapter 5, the domain $\Omega \subseteq \mathbb{R}^2$ is discretized using a finite element triangulation. The control cells of the original grid associated with our finite volume extension of the Nessyahu-Tadmor scheme are the triangles T_i of $\mathcal{T}_h$ and the cell average solution at even time steps will be defined at the centroids G_i of T_i, while the cells of the staggered dual grid are the quadrilaterals Q_{ij} (as described in chapter 4) and the cell average solution at odd time steps will be defined at the midpoints M_{ij} of the sides $a_i a_j$ of the triangulation.

Let the two-dimensional scalar conservation law

$$u_t + \frac{\partial}{\partial x} f(u) + \frac{\partial}{\partial y} g(u) = 0 \,, \qquad \text{for } t > 0 \,,\ (x, y) \in \Omega \tag{6.1}$$

with initial condition

$$u(x, y, 0) = u_0(x, y) \,.$$

As in the original NT scheme [44] and in its multi-dimensional extensions [2; 35; 14; 6; 3; 26; 27; 42], the method we propose evolves a piecewise linear numerical solution on two staggered grids.

The solution on the triangular cell T_i at time t^n is approximated by the linear interpolant:

$$L_i(x, y, t^n) = u_i^n + (x - x_{G_i})P_{i_x}^n + (y - y_{G_i})P_{i_y}^n \,, \tag{6.2}$$

where, $\left(P_{i_x}^n, P_{i_y}^n\right) \simeq \nabla u_i^n$ denotes the limited numerical gradient evaluated at G_i. The solution on the quadrilateral cell Q_{ij} at time t^{n+1} is approximated by the linear interpolant:

$$L_{ij}(x, y, t^{n+1}) = u_{ij}^{n+1} + (x - x_{M_{ij}})P_{ij_x}^{n+1} + (y - y_{M_{ij}})P_{ij_y}^{n+1} \,, \tag{6.3}$$

where, $(P_{ij_x}^{n+1}, P_{ij_y}^{n+1}) \simeq \nabla u_{ij}^{n+1}$ denotes the limited numerical gradient evaluated at M_{ij}.

We assume that the solution is known at time $t = t^n$ on the triangular cells T_i and is defined at the centroids G_i, i.e.

$$u_i^n = \frac{1}{\mathcal{A}(T_i)} \int_{T_i} L_i(x, y, t^n)\, d\mathcal{A} \,.$$

Integrating equation (6.1) over the volume $Q_{ij} \times [t^n, t^{n+1}]$,

$$\int_{t^n}^{t^{n+1}} \int_{Q_{ij}} \left(u_t + \frac{\partial}{\partial x} f(u) + \frac{\partial}{\partial y} g(u) \right) d\mathcal{A}\, dt = 0 \,, \tag{6.4}$$

and applying the divergence theorem to the spatial integral, we get

$$\begin{aligned} \int_{Q_{ij}} u(x, y, t^{n+1})\, d\mathcal{A} \;\; - \;\; & \int_{Q_{ij}} u(x, y, t^n)\, d\mathcal{A} \\ + \;\; & \int_{t^n}^{t^{n+1}} \int_{\partial Q_{ij}} \left(f(u(x, y, t))\nu_x + g(u(x, y, t))\nu_y \right) d\sigma\, dt = 0 \,, \end{aligned}$$

where ∂Q_{ij} denotes the boundary of Q_{ij} and $\nu = (\nu_x, \nu_y)$ denotes the unit outer normal vector to ∂Q_{ij}.

Since

$$Q_{ij} = (Q_{ij} \cap T_i) \cup (Q_{ij} \cap T_j) \,,$$

then,

$$\int_{Q_{ij}} u(x, y, t^n)\, d\mathcal{A} = \int_{Q_{ij} \cap T_i} u(x, y, t^n)\, d\mathcal{A} + \int_{Q_{ij} \cap T_j} u(x, y, t^n)\, d\mathcal{A} \,.$$

Equation (6.4) becomes

$$\begin{aligned} \int_{Q_{ij}} u(x, y, t^{n+1})\, d\mathcal{A} \;\; &= \;\; \int_{Q_{ij} \cap T_i} u(x, y, t^n)\, d\mathcal{A} + \int_{Q_{ij} \cap T_j} u(x, y, t^n)\, d\mathcal{A} \\ &\quad - \int_{t^n}^{t^{n+1}} \int_{\partial Q_{ij}} \left(f(u(x, y, t))\nu_x + g(u(x, y, t))\nu_y \right) d\sigma\, dt \,. \end{aligned} \tag{6.5}$$

Note that

$$\int_{Q_{ij}} u(x, y, t^{n+1})\, d\mathcal{A} = \mathcal{A}(Q_{ij}) u_{ij}^{n+1}.$$

Hence equation (6.5) becomes

$$\begin{aligned} \mathcal{A}(Q_{ij}) u_{ij}^{n+1} \;\; &= \;\; \int_{Q_{ij} \cap T_i} u(x, y, t^n)\, d\mathcal{A} + \int_{Q_{ij} \cap T_j} u(x, y, t^n)\, d\mathcal{A} \\ &\quad - \int_{t^n}^{t^{n+1}} \int_{\partial Q_{ij}} \left(f(u(x, y, t))\nu_x + g(u(x, y, t))\nu_y \right) d\sigma\, dt \,. \end{aligned} \tag{6.6}$$

In addition, since $L_i(x, y, t^n)$ is the piecewise linear reconstruction of the solution at time t^n defined on cell T_i by equation (6.2), then

$$\int_{Q_{ij} \cap T_i} u(x, y, t^n)\, d\mathcal{A} = \int_{Q_{ij} \cap T_i} L_i(x, y, t^n)\, d\mathcal{A} \,.$$

Let A_i, B_i and A_j be the function values of $L_i(x, y, t^n)$ obtained at the vertices of the triangle T_i i.e. $A_i = L_i(x_i, y_i, t^n)$, $A_j = L_i(x_j, y_j, t^n)$ and $B_i = L_i(x_{G_i}, y_{G_i}, t^n)$. The integral of $u(x, y, t^n)$ on $Q_{ij} \cap T_i$ is equal to the volume of the triangular prism with triangular base $a_i G_i a_j$:

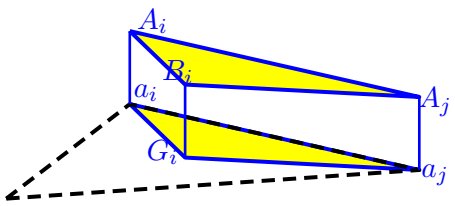

Figure 6.2: Prismatic regions for the computation of $\int_{Q_{ij}\cap T_i} u(x,y,t^n)\,dA$

$$
\begin{aligned}
&\int_{Q_{ij}\cap T_i} u(x,y,t^n)\,d\mathcal{A} \\
&\quad = \; vol(a_iG_ia_jA_iB_iA_j) \\
&\quad = \; \frac{1}{3}\mathcal{A}rea(a_iG_ia_j)\times\big(a_iA_i+G_iB_i+a_jA_j\big) \\
&\quad = \; \frac{1}{3}\mathcal{A}rea(a_iG_ia_j)\times\big(u_i^n+(x_i-x_{G_i})P_{ix}^n+(y_i-y_{G_i})P_{iy}^n \\
&\qquad\qquad\qquad +u_i^n+(x_{G_i}-x_{G_i})P_{ix}^n+(y_{G_i}-y_{G_i})P_{iy}^n \\
&\qquad\qquad\qquad +u_i^n+(x_j-x_{G_i})P_{ix}^n+(y_j-y_{G_i})P_{iy}^n\big) \\
&\quad = \; \frac{1}{3}\mathcal{A}rea(a_iG_ia_j)\times\Big(3u_i^n+(x_i+x_j-2x_{G_i})P_{ix}^n+(y_i+y_j-2y_{G_i})P_{iy}^n\Big)\;,
\end{aligned}
$$

In a similar way, the integral $\int_{Q_{ij}\cap T_j} u(x,y,t^n)\,d\mathcal{A}$ is computed.

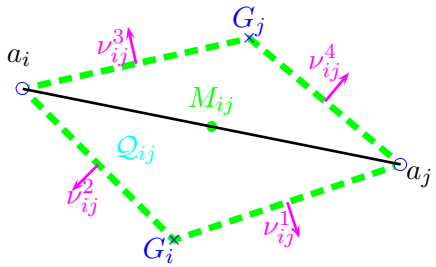

Figure 6.3: Quadrilateral cell $\mathcal{Q}_{ij} = a_iG_ia_jG_j$ with the normal vectors to its sides

Applying the midpoint quadrature rule to the flux time integral, we get

$$
\begin{aligned}
&\int_{t^n}^{t^{n+1}}\int_{\partial Q_{ij}}\big(f(u(x,y,t))\nu_x+g(u(x,y,t))\nu_y\big)\;d\sigma\,dt \\
&\qquad\cong\;\Delta t\int_{\partial Q_{ij}}\big(f(u(x,y,t^{n+1/2}))\nu_x+g(u(x,y,t^{n+1/2}))\nu_y\big)\,d\sigma\;. \qquad (6.7)
\end{aligned}
$$

We use a first-order Taylor series expansion and the conservation law (6.1) to approximate $u(x, y, t^{n+1/2})$, which becomes

$$u(x,y,t^{n+1/2}) \cong u(x,y,t^n) - \frac{\Delta t}{2}\left(f_u\left(u\left(x,y,t^n\right)\right)u_x\left(x,y,t^n\right) + g_u\left(u\left(x,y,t^n\right)\right)u_y\left(x,y,t^n\right)\right) . \tag{6.8}$$

Recall that $\nabla u_i^n \cong \left(P_{ix}^n, P_{iy}^n\right)$ and $u(x,y,t^n) = \begin{cases} L_i(x,y,t^n) & \text{if (x,y)} \in T_i \\ L_j(x,y,t^n) & \text{if (x,y)} \in T_j \end{cases}$

Since we want to approximate the integrals over the boundary of the quadrilateral cell Q_{ij}, then we need to find an approximate value of $u(x, y, t^n)$ on the line segments a_iG_i, a_iG_j, a_jG_j and G_ia_j.

One possibility is to choose the value of the linear interpolants $L_i(x, y, t^n)$ and $L_j(x, y, t^n)$ at the midpoints of these segments.

We then take for any (x,y) on a_iG_i

$$\begin{aligned} u_{a_iG_i}^n &\cong u_i^n + \left(\left(\frac{x_i + x_{G_i}}{2}\right) - x_{G_i}\right)P_{ix}^n + \left(\left(\frac{y_i + y_{G_i}}{2}\right) - y_{G_i}\right)P_{iy}^n \\ &\cong u_i^n + \frac{1}{2}(x_i - x_{G_i})P_{ix}^n + \frac{1}{2}(y_i - y_{G_i})P_{iy}^n , \end{aligned}$$

with similar estimates for $u_{G_ia_j}^n$, $u_{a_jG_j}^n$ and $u_{G_ja_i}^n$.

In view of equation(6.8), we approximate $u(x, y, t^{n+1/2})$ as follows:

$$\mathrm{u(x,y,}t^{n+1/2}) = \begin{cases} u^n_{a_iG_i} - \frac{\Delta t}{2}\left(f_u(u^n_{a_iG_i})P^n_{ix} + g_u(u^n_{a_iG_i})P^n_{iy}\right) & \text{along } a_iG_i \\ u^n_{G_ia_j} - \frac{\Delta t}{2}\left(f_u(u^n_{G_ia_j})P^n_{ix} + g_u(u^n_{G_ia_j})P^n_{iy}\right) & \text{along } G_ia_j \\ u^n_{a_jG_j} - \frac{\Delta t}{2}\left(f_u(u^n_{a_jG_j})P^n_{jx} + g_u(u^n_{a_jG_j})P^n_{jy}\right) & \text{along } a_jG_j \\ u^n_{G_ja_i} - \frac{\Delta t}{2}\left(f_u(u^n_{G_ja_i})P^n_{jx} + g_u(u^n_{G_ja_i})P^n_{jy}\right) & \text{along } G_ja_i \end{cases}$$

Let :

- $u^{n+1/2}_{a_iG_i}$ approximates the value of u(x,y,$t^{n+1/2}$) along a_iG_i,
- $u^{n+1/2}_{a_jG_i}$ approximates the value of u(x,y,$t^{n+1/2}$) along a_jG_i,
- $u^{n+1/2}_{a_iG_j}$ approximates the value of u(x,y,$t^{n+1/2}$) along a_iG_j, and
- $u^{n+1/2}_{a_jG_j}$ approximates the value of u(x,y,$t^{n+1/2}$) along a_jG_j .

We substitute these values in equation (6.7) and note that ν^1_{ij}, ν^2_{ij}, ν^3_{ij} and ν^4_{ij} are the outer unit normal vectors to the cell edges a_jG_i, a_iG_i, a_iG_j, and a_jG_j, respectively. We finally get

$$\begin{aligned} \int_{t^n}^{t^{n+1}} \int_{\partial Q_{ij}} & \left(f(u(x,y,t))\nu_x + g(u(x,y,t))\nu_y\right)\, d\sigma\, dt \\ & \cong \Delta t \Big(f(u^{n+1/2}_{a_jG_i})\nu^1_{ij_x}|a_jG_i| + f(u^{n+1/2}_{a_iG_i})\nu^2_{ij_x}|a_iG_i| \\ & \quad + g(u^{n+1/2}_{a_jG_i})\nu^1_{ij_y}|a_jG_i| + g(u^{n+1/2}_{a_iG_i})\nu^2_{ij_y}|a_iG_i| \\ & \quad + f(u^{n+1/2}_{a_iG_j})\nu^3_{ij_x}|a_iG_j| + f(u^{n+1/2}_{a_jG_j})\nu^4_{ij_x}|a_jG_j| \\ & \quad + g(u^{n+1/2}_{a_iG_j})\nu^3_{ij_y}|a_iG_j| + g(u^{n+1/2}_{a_jG_j})\nu^4_{ij_y}|a_jG_j|\Big) \ . \end{aligned} \tag{6.9}$$

In view of (6.7) and (6.9), equation (6.6) becomes

$$
\begin{aligned}
u_{ij}^{n+1} \;=\; & \frac{1}{\mathcal{A}(Q_{ij})}\mathcal{A}(Q_{ij}\cap T_i) \\
& \qquad \times \left(u_i^n + \frac{1}{3}(x_i + x_j - 2x_{G_i})P_{i_x}^n + \frac{1}{3}(y_i + y_j - 2y_{G_i})P_{i_y}^n \right) \\
& + \frac{1}{\mathcal{A}(Q_{ij})}\mathcal{A}(Q_{ij}\cap T_j) \\
& \qquad \times \left(u_j^n + \frac{1}{3}(x_i + x_j - 2x_{G_j})P_{j_x}^n + \frac{1}{3}(y_i + y_j - 2y_{G_j})P_{j_y}^n \right) \\
& - \frac{1}{\mathcal{A}(Q_{ij})}\Delta t \, \Big(f(u_{a_jG_i}^{n+1/2})\nu_{ij_x}^1 |a_jG_i| + f(u_{a_iG_i}^{n+1/2})\nu_{ij_x}^2 |a_iG_i| \\
& \qquad\qquad + g(u_{a_jG_i}^{n+1/2})\nu_{ij_y}^1 |a_jG_i| + g(u_{a_iG_i}^{n+1/2})\nu_{ij_y}^2 |a_iG_i| \\
& \qquad\qquad + f(u_{a_iG_j}^{n+1/2})\nu_{ij_x}^3 |a_iG_j| + f(u_{a_jG_j}^{n+1/2})\nu_{ij_x}^4 |a_jG_j| \\
& \qquad\qquad + g(u_{a_iG_j}^{n+1/2})\nu_{ij_y}^3 |a_iG_j| + g(u_{a_jG_j}^{n+1/2})\nu_{ij_y}^4 |a_jG_j| \Big) \;,
\end{aligned}
$$

We now construct the solution at time t^{n+2} on the triangular cells T_i by following the same strategy as in the first time step.

We integrate equation (6.1) over the volume $T_i \times [t^{n+1}, t^{n+2}]$ assuming that the solution at the quadrilateral cell Q_{ij} is known at time t^{n+1} as a piecewise linear solution, and is defined at the points M_{ij}.

Green's divergence formula yields

$$
\begin{aligned}
\int_{T_i} u(x,y,t^{n+2})\, d\mathcal{A} \;-\; & \int_{T_i} u(x,y,t^{n+1})\, d\mathcal{A} + \\
& \int_{t^{n+1}}^{t^{n+2}} \int_{\partial T_i} \big(f(u(x,y,t))\omega_x + g(u(x,y,t))\omega_y \big)\, d\sigma\, dt = 0 \,. \qquad (6.10)
\end{aligned}
$$

Note that $T_i = (T_i \cap Q_{ij}) \cup (T_i \cap Q_{il}) \cup (T_i \cap Q_{ik})$, hence equation (6.10) becomes

$$
\begin{aligned}
\int_{T_i} u(x,y,t^{n+2})\, d\mathcal{A} = & \int_{T_i\cap Q_{ij}} u(x,y,t^{n+1})\, d\mathcal{A} + \int_{T_i\cap Q_{il}} u(x,y,t^{n+1})\, d\mathcal{A} \qquad (6.11) \\
& + \int_{T_i\cap Q_{ik}} u(x,y,t^{n+1})\, d\mathcal{A} - \int_{t^{n+1}}^{t^{n+2}} \int_{\partial T_i} \big(f(u(x,y,t))\omega_x + g(u(x,y,t))\omega_y \big)\, d\sigma\, dt \,.
\end{aligned}
$$

Since $u(x, y, t^{n+2})$ is a piecewise linear solution defined at the cell centers, then

$$\int_{T_i} u(x, y, t^{n+2})\, d\mathcal{A} = \int_{T_i} L_i(x, y, t^{n+2})\, d\mathcal{A} = \mathcal{A}(T_i) u_i^{n+2} \,.$$

Equation (6.11) becomes

$$\mathcal{A}(T_i) u_i^{n+2} = \int_{T_i \cap Q_{ij}} u(x, y, t^{n+1})\, d\mathcal{A} + \int_{T_i \cap Q_{il}} u(x, y, t^{n+1})\, d\mathcal{A} \tag{6.12}$$
$$+ \int_{T_i \cap Q_{ik}} u(x, y, t^{n+1})\, d\mathcal{A} - \int_{t^{n+1}}^{t^{n+2}} \int_{\partial T_i} \left(f(u(x, y, t))\omega_x + g(u(x, y, t))\omega_y \right)\, d\sigma\, dt \,.$$

In addition, $L_{ij}(x, y, t^{n+1})$ is the piecewise linear function defined on the cell Q_{ij} by equation (6.3).

Let A_i, B_i, and A_j be the linear interpolant $L_{ij}(x, y, t^{n+1})$ values on Q_{ij} obtained on the three vertices of $T_i \cap Q_{ij} = (a_i G_i a_j)$, respectively,

i.e. $A_i = L_{ij}(x_i, y_i, t^{n+1})$, $A_j = L_{ij}(x_j, y_j, t^{n+1})$ and $B_i = L_{ij}(x_{G_i}, y_{G_i}, t^{n+1})$.

The double integral of u(x,y,t^{n+1}) on $T_i \cap Q_{ij}$ is equal to the volume of the triangular prism with triangular base $(a_i G_i a_j)$.

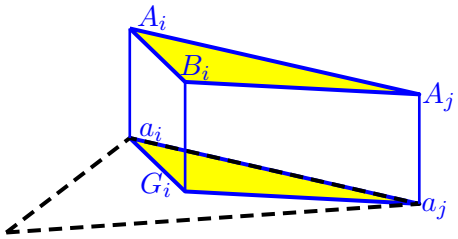

Figure 6.4: Prismatic regions for the computation of $\int_{T_i \cap Q_{ij}} u(x, y, t^{n+1})\, dA$

$$
\begin{aligned}
&\int_{T_i \cap Q_{ij}} u(x,y,t^{n+1})\, d\mathcal{A} \\
&\quad = \; vol(a_i G_i a_j A_i A_j B_i) \\
&\quad = \; \mathcal{A}rea(a_i G_i a_j) \times \left(\frac{a_i A_i + G_i B_i + a_j A_j}{3} \right) \\
&\quad = \; \frac{1}{3} \mathcal{A}rea(a_i G_i a_j) \times (u_{ij}^{n+1} + (x_i - x_{M_{ij}}) P_{ij_x}^{n+1} + (y_i - y_{M_{ij}}) P_{ij_y}^{n+1} \\
&\qquad\qquad\qquad\qquad u_{ij}^{n+1} + (x_{G_i} - x_{M_{ij}}) P_{ij_x}^{n+1} + (y_{G_i} - y_{M_{ij}}) P_{ij_y}^{n+1} \\
&\qquad\qquad\qquad\qquad u_{ij}^{n+1} + (x_j - x_{M_{ij}}) P_{ij_x}^{n+1} + (y_j - y_{M_{ij}}) P_{ij_y}^{n+1}) \\
&\quad = \; \frac{1}{3} \mathcal{A}rea(a_i G_i a_j) \\
&\qquad \times \left(3u_{ij}^{n+1} + (x_i + x_{G_i} + x_j - 3x_{M_{ij}}) P_{ij_x}^{n+1} + (y_i + y_{G_i} + y_j - 3y_{M_{ij}}) P_{ij_y}^{n+1} \right) \\
&\quad = \; \frac{1}{3} \mathcal{A}rea(a_i G_i a_j) \times \left(3u_{ij}^{n+1} + (x_{G_i} - x_{M_{ij}}) P_{ij_x}^{n+1} + (y_{G_i} - y_{M_{ij}}) P_{ij_y}^{n+1} \right) \quad (6.13)
\end{aligned}
$$

$\int_{T_i \cap Q_{ik}} u(x,y,t^{n+1})\, d\mathcal{A}$ and $\int_{T_i \cap Q_{il}} u(x,y,t^{n+1})\, d\mathcal{A}$ are computed similarly.

Applying the midpoint quadrature rule to the flux integral with respect to time we obtain

$$
\begin{aligned}
&\int_{t^{n+1}}^{t^{n+2}} \int_{\partial T_i} \left(f(u(x,y,t))\omega_x + g(u(x,y,t))\omega_y \right) d\sigma\, dt \\
&\qquad \cong \; \Delta t \int_{\partial T_i} \left(f(u(x,y,t^{n+3/2}))\omega_x + g(u(x,y,t^{n+3/2}))\omega_y \right) d\sigma\,. \qquad (6.14)
\end{aligned}
$$

Again, we use a first-order Taylor series expansion and the conservation law (6.1) to approximate $u(x,y,t^{n+3/2})$, we get

$$
\begin{aligned}
u(x,y,t^{n+3/2}) \cong u(x,y,t^{n+1}) - \qquad\qquad\qquad\qquad\qquad\qquad (6.15) \\
\frac{\Delta t}{2} \left(f_u(u(x,y,t^{n+1}))u_x(x,y,t^{n+1}) + g_u(u(x,y,t^{n+1}))u_y(x,y,t^{n+1}) \right)\,.
\end{aligned}
$$

Note that:

- on Q_{ij}(and thus on $Q_{ij} \cap T_i$) we have chosen $u_x(x, y, t^{n+1}) = P_{ij_x}^{n+1}$ and $u_y(x, y, t^{n+1}) = P_{ij_y}^{n+1}$,
- on Q_{il}(and thus on $Q_{il} \cap T_i$) we have chosen $u_x(x, y, t^{n+1}) = P_{il_x}^{n+1}$ and $u_y(x, y, t^{n+1}) = P_{il_y}^{n+1}$, and
- on Q_{ik}(and thus on $Q_{ik} \cap T_i$) we have chosen $u_x(x, y, t^{n+1}) = P_{ik_x}^{n+1}$ and $u_y(x, y, t^{n+1}) = P_{ik_y}^{n+1}$.

$$\text{and } u(x, y, t^{n+1}) = \begin{cases} L_{ij}(x, y, t^{n+1}) & \text{if (x,y)} \in Q_{ij} \\ L_{il}(x, y, t^{n+1}) & \text{if (x,y)} \in Q_{il} \\ L_{ik}(x, y, t^{n+1}) & \text{if (x,y)} \in Q_{ik} \end{cases}$$

Since we want to estimate the integrals over the boundary of the triangle T_i, then we need to find an approximate value of $u(x, y, t^{n+1})$ on the line segments $a_i a_k$, $a_i a_j$, and $a_j a_k$. One possible choice consists of choosing the values of the linear interpolants $L_{ij}(x, y, t^{n+1})$, $L_{jk}(x, y, t^{n+1})$ and $L_{ik}(x, y, t^{n+1})$ at the midpoints of their corresponding segments.

We then take for any (x, y) on $a_i a_j$: $\quad u(x, y, t^{n+1}) \cong u_{a_i a_j}^{n+1} \cong u_{ij}^{n+1}$.

The numerical solutions on $a_i a_k$ and $a_j a_k$ at time t^{n+1} are defined similarly.

From these equations and in view of equation(6.15), we approximate $u(x, y, t^{n+3/2})$ as follows:

$$\text{u(x,y,}t^{n+3/2}) = \begin{cases} u_{a_i a_j}^{n+1} - \frac{\Delta t}{2}\left(f_u(u_{a_i a_j}^{n+1}) P_{ij_x}^{n+1} + g_u(u_{a_i a_j}^{n+1}) P_{ij_y}^{n+1}\right) & \text{along } a_i a_j \\ u_{a_i a_k}^{n+1} - \frac{\Delta t}{2}\left(f_u(u_{a_i a_k}^{n+1}) P_{il_x}^{n+1} + g_u(u_{a_i a_k}^{n+1}) P_{il_y}^{n+1}\right) & \text{along } a_i a_k \\ u_{a_j a_k}^{n+1} - \frac{\Delta t}{2}\left(f_u(u_{a_j a_k}^{n+1}) P_{ik_x}^{n+1} + g_u(u_{a_j a_k}^{n+1}) P_{ik_y}^{n+1}\right) & \text{along } a_j a_k \end{cases}$$

Let :

- $u_{a_i a_j}^{n+3/2}$ denote the value of u(x,y,$t^{n+3/2}$) along $a_i a_j$,
- $u_{a_i a_k}^{n+3/2}$ denote the value of u(x,y,$t^{n+3/2}$) along $a_i a_k$, and
- $u_{a_j a_k}^{n+3/2}$ denote the value of u(x,y,$t^{n+3/2}$) along $a_j a_k$.

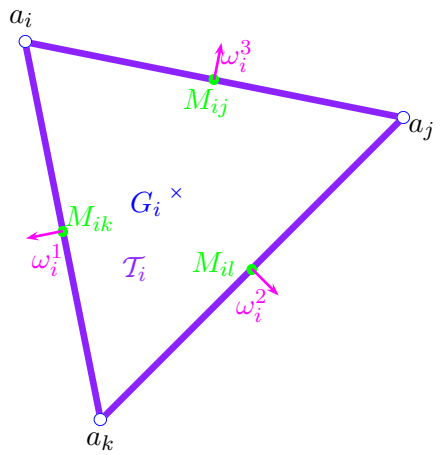

Figure 6.5: Triangular cell T_i with the normal vectors to its sides

We substitute these values in equation (6.14) and note that ω_i^1, ω_i^2, and ω_i^3 are the unit outer normal vectors to the cell edges $a_i a_k, a_k a_j, a_i a_j$, respectively. We finally obtain

$$\begin{aligned}
&\int_{t^{n+1}}^{t^{n+2}} \int_{\partial T_i} \left(f(u(x,y,t))\omega_x + g(u(x,y,t))\omega_y \right) \, d\sigma \, dt \\
&\qquad \cong \quad \Delta t \Big(f(u_{a_i a_k}^{n+3/2})\omega_{i_x}^1 |a_i a_k| + f(u_{a_k a_j}^{n+3/2})\omega_{i_x}^2 |a_k a_j| \\
&\qquad\qquad + g(u_{a_i a_k}^{n+3/2})\omega_{i_y}^1 |a_i a_k| + g(u_{a_k a_j}^{n+3/2})\omega_{i_y}^2 |a_k a_j| \\
&\qquad\qquad + f(u_{a_i a_j}^{n+3/2})\omega_{i_x}^3 |a_i a_j| + g(u_{a_i a_j}^{n+3/2})\omega_{i_y}^3 |a_i a_j| \Big) \, . \qquad (6.16)
\end{aligned}$$

In view of equations (6.13) and (6.16), equation (6.12) becomes

$$
\begin{aligned}
u_i^{n+2} &= \frac{1}{\mathcal{A}(T_i)}\mathcal{A}(T_i \cap Q_{ij}) \\
&\qquad \times \left(u_{ij}^{n+1} + \frac{1}{3}(x_{G_i} - x_{M_{ij}})P_{ij_x}^{n+1} + \frac{1}{3}(y_{G_i} - y_{M_{ij}})P_{ij_y}^{n+1} \right) \\
&+ \frac{1}{\mathcal{A}(T_i)}\mathcal{A}(T_i \cap Q_{il}) \\
&\qquad \times \left(u_{il}^{n+1} + \frac{1}{3}(x_{G_i} - x_{M_{il}})P_{il_x}^{n+1} + \frac{1}{3}(y_{G_i} - y_{M_{il}})P_{il_y}^{n+1} \right) \\
&+ \frac{1}{\mathcal{A}(T_i)}\mathcal{A}(T_i \cap Q_{ik}) \\
&\qquad \times \left(u_{ik}^{n+1} + \frac{1}{3}(x_{G_i} - x_{M_{ik}})P_{ik_x}^{n+1} + \frac{1}{3}(y_{G_i} - y_{M_{ik}})P_{ik_y}^{n+1} \right) \\
&- \frac{1}{\mathcal{A}(T_i)}\Delta t(f(u_{a_i a_k}^{n+3/2})\omega_{i_x}^1 |a_i a_k| + f(u_{a_k a_j}^{n+3/2})\omega_{i_x}^2 |a_k a_j| \\
&\qquad\qquad + g(u_{a_i a_k}^{n+3/2})\omega_{i_y}^1 |a_i a_k| + g(u_{a_k a_j}^{n+3/2})\omega_{i_y}^2 |a_k a_j| \\
&\qquad\qquad + f(u_{a_i a_j}^{n+3/2})\omega_{i_x}^3 |a_i a_j| + g(u_{a_i a_j}^{n+3/2})\omega_{i_y}^3 |a_i a_j|) \,, \qquad (6.17)
\end{aligned}
$$

6.1 Linear interpolants reconstruction

In general, the reconstruction of the piecewise linear approximation from the values obtained at the centers of the control volumes (triangles or quadrilateral) depends mainly on the system at hand since it involves a computation of the jacobian of the flux vector. In this thesis we considered different gradients and slope limiters to construct the linear interpolants.

6.1.1 Minimum Angle Plane reconstruction

The minimum angle plane reconstruction MAPR [14] is based on the selection of an interpolation stencil yielding a linear reconstruction of the solution from its cell averages with minimal angle with respect to the horizontal.

Remark 3 *The gradient* $\nabla u_i^n \approx \left(P_{ix}^n, P_{iy}^n\right)$ *uniquely determines each linear interpolant.*

Numerical results are presented in the following chapter for both hyperbolic systems of conservation laws with convex and non convex flux functions. Also it will be shown that the MAPR is able to capture composite waves accurately. Composite waves consist of joined rarefaction and shock waves. A generic case is a shock adjacent to a rarefaction wave.

Consider an element of the original grid T_i with its triangle neighbors, which we define as the elements of the original grid sharing an edge with T_i. Note that T_i may have one, two, or three neighbors, which we denote by T_j, T_k, and T_l.
Therefore we have three cases to consider:

- T_i has only two neighbors (i.e. one of T_i's edges lie on $\partial\Omega$) then only one plane can be constructed and it is therefore the minimum angle plane.

- T_i has only one neighbor, T_j (i.e. two of T_i's edges lie on $\partial\Omega$). T_j has two further neighbors: T_{j_1} and T_{j_2}. Due to the lack of information at the boundaries, we consider T_j, T_{j_1} and T_{j_2} as the three neighbors of T_i. From these defined neighbors we can then construct four planes and then choose the minimum angle plane.

- T_i has three neighbors. We begin the minimum angle plane construction by defining the four planes that pass through the images of the centroids on the plane with the third component being the numerical approximation of the solution at time t^n obtained at the centroids of the triangular cells.

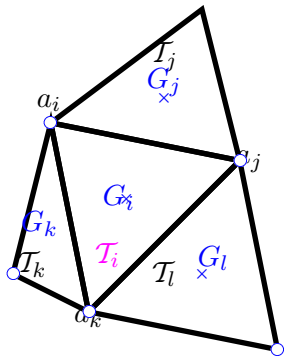

– **Plane 1**: passing through $(x_{G_i}, y_{G_i}, u_i^n)$, $(x_{G_j}, y_{G_j}, u_j^n)$, and $(x_{G_k}, y_{G_k}, u_k^n)$

Define A, B, C, and D as follows:

$$\begin{aligned}
A &= y_{G_i}\left(u_j^n - u_k^n\right) + y_{G_j}\left(u_k^n - u_i^n\right) + y_{G_k}\left(u_i^n - u_j^n\right) \\
B &= u_i^n\left(x_{G_j} - x_{G_k}\right) + u_j^n\left(x_{G_k} - x_{G_i}\right) + u_k^n\left(x_{G_i} - x_{G_j}\right) \\
C &= x_{G_i}\left(y_{G_j} - y_{G_k}\right) + x_{G_j}\left(y_{G_k} - y_{G_i}\right) + x_{G_k}\left(y_{G_i} - y_{G_j}\right) \\
D &= -Ax_{G_i} - By_{G_i} - Cu_i^n
\end{aligned}$$

Therefore the equation of the plane is given by:

$$z = f(x, y) = -\frac{A}{C}x - \frac{B}{C}y - \frac{D}{C}$$

Similar strategy will lead to the equations of:

– **Plane 2**: passing through $(x_{G_i}, y_{G_i}, u_i^n)$, $(x_{G_j}, y_{G_j}, u_j^n)$, and $(x_{G_l}, y_{G_l}, u_l^n)$,

– **Plane 3**: passing through $(x_{G_i}, y_{G_i}, u_i^n)$, $(x_{G_l}, y_{G_l}, u_l^n)$, and $(x_{G_k}, y_{G_k}, u_k^n)$, and

– **Plane 4**: passing through $(x_{G_l}, y_{G_l}, u_l^n)$, $(x_{G_j}, y_{G_j}, u_j^n)$, and $(x_{G_k}, y_{G_k}, u_k^n)$.

Upon the construction of the four possible planes, we set ∇u_i^n using the gradient of the plane that gives the smallest angle with the horizontal. The angle is always corrected to the first quadrant because the orientation of the plane does not matter. That is, let $v = (v_x, v_y, v_z)$ denote the unit normal vector for any of the above

planes. The normal vector is given by $v = (A, B, C)$.

Another method of computing the normal vector without constructing the planes is as follows: Denote by P_1, P_2, and P_3 the vectors from the origin of $\mathbb{R}^3$ to the three points defining the plane then,

$$v = \frac{(P_3 - P_1) \times (P_2 - P_1)}{\|(P_3 - P_1) \times (P_2 - P_1)\|} \tag{6.18}$$

where $\times$ denotes the cross or vector product and $\|.\|$ denotes the usual Euclidean norm over $\mathbb{R}^3$.

The angle of this plane with respect to the horizontal is given by [14]:

$$\theta = \begin{cases} \arccos(v_z) & \arccos(v_z) \leq \frac{\pi}{2} \\ \pi - \arccos(v_z) & \text{else} \end{cases}$$

Once we find the minimum angle plane over some T_i at $t = t^n$ and its unit normal vector v then the limited gradient evaluated at the centroid of T_i is given by:

$$\nabla L_i^n = \begin{cases} -\left(\frac{v_x}{v_z}, \frac{v_y}{v_z}\right)^T & (v_z) > \varepsilon \\ (0,0)^T & \text{else} \end{cases}$$

Note that the second case prevents the selection of a vertical minimum angle plane. The tolerance ε can be taken to be the machine accuracy.

Consider an element of the staggered grid Q_{ij} with its neighbors which we define as the elements of the staggered grid sharing an edge with Q_{ij}. Q_{ij} may have one, two, three, or four neighbors.

- If Q_{ij} has only 2 neighbors then only one plane can be constructed and is therefore the minimum angle plane.

- If Q_{ij} has more than 2 neighbors then we begin the minimum angle plane construction by defining the planes that pass through $\left(x_{M_{ij}}, y_{M_{ij}}, u_{ij}^{n+1}\right)$ and the corresponding points of the neighboring quadrilaterals.

Then we define the normal vectors to the planes and compute the gradients ∇u_{ij}^{n+1} using the same strategy used for computing ∇u_i^n.

6.1.2 Least squares gradient method

Let T_i be a triangle with centroid G_i and let T_j $(j = 1, 2, 3)$ be the neighboring triangles to T_i (sharing a common side with T_i), with centroids G_j.

Note by u_j^n the values of the numerical solution at the centroids of the neighboring triangles T_j.

Assume that the solution is known at the centers of the four triangles. Suppose a linear reconstruction:

$$u(x_M, y_M, t^n) \approx L_i(x_M, y_M, t^n) = u_i^n + \nabla u_i^n \overrightarrow{G_i M}, \quad \text{where } \overrightarrow{G_i M} = \begin{pmatrix} x_M - x_{G_i} \\ y_M - y_{G_i} \end{pmatrix}.$$

We want to minimize the sum of squares of the difference in the solution between the triangle T_i and its neighbors [2]; i.e. the least squares gradient $\nabla u_i^n = (P_i^n, Q_i^n)$ for triangle T_i will be chosen such as to minimize the functional:

$$I = \sum_{j=1}^{3} \left\{ u_i^n - u_j^n + \nabla u_i^n \overrightarrow{G_i G_j} \right\}^2 \qquad \text{where } \overrightarrow{G_i G_j} = \begin{pmatrix} x_{G_j} - x_{G_i} \\ y_{G_j} - y_{G_i} \end{pmatrix}.$$

The minimum is obtained when

$$\frac{\partial I}{\partial P_i^n} = \frac{\partial I}{\partial Q_i^n} = 0\,.$$

Deriving I with respect to P_i^n and Q_i^n, we get the following system:

$$\sum_{j \in N_i} \begin{pmatrix} \Delta x^2 & \Delta x \Delta y \\ \Delta y \Delta x & \Delta y^2 \end{pmatrix} \begin{pmatrix} P_i^n \\ Q_i^n \end{pmatrix} = \sum_{j \in N_i} \left(u_j^n - u_i^n \right) \begin{pmatrix} \Delta x \\ \Delta y \end{pmatrix}.$$

Solving this system one gets:

$$\begin{aligned} P_i^n &= \frac{1}{D}\sum_{j=1}^{3}(y_{G_j}-y_{G_i})^2\sum_{j=1}^{3}(u_j^n-u_i^n)(x_{G_j}-x_{G_i}) \\ &\quad -\frac{1}{D}\sum_{j=1}^{3}(x_{G_j}-x_{G_i})(y_{G_j}-y_{G_i})\sum_{j=1}^{3}(u_j^n-u_i^n)(y_{G_j}-y_{G_i}) \\ Q_i^n &= \frac{1}{D}\sum_{j=1}^{3}(x_{G_j}-x_{G_i})^2\sum_{j=1}^{3}(u_j^n-u_i^n)(y_{G_j}-y_{G_i}) \\ &\quad -\frac{1}{D}\sum_{j=1}^{3}(x_{G_j}-x_{G_i})(y_{G_j}-y_{G_i})\sum_{j=1}^{3}(u_j^n-u_i^n)(x_{G_j}-x_{G_i})\,, \end{aligned}$$

where the denominator

$$D=\sum_{j=1}^{3}(x_{G_j}-x_{G_i})^2\sum_{j=1}^{3}(y_{G_j}-y_{G_i})^2-\left[\sum_{j=1}^{3}\left(x_{G_j}-x_{G_i}\right)\left(y_{G_j}-y_{G_i}\right)\right]^2\,,$$

which is strictly positive for any non degenerate triangle.

For the quadrilateral cells Q_{ij}, the procedure is quite similar to the one described above for triangular cells. Alternatively, for a quadrilateral cell Q_{ij} with center M_{ij}, we could first compute the least squares gradient $\nabla u_j^{n+1}=(P_j^{n+1},Q_j^{n+1})$ of each triangle T_j intersecting with Q_{ij} (such that $M_{ij}\in T_j$) and then take the cell gradient

$$\nabla u_{ij}^{n+1}=average\left\{\nabla u_j^{n+1}\right\}.$$

Unfortunately, this procedure does not preserve the monotonicity of the solution in the usual van Leer sense described below, and allows the creation of local extremas between the nodes; this phenomena may lead to (or amplifies already existing) spurious oscillations, with the associated loss of stability and convergence difficulties in the case of steady flows. Therefore, we need to introduce some slope limiting in the computation of the gradients.

6.2 Slope Limiting

To prevent the generation of spurious oscillations in regions of strong gradients (neighborhood of shocks and discontinuities), we must perform a slope limiting correction [44].

6.2.1 Van Leer Limiting Approach

Following the van Leer approach [38; 39; 40], in which the value at some interface point $x_{i+1/2}$, in the one-dimensional case, must fall within the range of values spanned by the adjacent grid values, u_{i-1} and u_{i+1}, in a 2D context, we limit the gradient of the linear interpolant L to ensure that its values at the centers of the cells are bounded by u_i^n (or u_{ij}^{n+1}) the values at the centers of its neighboring cells. The limiting procedure is implemented on each cell as follows:

Let

$$\nabla u_i^n = \begin{pmatrix} P_i \\ Q_i \end{pmatrix}$$

denote the numerical gradient of u_i^n on the cell T_i.

If u satisfies the van Leer requirement we choose:

$$\begin{aligned}
P_i^{lim} &= minmod_{j\in\mathcal{N}_j}\{P_j\}, \text{ with } \mathcal{N}_j\text{=set of centroids } j \text{ adjacent to centroid } i \\
&= \frac{1}{2}\left\{\min_{T_i\in\mathcal{T}} \operatorname{sign}(P_j) + \max_{T_i\in\mathcal{T}} \operatorname{sign}(P_j)\right\} \min_{T\in\mathcal{T}} |P_j| \,, \\
Q_i^{lim} &= minmod_{j\in\mathcal{N}_j}\{Q_j\} \\
&= \frac{1}{2}\left\{\min_{T_i\in\mathcal{T}} \operatorname{sign}(Q_j) + \max_{T_i\in\mathcal{T}} \operatorname{sign}(Q_j)\right\} \min_{T\in\mathcal{T}} |Q_j|.
\end{aligned}$$

$$\text{where sign(x)} = \begin{cases} 1 & \text{if } x > 0 \\ -1 & \text{if } x < 0 \end{cases}$$

We proceed in a similar way on quadrilateral cells Q_{ij}.

6.2.2 Barth and Jespersen slope limiter

Barth and Jespersen slope limiter [9] is based on the idea that the gradients must be limited in a way to force locally the maximum principle. Let $u^n_{i_{max}}$ and $u^n_{i_{min}}$ be the maximum and minimum values of the solution at the centers of the neighboring cells of cell T_i i.e.

$$u^n_{i_{max}} = \max_{k\in\mathcal{N}(i)}\{u^n_k\} \qquad \text{and} \qquad u^n_{i_{min}} = \min_{k\in\mathcal{N}(i)}\{u^n_k\}$$

We thus want to impose on the reconstructed solution the following condition

$$u^n_{i_{min}} \leq u^n_i(x,y) \leq u^n_{i_{max}} \qquad\qquad \forall i, \quad \forall n$$

Theorem 6.2.1 *It is sufficient to impose this condition only at the quadrature points, i.e. at the points where we evaluate the reconstruction.*

For the proof of this theorem, we refer to [9].

Let M be a quadrature point, in our 2D extension of the NT scheme M is the midpoint of a side of the cell T_i.

Suppose a limited reconstruction:

$$u(x,y,t^n)|_{T_i} = L(x,y,t^n) = u^n_i + \Psi_i \nabla u^n_i \overrightarrow{G_iM} \qquad \text{where } \overrightarrow{G_iM} = \begin{pmatrix} x_M - x_{G_i} \\ y_M - y_{G_i} \end{pmatrix}$$

The directed slope in the direction of $\overrightarrow{G_iM}$ will be defined by:

$$u^n_M - u^n_i = u^n(x_M, y_M)|_{T_i} - u^n_i = \nabla u^n_i \overrightarrow{G_iM}$$

which is in fact $u(x,y,t^n)|_{T_i}$ evaluated at the point M with $\Psi_i = 1$.

The limiter is computed as follows:

$$\Psi_M = \begin{cases} \psi\left(\frac{\delta_+}{\delta_-}\right) & \text{with } \delta_+ = u^n_{i_{max}} - u^n_i \quad \text{if } u^n_M > u^n_i \\ \psi\left(\frac{\delta_+}{\delta_-}\right) & \text{with } \delta_+ = u^n_{i_{min}} - u^n_i \quad \text{if } u^n_M < u^n_i \\ 1 & \qquad\qquad\qquad\qquad\quad \text{if } u^n_M = u^n_i \end{cases}$$

where, $\delta_- = u^n_M - u^n_i$.

The limiter function is defined as: $\psi\left(\frac{\delta_+}{\delta_-}\right) = \min\left(1, \frac{\delta_+}{\delta_-}\right)$

The final limiter value Ψ_i is obtained by taking the minimum of the values at the quadrature points of cell T_i:

$$\Psi_i = \min_M \Psi_M$$

Remark 4 *In practice, we need to specify a tolerance $\epsilon_{machine}$ based on the machine number and accordingly define the limiter as follows:*

$$\Psi_M = \begin{cases} \psi\left(\frac{\delta_+}{\delta_-}\right) & \textit{with } \delta_+ = u^n_{i_{max}} - u^n_i \quad \textit{if } u^n_M - u^n_i > \epsilon_{machine} \\ \psi\left(\frac{\delta_+}{\delta_-}\right) & \textit{with } \delta_+ = u^n_{i_{min}} - u^n_i \quad \textit{if } u^n_M - u^n_i < -\epsilon_{machine} \\ 1 & \qquad\qquad\qquad\qquad\quad \textit{if } |u^n_M - u^n_i| < |\epsilon_{machine}| \end{cases}$$

Note 1 *A disadvantage of the Barth-Jespersen slope limiter is that it introduces non-differentiability in the computation of the reconstructed gradient due to the use of the non-differentiable operator* min.

6.2.3 Venkatakrishnan slope limiter

Venkatakrishnan (1995) [43] addressed the problem of obtaining convergence to steady state using the Bath and Jespersen slope limiter.

The min function has been replaced by a differentiable function

$$\psi\left(\frac{\delta_+}{\delta_-}\right) = \frac{\delta_+^2 + 2\delta_+\delta_- + \epsilon^2}{\delta_+^2 + \delta_+\delta_- + 2\delta_-^2 + \epsilon^2}$$

The parameter ϵ^2 has been introduced to avoid division by zero in regions where the numerical solution is almost constant and ϵ^2 is taken as $(\mathcal{K}\Delta x)^3$ with $\mathcal{K}$ being a user specified constant representing the tolerance to oscillations, and Δx is a characteristic length representing the local mesh size. In our numerical examples we take Δx to be the largest side. If $\mathcal{K} = 0$ the limiter is active all around the mesh.

CHAPTER 7

NUMERICAL EXPERIMENTS

In this chapter we apply the developed numerical central schemes and solve classical problems arising in gas dynamics. For some problems, we compare the numerical results obtained using these schemes with the exact solution.

7.1 Linear advection test case

We first validate our proposed methods and calculate the numerical orders of accuracy by considering the following initial-value problem for the oblique linear advection equation:

$$\begin{cases} \partial_t u + \partial_x u + \partial_y u = 0 \qquad (x, y, t) \in [0,1]^2 \times (0,1] \\ u(x, y, 0) = \sin(\pi(x + y)) \end{cases}$$

subject to exact boundary conditions prescribed via the exact solution given by:

$$u(x, y, t) = \sin(\pi(x + y - 2t))$$

Figure 7.1 shows a cross section along the line $y = x$ of the solution obtained using $40^2 \times 4$ triangular cells and, compares the profile of the solutions obtained using the 2D extension of the LF scheme and the 2D extension of the NT scheme to the exact solution of the corresponding one-dimensional problem.

As we can see from the plots, the numerical solutions obtained using both schemes reproduce the behavior of the exact solution very well. We can observe little diffusion after we zoom the plot of the solution. The 2D extension of the NT method returns more accurate results than the 2D extension of the LF scheme. We can also notice

(fig.7.1(b)) that the quality of the results obtained using our extension of the NT scheme varies according to the limiter used.

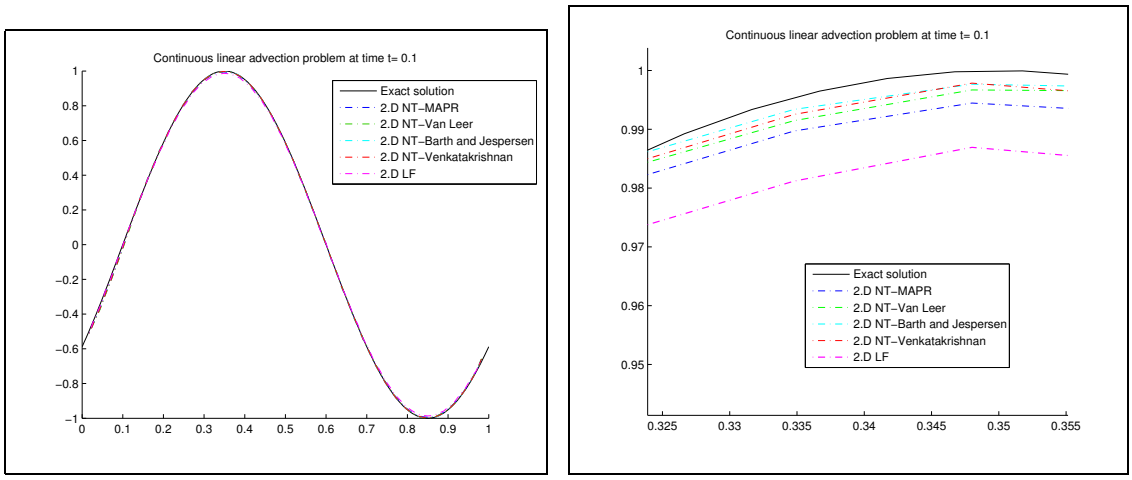

(a) Numerical Solutions (b) zoomed version of the plot

Figure 7.1: Linear advection problem: 1D cross section of the numerical and exact solutions along the line y=x.

The Least Squares (LS) gradient approximation with the Barth-Jespersen [9] slope limiter and the LS gradient approximation with the Venkatakrishnan [43] slope limiter return the best numerical results. However we will see later (in the results of the Sod shock tube problem fig.7.14) that the NT scheme with LS gradient approximation and Barth-Jespersen slope limiter produces spurious oscillations near shock discontinuities. On the other hand, the 2D extension of the NT scheme with minimum angle plane reconstruction(MAPR) [14] returns the least accurate numerical solution. Therefore the LS gradient approximation with Venkartakrishnan slope limiter gives the best numerical solution whereas the MAPR limited gradient reconstruction produces the most diffusive numerical solution among the other limiters introduced in this thesis.

For this problem, we have validated the numerical accuracy of the proposed schemes and calculated their orders of convergence. The orders of the error are relative to

a certain measure of fitness h, which can be the minimal altitude $h1$ among all triangles in the mesh, or the largest side $h2$ of the triangulation.

The error is taken to be the absolute difference between the exact solution and the numerical one. The order of the error is computed as follows:

$$\mathcal{O}_h(error) = \frac{\log(||Error_r||) - \log(||Error_{nr}||)}{\log(h_r) - \log(h_{nr})},$$

where, $Error_r$ is the error obtained on the refined grid and $Error_{nr}$ is the error obtained on the less refined grid. Similar notations are used for the measures of fitness h.

- Numerical Accuracy of our 2D extension of the LF scheme

- Norms and orders of the errors with respect to space discretization.

Grid Size	Minimal Altitude(h1)	Largest Side(h2)	$\|Error\|_\infty$	$\mathcal{O}_{h_1}$(error)	$\mathcal{O}_{h_2}$(error)
40x40	0.01282	0.02632	0.01395	-	-
80x80	0.006329	0.01282	0.006843	1.01	0.99
160x160	0.003145	0.006329	0.003399	0.977	0.969

Table 7.1: Linear advection problem: L_∞ norms and order of the errors using our 2D extension of the LF scheme.

Grid Size	Minimal Altitude(h1)	Largest Side(h2)	$\|Error\|_1$	$\mathcal{O}_{h_1}$(error)	$\mathcal{O}_{h_2}$(error)
40x40	0.01282	0.02632	0.005052	-	-
80x80	0.006329	0.01282	0.002546	0.97	0.95
160x160	0.003145	0.006329	0.001263	1.00	0.99

Table 7.2: Linear advection problem: L_1 norms and order of the errors using our 2D extension of the LF scheme.

Grid Size	Minimal Altitude(h1)	Largest Side(h2)	$\|Error\|_2^2$	$\mathcal{O}_{h_1}$(error)	$\mathcal{O}_{h_2}$(error)
40x40	0.01282	0.02632	$7.1707 * 10^{-5}$	-	-
80x80	0.006329	0.01282	1.8896×10^{-5}	0.944	0.92
160x160	0.00314	0.006329	4.63371×10^{-6}	1.00	0.99

Table 7.3: Linear advection problem: L_2 norms and order of the errors using our 2D extension of the LF scheme.

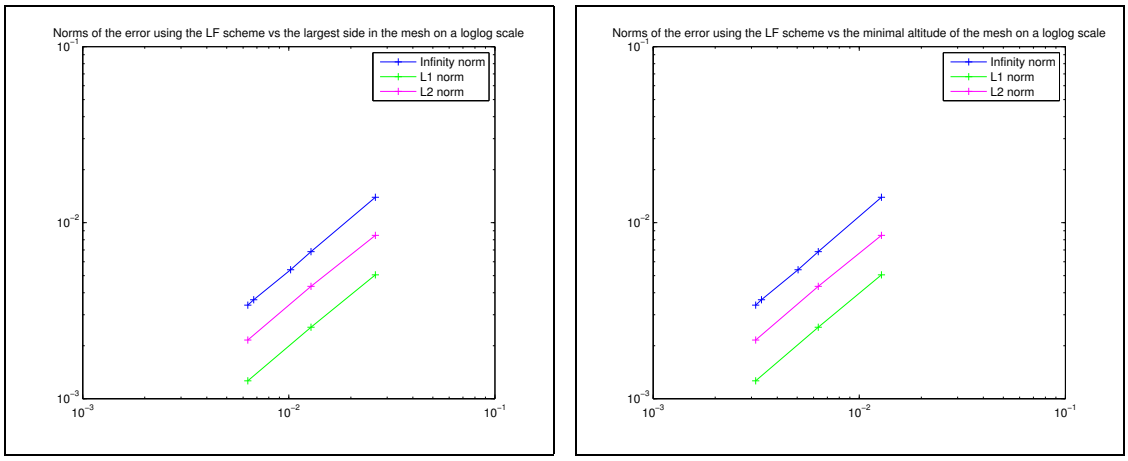

(a) Linear advection problem: Loglog plot of the norm of the error vs the largest side in the mesh for our 2D extension of the LF scheme.

(b) Linear advection problem: Loglog plot of the norm of the error vs the minimal altitude in the mesh for our 2D extension of the LF scheme.

Figure 7.2: Linear advection problem: Loglog plot of the norm of the error vs the measures of fitness for our 2D extension of the LF scheme.

- Norms and orders of the errors with respect to time discretization.

We consider an 80x80x4 grid, and an initial time step dt_0 and compute the $L\infty$, L1, and L2 norms and orders of the error. dt_0 is chosen to be the smallest time step taken by the scheme according to the CFL condition.

Norms \ Time Step	dt_0=0.001		$\frac{dt_0}{2} = 0.0005$		$\frac{dt_0}{4} = 0.00025$		$\frac{dt_0}{8} = 0.000125$	
	Norm	$\mathcal{O}$(error)	Norm	$\mathcal{O}$(error)	Norm	$\mathcal{O}$(error)	Norm	$\mathcal{O}$(error)
$\|Error\|_\infty$	0.00684	-	0.01352	0.98	0.02651	0.97	0.05186	0.968
$\|Error\|_1$	0.002546	-	0.004992	0.97	0.009797	0.97	0.01926	0.975
$\|Error\|_2^2$	$1.8896e^{-5}$	-	$7.27587e^{-5}$	0.964	$2.7496e^{-4}$	0.968	$1.06186e^{-3}$	0.975

Table 7.4: Linear advection problem: Norms and orders of the errors with respect to the time using our 2D extension of the LF scheme.

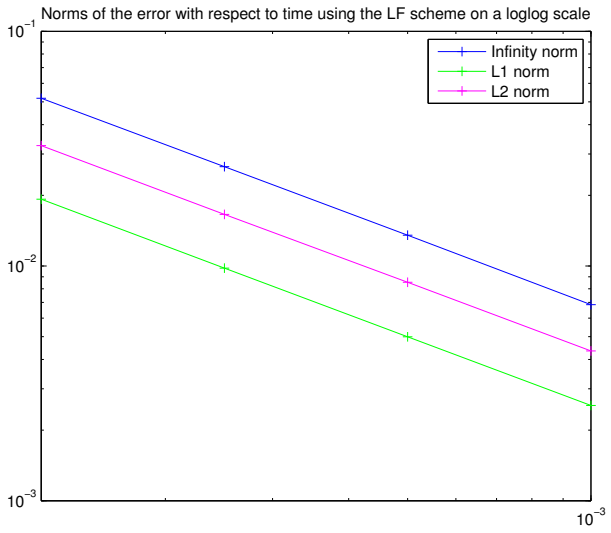

Figure 7.3: Linear advection problem: Loglog plot of the norm of the error vs the time step for our 2D extension of the LF scheme.

These numerical results confirm the first-order of accuracy in space and time of the Lax-Friedrichs scheme.

- Numerical Accuracy of our 2D extension of the NT scheme with Venkatakrishnan slope limiter

- Norms and orders of the errors with respect to space discretization.

Grid Size	Minimal Altitude(h1)	Largest Side(h2)	$\|Error\|_\infty$	$\mathcal{O}_{h_1}$(error)	$\mathcal{O}_{h_2}$(error)
40x40	0.012820513	0.02632	0.01096	-	-
80x80	0.006329	0.01282	0.003975	1.44	1.41
160x160	0.003145	0.006329	$1.2933e^{-3}$	1.605	1.59

Table 7.5: Linear advection problem: L_∞ norms and order of the errors using our 2D extension of the NT scheme.

Grid Size	Minimal Altitude(h1)	Largest Side(h2)	$\|Error\|_1$	$\mathcal{O}_{h_1}$(error)	$\mathcal{O}_{h_2}$(error)
40x40	0.01282	0.02632	$3.8228e^{-3}$	-	-
80x80	0.006329	0.01282	$1.0517e^{-3}$	1.82	1.79
160x160	0.003145	0.006329	$2.8315e^{-4}$	1.876	1.86

Table 7.6: Linear advection problem: L_1 norms and order of the errors using our 2D extension of the NT scheme.

Grid Size	Minimal Altitude(h1)	Largest Side(h2)	$\|Error\|_2^2$	$\mathcal{O}_{h_1}$(error)	$\mathcal{O}_{h_2}$(error)
40x40	0.01282	0.02632	$5.4263e^{-5}$	-	-
80x80	0.006329	0.01282	$4.7458e^{-6}$	1.726	1.69
160x160	0.003145	0.006329	$4.0365e^{-7}$	1.76	1.746

Table 7.7: Linear advection problem: L_2 norms and order of the errors using our 2D extension of the NT scheme.

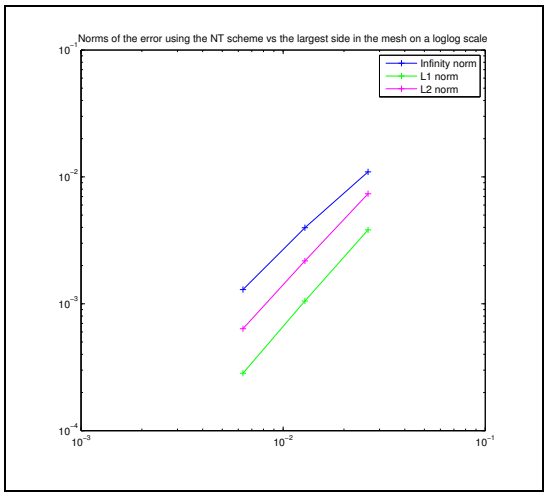

(a) Linear advection problem: Loglog plot of the norm of the error vs the largest side in the mesh for our 2D extension of the NT scheme.

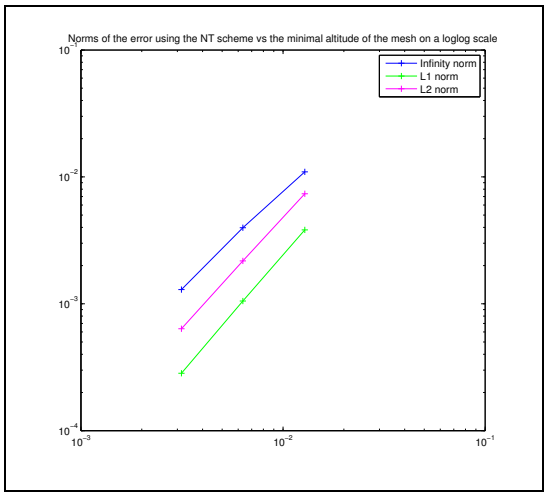

(b) Linear advection problem: Loglog plot of the norm of the error vs the minimal altitude in the mesh for our 2D extension of the NT scheme.

Figure 7.4: Linear advection problem: Loglog plot of the norm of the error vs the measures of fitness for our 2D extension of the NT scheme.

- Norms and orders of the errors with respect to time discretization.

Time Step / Norms	dt_0=0.001		$\frac{dt_0}{2} = 0.0005$		$\frac{dt_0}{4} = 0.00025$		$\frac{dt_0}{8} = 0.000125$	
	Norm	$\mathcal{O}$(error)	Norm	$\mathcal{O}$(error)	Norm	$\mathcal{O}$(error)	Norm	$\mathcal{O}$(error)
$\|Error\|_\infty$	0.003975	-	0.01139	1.52	0.03450	1.59	0.10723	1.636
$\|Error\|_1$	$1.0517e^{-3}$	-	0.003693	1.81	0.013289	1.847	0.04735	1.83
$\|Error\|_2^2$	$4.7458e^{-6}$	-	$5.485345e^{-5}$	1.765	$6.5348e^{-4}$	1.787	$7.59693e^{-3}$	1.77

Table 7.8: Linear advection problem: Norms and orders of the errors with respect to the time steps using our 2D extension of the NT scheme.

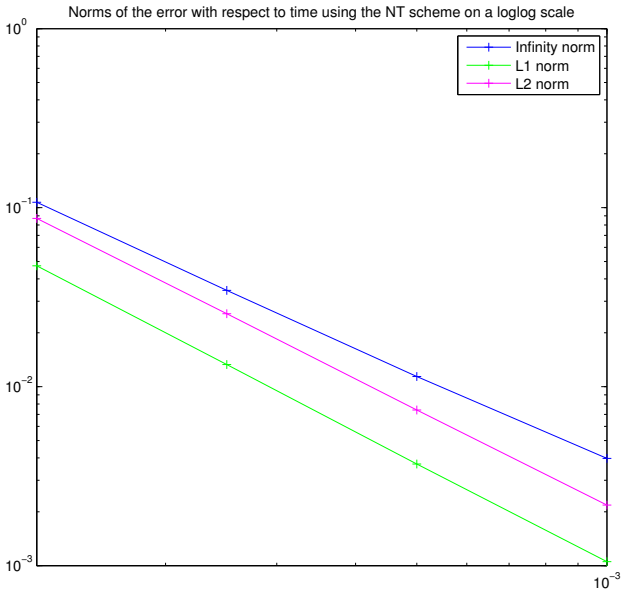

Figure 7.5: Linear advection problem: Loglog plot of the norm of the error vs the time step for our 2D extension of the NT scheme.

These numerical results confirm the second-order of accuracy in space and time of the Nessyahu-Tadmor scheme and compare very well to those presented in [15].

7.2 Burgers' equation

Next, we consider the two-dimensional inviscid Burgers equation:

$$\partial_t u + \partial_x \left(\frac{1}{2}u^2\right) + \partial_y \left(\frac{1}{2}u^2\right) = 0 \qquad \text{(x,y)} \in [0,1]^2$$

subject to the following initial condition:

$$u(x,y,0) = \begin{cases} 2, & x < 0.25, y < 0.25 \\ 3, & x > 0.25, y > 0.25 \\ 1, & \text{else} \end{cases}$$

The solution is calculated at time $t = \frac{1}{12}$. The computational domain is discretized using $100^2 \times 4$ triangular cells.

The exact solution of this initial value problem [15] consists of two shock waves and two rarefactions, which meet toward the middle of the domain to form a cusp. Figure 7.6(a) shows the profile of the numerical solution at the final time obtained using the 2D extension of the LF scheme while 7.6(b) shows the contour lines of the solution. Similar information is shown in figures 7.7(a) and 7.7(b) obtained using the NT scheme with Venkatakrishnan slope limiter.

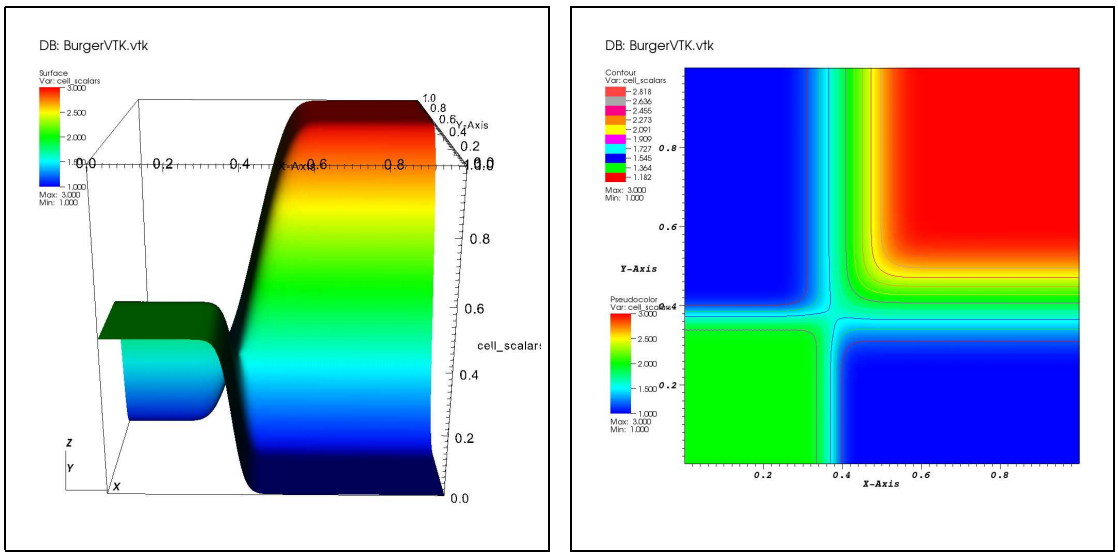

(a) 3D surface plot (b) Contour lines

Figure 7.6: Burgers' equation: Numerical solution obtained using our 2D extension of the LF scheme.

Figure 7.8 shows the cross sections of the numerical solutions along the $y = x$ axis, obtained using the 2D extension of the NT scheme with MAPR limited gradient reconstruction (dotted line), the 2D extension of the NT scheme with LS gradient reconstruction and Venkatakrishnan slope limiter (solid line), and the 2D extension of the LF scheme (dashed line).

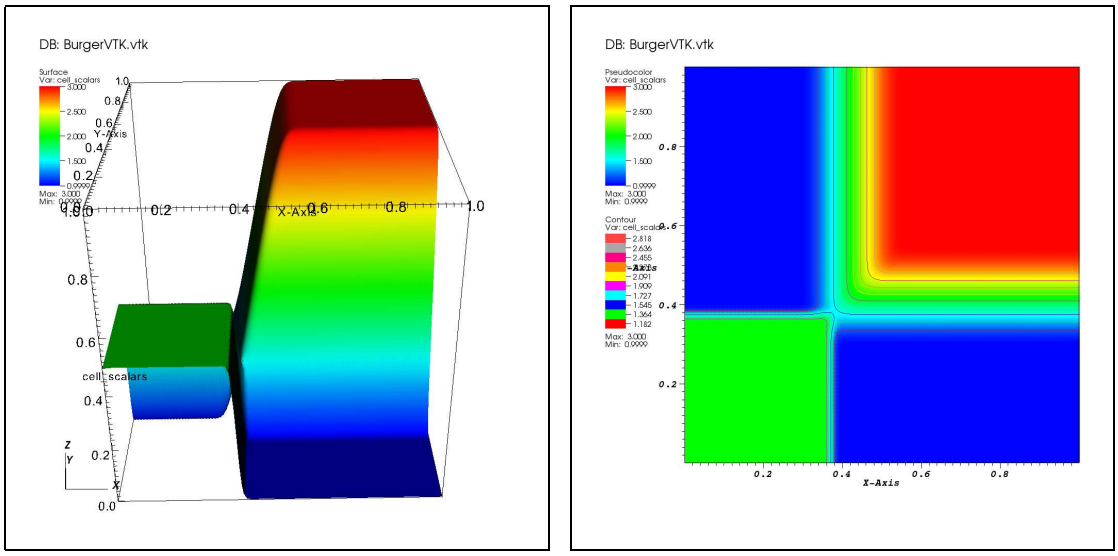

(a) 3D surface plot (b) Contour lines

Figure 7.7: Burgers' equation: Numerical solution obtained using our 2D extension of the NT scheme with the Venkatakrishnan slope limiter.

We have chosen to plot the least accurate among the numerical solutions obtained with the NT scheme i.e. using the MAPR gradient reconstruction in order to show that even the least accurate solution returned by the NT scheme gives much sharper results than the LF scheme.

We have also plotted the result obtained using the LS gradient reconstruction with Venkatakrishnan slope limiter in order to show how sharp can be the numerical solution obtained using the NT scheme.

The numerical results obtained using both schemes are in good agreement with those obtained by Christov and Popov in [15].

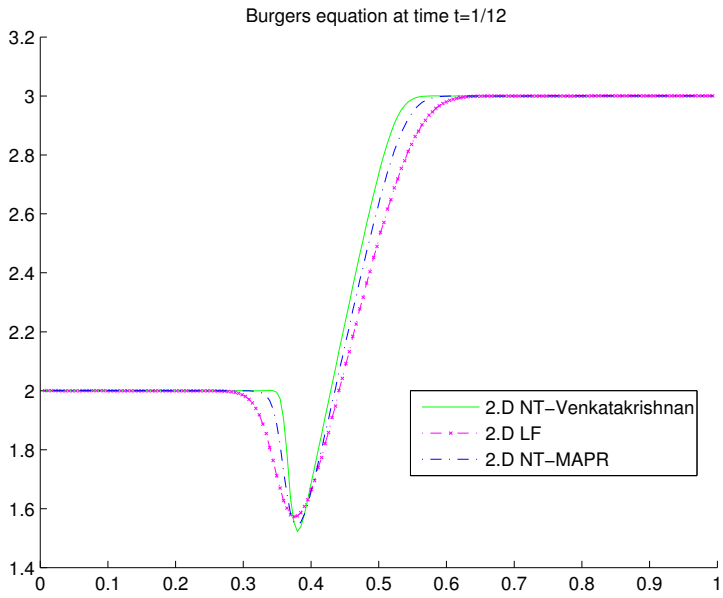

Figure 7.8: Burgers' equation: 1D cross section along the axis $y = x$ of our 2D extension of the NT scheme and our 2D extension of the LF scheme.

7.3 Nonconvex Fluxes test case

The following example shows the capability of our scheme to capture composite waves. We consider the scalar conservation law with nonconvex fluxes (i.e. $f''(u)$ and $g''(u)$ change sign):

$$\partial_t u + \partial_x \left(\sin(u)\right) + \partial_y \left(\cos(u)\right) = 0\,, \qquad (x, y, t) \in [-2, 2] \times [-2.5, 1.5] \times (0, 1]$$

subject to the initial condition

$$u(x, y, 0) = \begin{cases} 3.5\pi\,, & \text{if } x^2 + y^2 < 1 \\ 0.25\pi\,, & \text{else} \end{cases}$$

For this initial condition, the x-direction flux has three inflection points, and the y-direction flux has four [34; 15]. This makes the problem more challenging because it gives the limiter more room for error. We discretize the domain using $100^2 \times 4$ triangular cells and compute the solution at time $t = 1$.

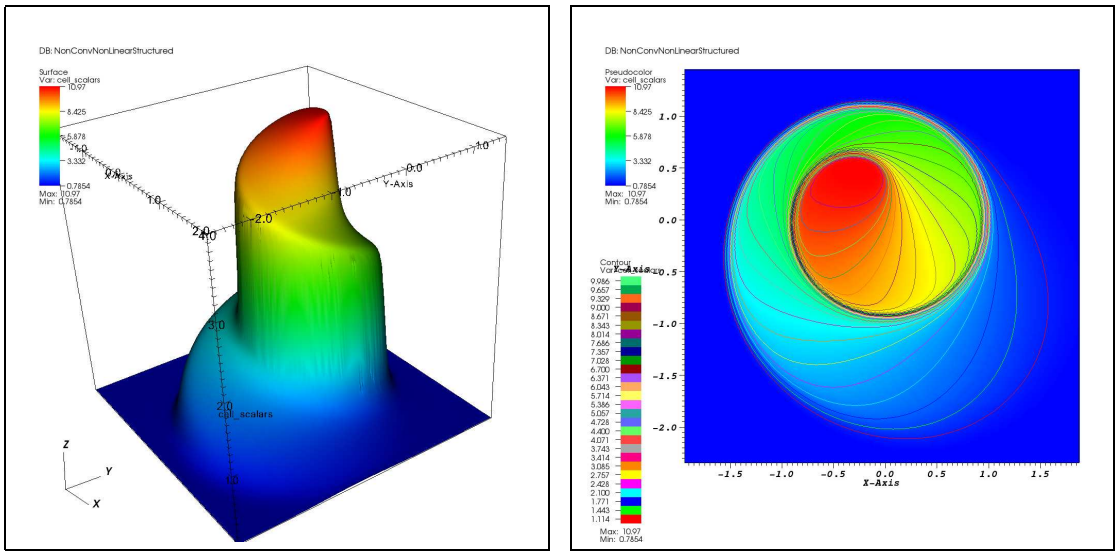

(a) 3D surface plot (b) Contour lines

Figure 7.9: Nonconvex problem: Numerical solution obtained using our 2D extension of the LF scheme.

Figure 7.9 shows the profile of the numerical solution at the final time (left) and the contour lines (right) obtained using the 2D extension of the LF scheme. Similar information for the solution obtained using the 2D extension of the NT scheme is shown in figure 7.10. The contour lines show the ability of our numerical schemes to reproduce the spiral movement of the exact solution and are in good agreement with the corresponding ones presented in [15].

The composite wave structure is captured very well by both schemes (especially the curved discontinuity). Unlike the WENO scheme with the Superbee limiter [34], our proposed extension of the NT scheme is capable to generate the exact profile when used with MAPR or the Venkatakrishnan gradient limiters.

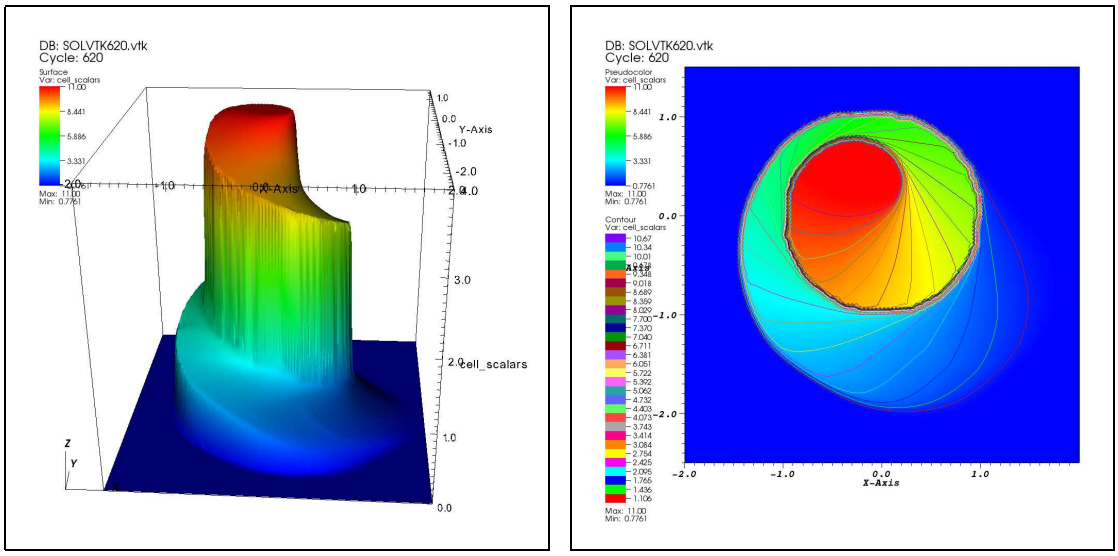

(a) 3D surface plot (b) Contour lines

Figure 7.10: Nonconvex problem: Numerical solution obtained using our 2D extension of the NT scheme with the Venkatakrishnan slope limiter.

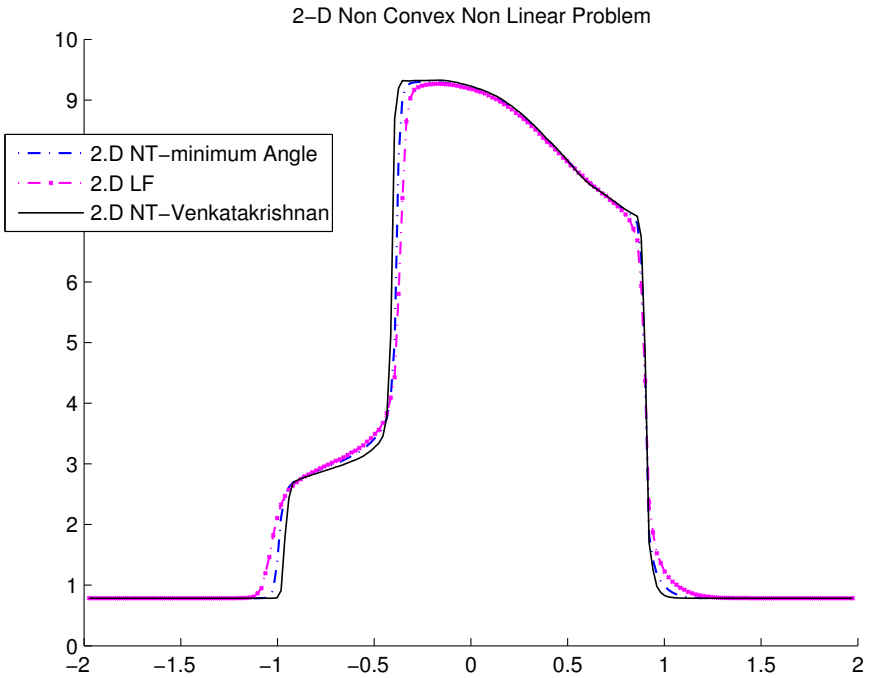

Figure 7.11: Nonconvex problem: 1D cross section along the axis $y = x$ of our 2D extension of the NT scheme and our 2D extension of the LF scheme.

7.4 Euler Equations

We now consider the two-dimensional Euler equations associated with different types of initial conditions: circular, two states, and four states.

The two-dimensional Euler equations are given by:

$$\frac{\partial}{\partial t}\begin{pmatrix}\rho\\ \rho u\\ \rho v\\ E\end{pmatrix}+\frac{\partial}{\partial x}\begin{pmatrix}\rho u\\ \rho u^2+p\\ \rho uv\\ u(E+p)\end{pmatrix}+\frac{\partial}{\partial y}\begin{pmatrix}\rho v\\ \rho uv\\ \rho v^2+p\\ v(E+p)\end{pmatrix}=0$$

here ρ is the gas density, (u, v) is the velocity field, p is the gas pressure, and E is the gas energy. E, ρ and p are related by the state equation:

$$E=\frac{p}{\gamma-1}+\frac{\rho\left(u^2+v^2\right)}{2}.$$

7.4.1 2 states: Left and right

We consider here the Euler equations subject to the following initial condition:

$$U(x,y,0)=\begin{cases}(1,0,0,2.5)\,, & \text{if } x<0.5\\ (0.125,0,0,0.25)\,, & \text{otherwise}\end{cases}$$

where the computational domain $[0,1]^2$ is discretized using $100^2\times 4$ triangles.

This is known by the Sod shock tube problem, a classical experiment in gas dynamics. To perform it one takes a long cylindrical tube separated into two halves by a thin membrane. A gas is placed into each side, with both sides at rest (velocity in the x and y direction in both sides is equal to zero), but with different pressures and densities. The membrane is then suddenly removed at time t=0, and the evolution of the gas is observed. One can then see the expansion of three waves: A rarefaction wave, a contact discontinuity, and a shock wave.

The numerical solution is calculated at time $t = 0.164$.

Figure 7.12 shows the profile of the gas density (left) and the contour lines (right) of the solution obtained using the NT scheme extension with a Venkatakrishnan gradient limiter.

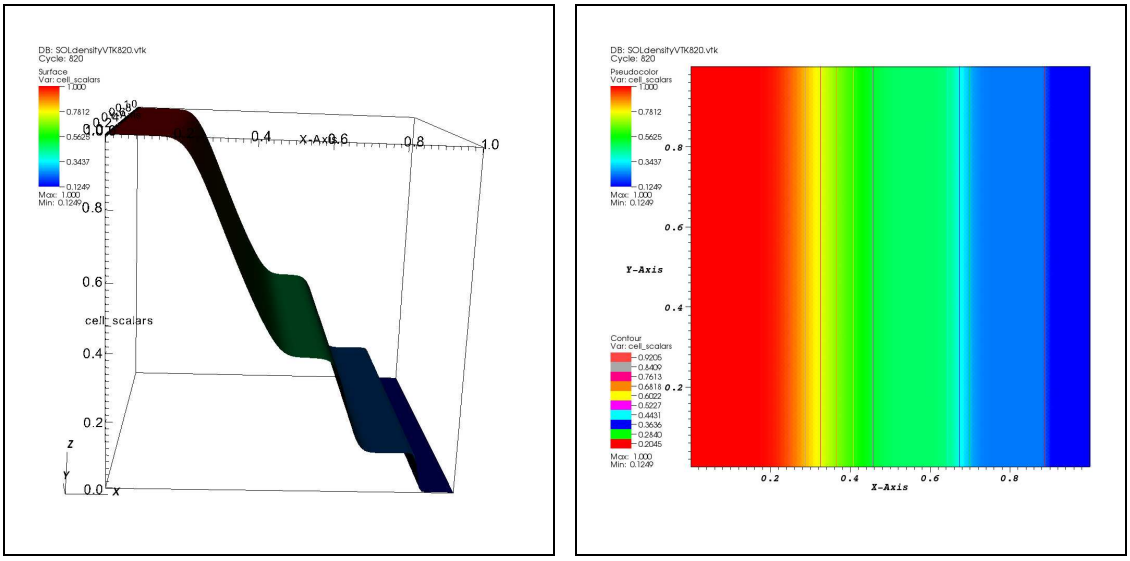

(a) 3D surface plot of the gas density (b) Contour lines

Figure 7.12: Numerical solution of the Sod shock tube problem using our 2D extension of the NT scheme.

Figure 7.13 shows cross sections of the mass density along the line $y = 0.5$ obtained using the LF and the NT extensions (dashed lines) using different limiters; the reference solution (solid line) is the exact solution of the corresponding one-dimensional problem.

Although the Barth-Jespersen slope limiter returns the sharpest numerical solution among the other limiters (fig. 7.13), it produces spurious oscillations near the shock discontinuity (fig. 7.14). These spurious oscillations might be resulting from the non-differentiability of the reconstructed gradient as discussed in [9].

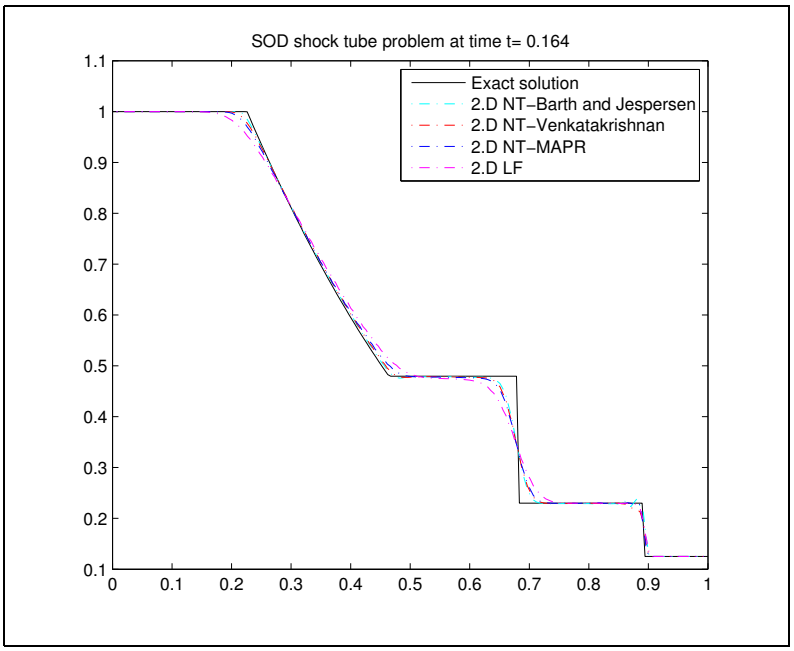

(a) cross section along y=0.5 direction

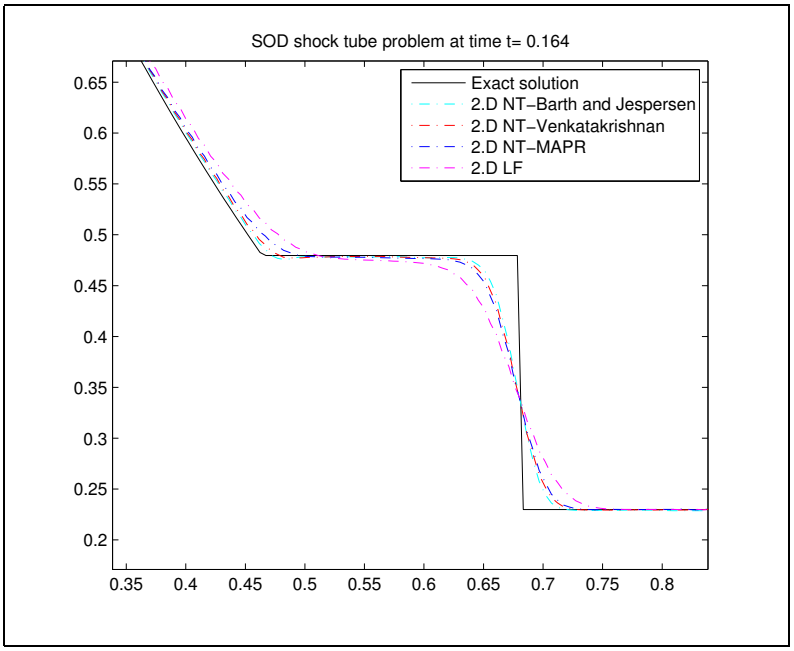

(b) zoom on the contact discontinuity and the rarefaction wave

Figure 7.13: Sod problem: 1D cross section of the 2D numerical the gas density using our extensions of the NT and LF schemes with the exact solution.

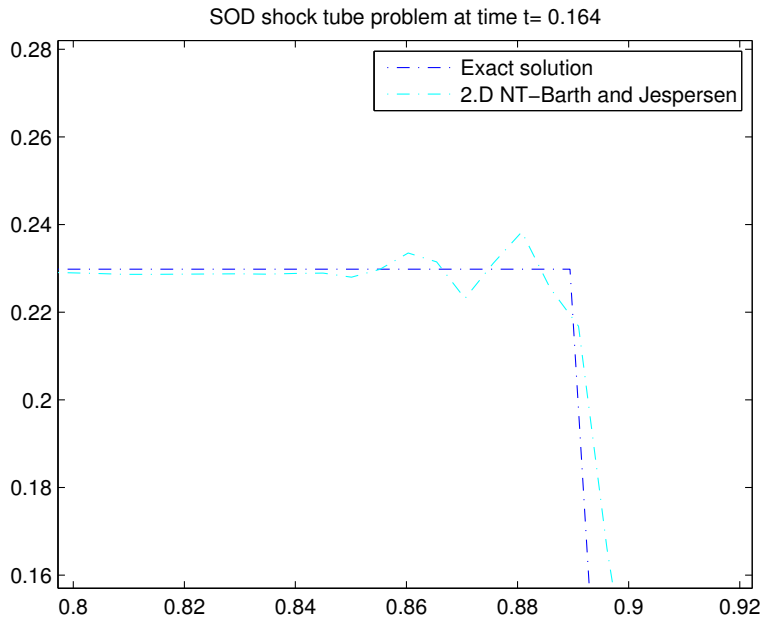

Figure 7.14: Sod problem: Barth-Jespersen gradient limiter returns spurious oscillations near the shock.

7.4.2 Circular Riemann Problem Problem

This problem tests the symmetric shock capturing capability of the proposed schemes. The computational domain $[0,1]^2$ is discretized using $100^2 \times 4$ triangular cells. The initial condition comprises two constant states separated by a cylindrical membrane of radius 0.1 as given below:

$$U(x,y,0) = \begin{cases} (1,0,0,2.5) & \text{if } \sqrt{(x-0.5)^2+(y-0.5)^2} < 0.1 \\ (0.125,0,0,0.25) & \text{otherwise} \end{cases}$$

Figure 7.15 shows the profile of the gas density at time $t = 0.1$ (left) and the corresponding contour lines (right); a circular shock wave propagating radially outward is about to exit the computational domain and an inner rarefaction wave is about to reach the center of the domain. By the time $t = 0.35$ the rarefaction wave has reached the center of the domain and has reflected creating a new outgoing radial

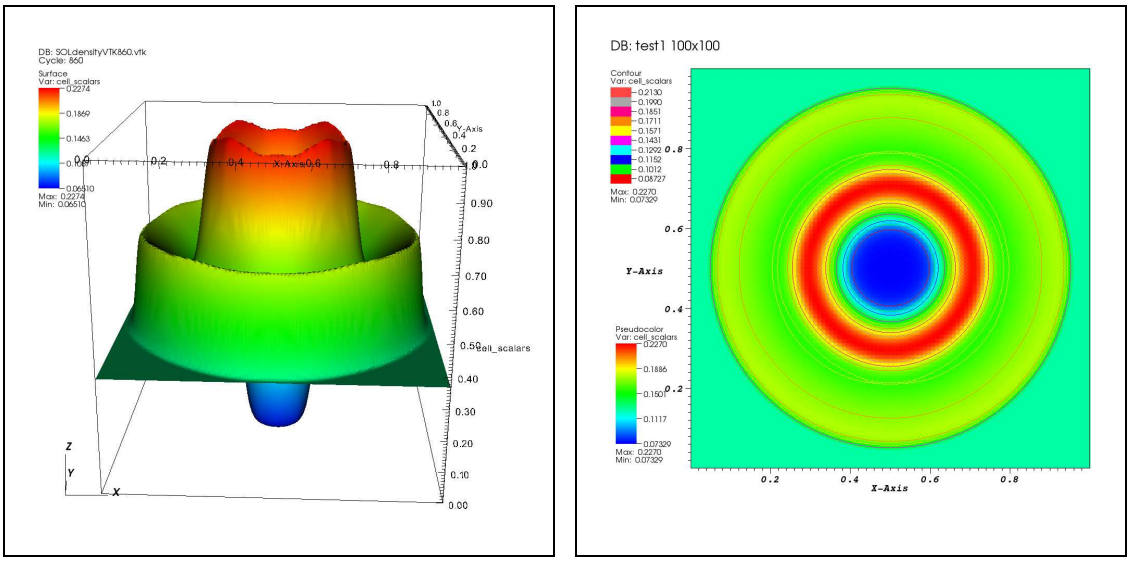

(a) 3D surface plot (b) Contour lines

Figure 7.15: Gas density at time t=0.1 using our 2D extension of the NT scheme with Venkatakrishnan gradient limiter.

shock wave (fig. 7.16). For both schemes, the two dimensional contours of the density of the gas present perfect symmetric flow behavior. Figure 7.17 shows a one-dimensional cross section along the $y = x$ line of the gas density at the final time obtained using the extensions of the LF scheme (dashed line) and the NT scheme with Venkatakrishnan slope limiter (solid line).

7.4.3 4 states Riemann Problem

We numerically solve the Euler equations subject to an initial condition with 4 different states. These states admit 19 different configurations as discussed in [36]. We will be testing our schemes on some of these configurations.

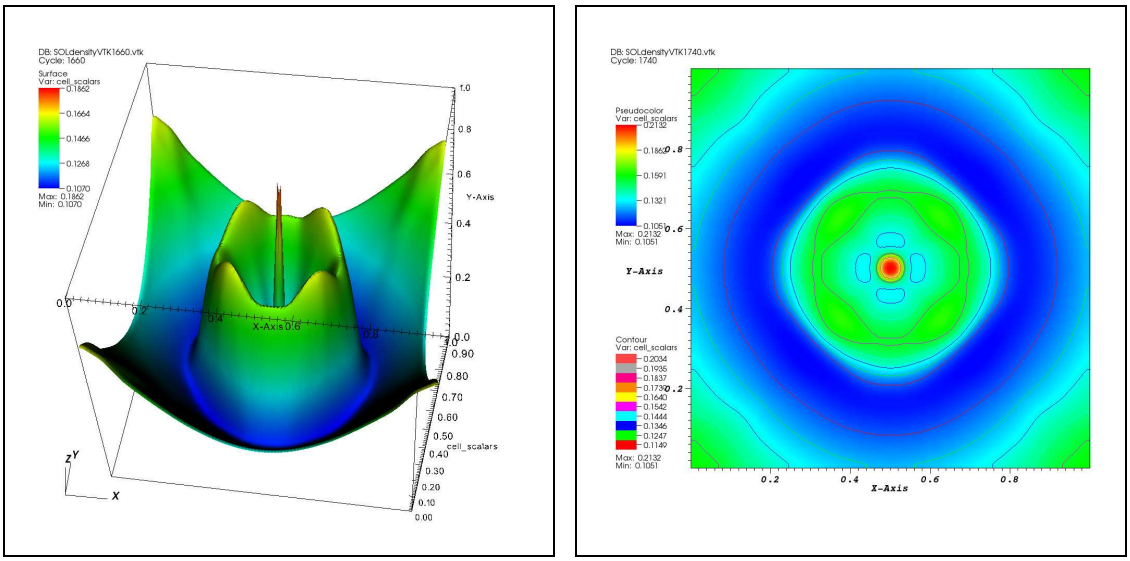

(a) 3D surface plot (b) Contour lines

Figure 7.16: Circular Riemann Problem: Gas density at the final time t=0.35 using our 2D extension of the NT scheme with Venkatakrishnan gradient limiter.

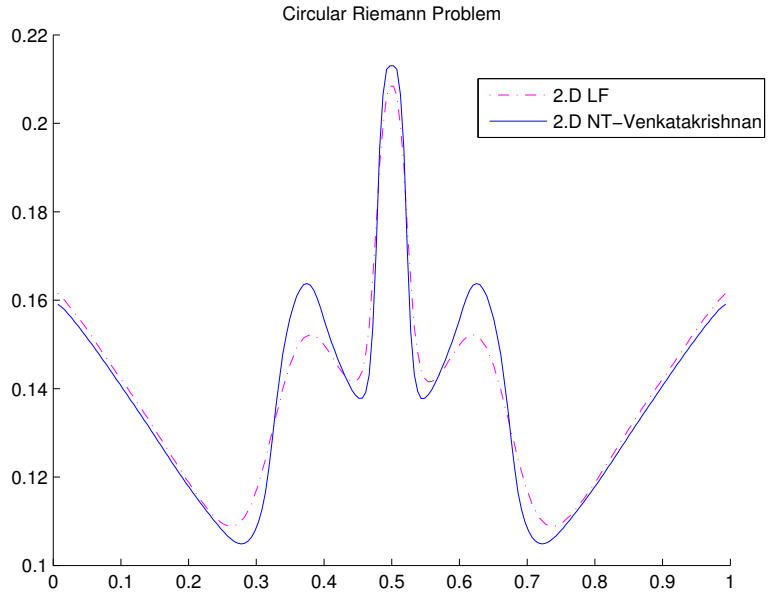

Figure 7.17: Circular Riemann Problem: 1D cross section along the axis $y = x$ of our 2D extensions of the NT scheme (solid line) and LF scheme (dashed line) at time t=0.35.

7.4.3.1 Problem A: 4 forward rarefaction waves.

The initial condition is given by:

$$(p,\rho,u,v)(x,y,0) = \begin{cases} (1,1,0,0) & \text{if } x > 0.5, y > 0.5 \\ (0.4,0.5197,-0.7259,0) & \text{if } x < 0.5, y > 0.5 \\ (0.0439,0.1072,-0.7259,-1.4045) & \text{if } x < 0.5, y < 0.5 \\ (0.15,0.2579,0,-1.4045) & \text{if } x > 0.5, y < 0.5 \end{cases}$$

The computational domain $[0,1]^2$ is discretized using $100^2 \times 4$ triangular cells and the numerical solution is calculated at time $t = 0.164$ using our extensions of the LF and NT schemes. This example corresponds to configuration 1 of [36].

Figure 7.18 shows the profile of the gas density (left) and the contour lines (right) obtained using our 2D extension of the NT scheme with Venkatakrishnan slope limiter at the final time.

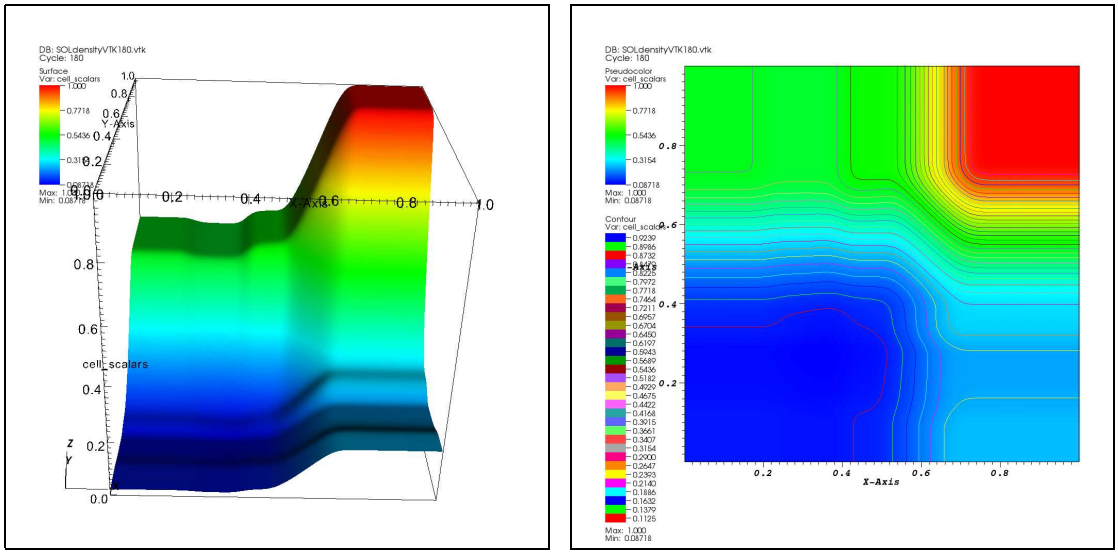

(a) 3D surface plot (b) Contour lines

Figure 7.18: Euler's equations with 4 forward rarefaction waves: Gas density obtained using the 2D extension of the NT scheme.

Figure 7.19 show cross sections along the $y = x$ (left) and the $y = -x$ (right) directions of the gas density obtained using our 2D extensions of the LF scheme (dashed line) and the NT scheme (solid line).

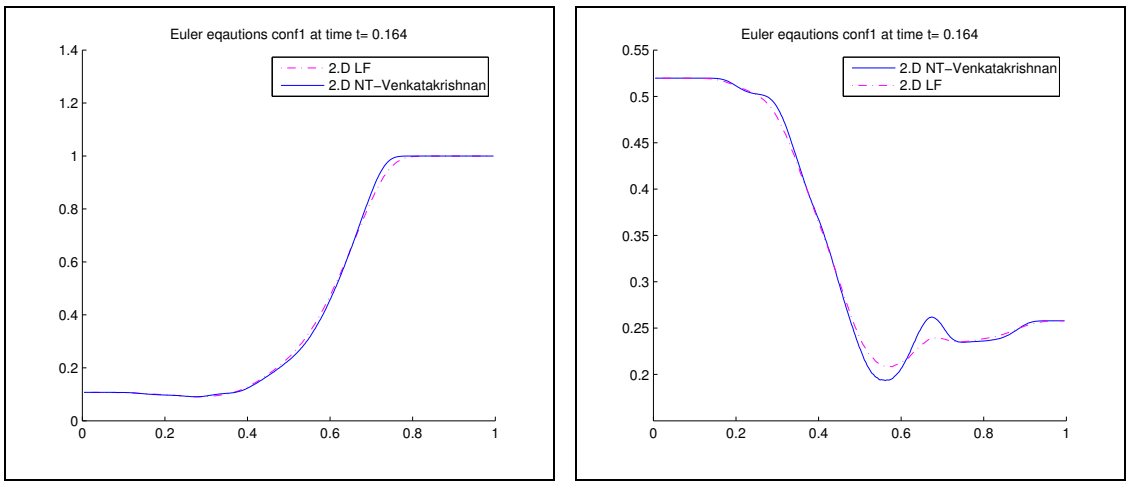

Figure 7.19: Euler's equations with 4 forward rarefaction waves: 1D cross section along the axes $y = x$ (left) and $y = -x$ (right) of the gas density obtained using the extensions of the NT scheme (solid line) and the LF scheme (dashed line).

7.4.3.2 Problem B: 2 forward and 2 backward rarefaction waves

The initial condition is given by:

$$(p, \rho, u, v)(x, y, 0) = \begin{cases} (1, 1, 0, 0) & \text{if } x > 0.5, y > 0.5 \\ (0.4, 0.5197, -0.7259, 0) & \text{if } x < 0.5, y > 0.5 \\ (1, 1, -0.7259, -0.7259) & \text{if } x < 0.5, y < 0.5 \\ (0.4, 0.5197, 0, -0.7259) & \text{if } x > 0.5, y < 0.5 \end{cases}$$

The computational domain $[0, 1]^2$ is discretized using $100^2 \times 4$ triangles and the numerical solution is calculated at time $t = 0.2$ using our extensions of the LF and NT schemes. This example corresponds to configuration 2 of [36].

Figure 7.20 shows the profile of the gas density (left) and the contour lines (right) obtained using the NT extension with a Venkatakrishnan slope limiter. On the other hand, figure 7.21 shows one-dimensional cross sections along the axis $y = x$

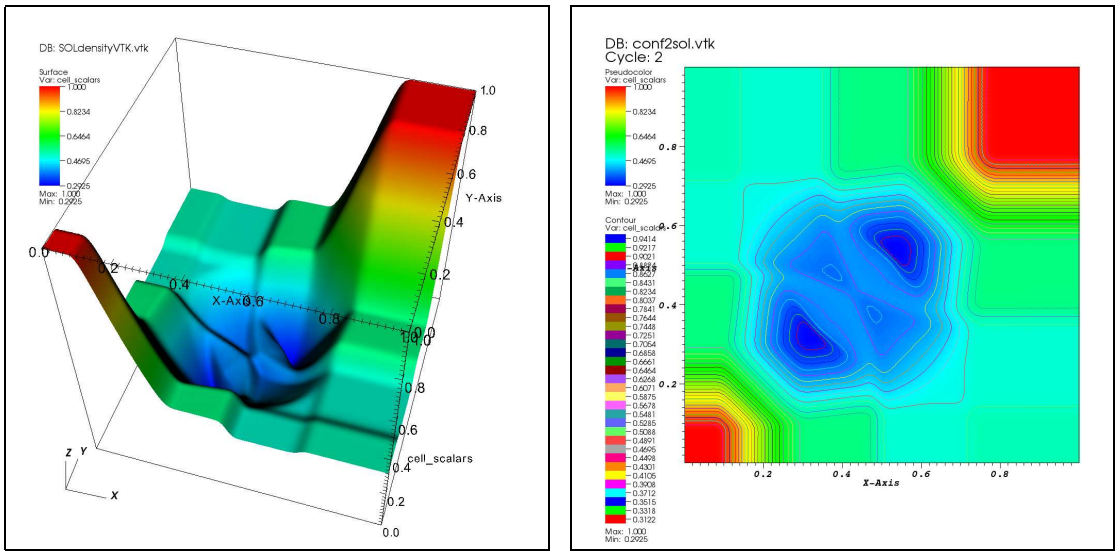

(a) 3D surface plot of the density (b) Contour lines

Figure 7.20: Euler's equations with 2 forward and 2 backward rarefaction waves: Gas density obtained using the 2D extension of the NT scheme.

and $y = -x$ of the gas density obtained at the final time using our 2D extensions of the LF (dashed line) and the NT (solid line) schemes.

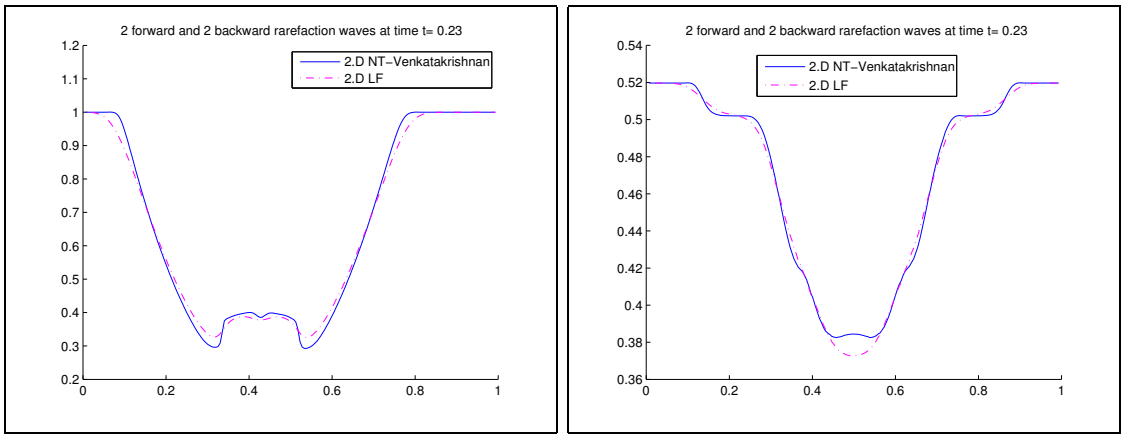

Figure 7.21: Euler's equations with 2 forward and 2 backward rarefaction waves: 1D cross section along the axes $y = x$ (left) and $y = -x$ (right) of the gas density obtained using the extensions of the NT scheme (solid line) and the LF scheme (dashed line).

As we can see, the numerical solution presents outward propagating rarefaction waves which are in good agreement with the results presented in [36].

7.4.3.3 Problem C: 2 forward and 2 backward shock waves

The initial condition is given by:

$$(p,\rho,u,v)(x,y,0) = \begin{cases} (1.1, 1.1, 0, 0) & \text{if } x > 0.5, y > 0.5 \\ (0.35, 0.5065, 0.8939, 0) & \text{if } x < 0.5, y > 0.5 \\ (1.1, 1.1, 0.8939, 0.8939) & \text{if } x < 0.5, y < 0.5 \\ (0.35, 0.35, 0, 0.8939) & \text{if } x > 0.5, y < 0.5 \end{cases}$$

The computational domain $[0,1]^2$ is discretized using $100^2 \times 4$ triangular cells and the numerical solution is calculated at time $t = 0.25$ using our extensions of the LF and NT schemes. This example corresponds to configuration 4 of [36].

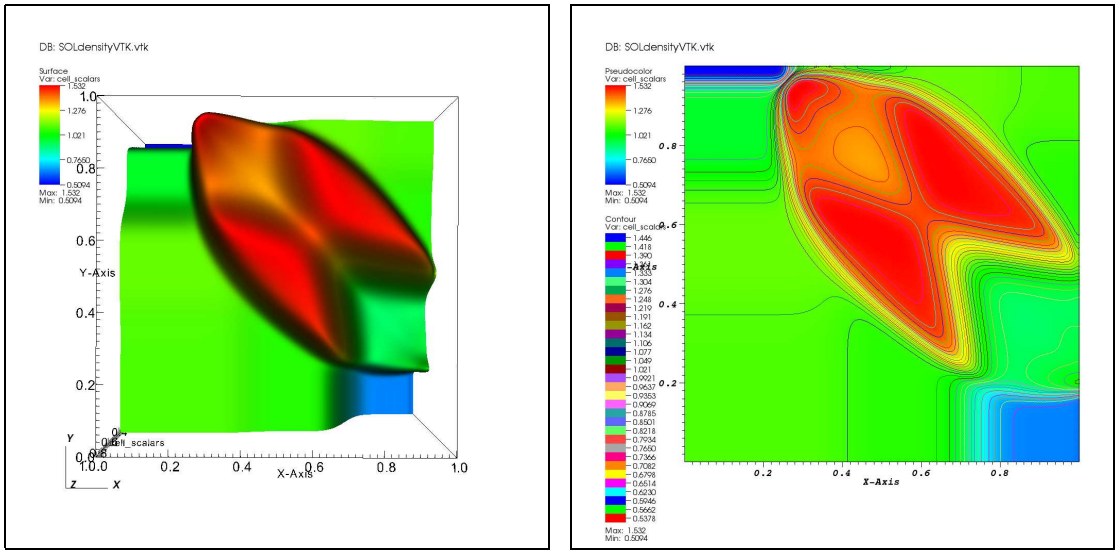

(a) 3D surface plot of the density (b) Contour lines

Figure 7.22: Euler's equations with 2 forward and 2 backward shock waves: Gas density obtained using the 2D extension of the NT scheme.

Figure 7.22 shows the 3D plot (left) and contour lines (right) of the mass density obtained using the 2D extension of the NT scheme with the Venkatakrishnan slope

limiter at time $t = 0.25$.

Figure 7.23 presents a one-dimensional cross section along the $y = x$ direction of the gas density obtained using our extensions of the LF (dashed line) and NT (solid line) schemes.

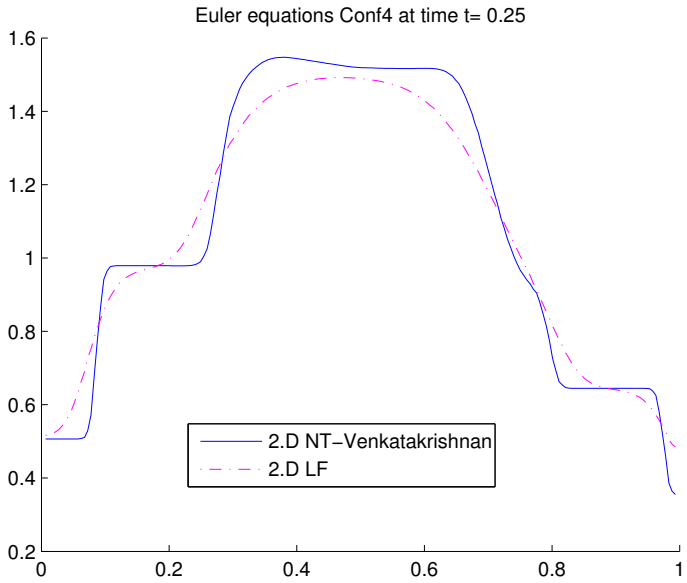

Figure 7.23: Euler's equations with 2 forward and 2 backward shock waves: 1D cross section along the axes $y = x$ of the gas density obtained using the extensions of the NT scheme (solid line) and the LF scheme (dashed line).

7.4.3.4 Problem D: 4 negative contact discontinuities

The initial condition is given by:

$$(p, \rho, u, v)(x, y, 0) = \begin{cases} (1, 1, -0.75, -0.5) & \text{if } x > 0.5, y > 0.5 \\ (1, 2, -0.75, 0.5) & \text{if } x < 0.5, y > 0.5 \\ (1, 1, 0.75, 0.5) & \text{if } x < 0.5, y < 0.5 \\ (1, 3, 0.75, -0.5) & \text{if } x > 0.5, y < 0.5 \end{cases}$$

The computational domain $[0, 1]^2$ is discretized using $100^2 \times 4$ triangular cells and the numerical solution is calculated at time $t = 0.23$ using our extensions of the LF and NT schemes. This example corresponds to configuration 5 of [36].

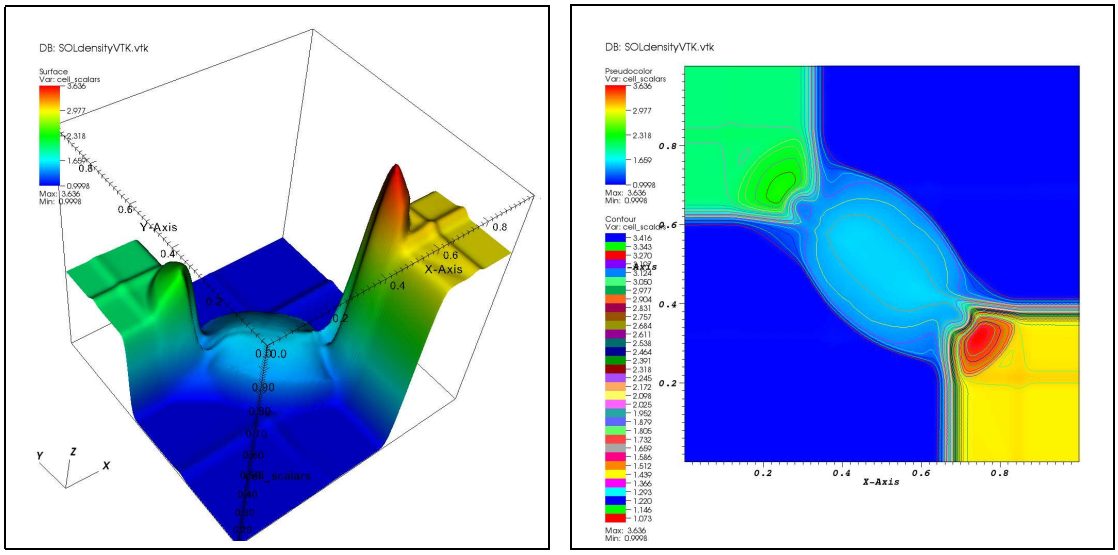

(a) 3D surface plot of the density (b) Contour lines

Figure 7.24: Euler's equations with 4 negative contact discontinuities: Gas density obtained using the 2D extension of the NT scheme.

Figure 7.24 shows a surface plot (left) and the contour lines (right) of the gas density obtained using our 2D extension of the NT scheme with Venkatakrishnan slope limiter at the final time $t = 0.23$. Figure 7.25 shows cross sections along the $y = x$ and the $y = -x$ axis of the mass density obtained using the extensions of the LF (dashed line) and the NT (solid line) schemes.

The 2D extension of the NT scheme returns sharper results than the 2D extension of the LF scheme. These results are in good agreement with the ones presented in [36].

The obtained numerical results for the problems A through D are in good agreement with their corresponding ones presented in [36] thus confirming the efficiency and the potential of the developed schemes.

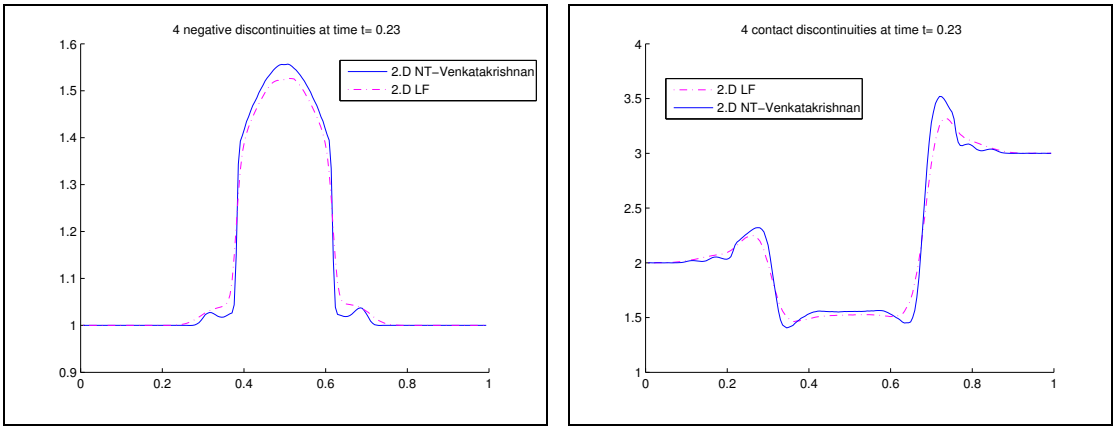

Figure 7.25: Euler's equations with 4 negative contact discontinuities: 1D cross section along the axes $y = x$ (left) and $y = -x$ (right) of the gas density obtained using the extensions of the NT scheme (solid line) and the LF scheme (dashed line).

CHAPTER 8

CONCLUSION AND FUTURE WORK

In this thesis we have presented two central finite volume schemes for approximating the solutions of hyperbolic systems of conservation laws. The proposed methods are new extensions of the one-dimensional Lax-Friedrichs and Nessyahu-Tadmor schemes to unstructured grids. The main feature of the proposed extensions is that they avoid the resolution of the Riemann problems arising at the cell interfaces thanks to two staggered grids. The control cells of the original grid are the triangles of a finite element triangulation whereas the dual staggered cells are the quadrilaterals obtained by joining the centroids of two neighboring triangles to the vertices of their common side.

In contrast with the extension of the Lax-Friedrichs scheme that evolves a piecewise constant numerical solution, the NT extension evolves a piecewise linear solution and thus ensures second-order of accuracy.

The introduced schemes have comparable performance and accuracy to the one-dimensional Lax-Friedrichs and Nessyahu-Tadmor schemes as well as their two-dimensional extensions to Cartesian or unstructured grids. Working on unstructured grids is preferred especially when irregular geometries are considered. On the other hand, the main advantage of these schemes over the already existing unstructured methods is the simplicity of the discretization and therefore of the computations.

The numerical experiments show the ability of the schemes to reproduce very well the profile of the exact solutions, and discontinuities and shock waves are very well captured by both schemes. The two-dimensional extension of the Nessyahu-Tadmor scheme returns sharper results than the two-dimensional extension of the Lax-Friedrichs scheme. The order of accuracy of the 2D extension of

the Nessyahu-Tadmor scheme varies according to the gradient limiter used; the best orders of the error are obtained using a Least squares gradient approximation associated with a Venkatakrishnan slope limiter.

Higher order of accuracy can be achieved by following the same strategy as the 2D extension of the Nessyahu-Tadmor and by replacing the piecewise linear reconstruction by a piecewise quadratic, or cubic functions. Furthermore, convergence and stability investigations of the proposed methods can be explored. In addition, the schemes can be extended to three-dimensions working on unstructured tetrahedral grids instead of the triangular grids used in two-dimensions. We are also interested in adapting our unstructured extension of the NT scheme to the case of balanced conservation laws.

REFERENCES

[1] G.D. Van Albada, W.W. Roberts, B. Van Leer, *A Comparative Study of computational methods in cosmic gas dynamics*, Astron. Astrophys. **vol.108** (1982), pp. 76–84.

[2] P. Arminjon, A. Madrane, M.C. Viallon, *A Finite Volume Extension of the Lax-Friedrichs and Nessyahu-Tadmor schemes for Conservation laws on Unstructured grids, revisited version with numerical applications*, Int. J. of Comp. Fluid Dynamics **vol.9** (1997), no. 1, pp. 1–22.

[3] P. Arminjon, A. St-Cyr, A. Madrane, *New Lax-Friedrichs-type finite volume schemes on 2 and 3D Cartesian staggered grids*, 7^{th} annual conference of the CFD Society of Canada, Halifax, J. Militzer, May 30 – Jun 1 1999, pp. 3–3, 3–10.

[4] P. Arminjon, R. Touma, *Central finite volume methods with constrained transport divergence treatment for ideal MHD*, Journal of Computational Physics **vol. 204 issue 2** (2005), pp. 737–759.

[5] P. Arminjon, M.C. Viallon, *Convergence du schéma de Nessyahu-Tadmor sur des maillages non structurés pour une équation hyperbolique linéaire bidimensionnelle*, Rapport de recherche (1994), no. C.N.R.S. U.R.A. 740, Équipe d'Analyse Numérique, Universités de Lyon et Saint-Étienne.

[6] P. Arminjon, M.C. Viallon, *Généralization du schéma de Nessyahu-Tadmor pour une équation hyperbolique à deux dimensions d'espace*, C. R. Acad. Sci. Paris, t.320 (1995), pp. 85–88.

[7] P. Arminjon, M.C. Viallon, *Convergence of a finite volume extension of the Nessyahu-Tadmor scheme on unstructured grid for a two-dimensional linear hyperbolic equation*, SIAM J.Num.Anal **vol.36** (1999), no. 3, pp. 738–771.

[8] P. Arminjon, M.C. Viallon, D. Stanscu, *A two dimensional finite volume extension of the Lax-Friedrichs and Nessyahu-Tadmor schemes for compressible flows*, vol. IV, Proc. of the 6^{th}. Int. Symp on Comp Fluid Dynamics, Sep 4 – Sep 8 1995, pp. 7–14.

[9] T.J. Barth, D.C. Jespersen, *The design and application of upwind schemes on unstructured meshes*, AIAA paper (1989), no. No.89-0366, 27^{th} Aerospace sciences meeting.

[10] J. Blazek, *Computational Fluid Dynamics: Principles and Applications*, Elsevier Science, 2001, chap. 5, pp. 134-135.

[11] J.P. Boris, D.L. Book, *Flux Corrected Transport SHASTA, a fluid transport algorithm that works*, J.Comp. Phys. **vol.11** (1973), pp. 38–69.

[12] C. Chainais-Hillairet, *Finite volume schemes for a nonlinear hyperbolic equation. Convergence towards the entropy solution and error estimate*, Math. Model. Numer. Anal. **vol.33** (1999), pp. 129–156.

[13] G-Q. Chen, *Shock capturing and Related Numerical methods in computational fluid dynamics*, Acta Math. univ. Comenianae **vol. L.XX** (2001), pp.51–73.

[14] I. Christov, B. Popov, *A Jiang-Tadmor scheme on unstructured triangulations*, Technical report isc-06-05, Math Institute for Scientific Computation, Texas, A&M University College Station, TX, 2006.

[15] I. Christov, B. Popov, *New nonoscillatory central schemes on unstructured tri-*

angulations for hyperbolic systems of conservation laws, Journal of Computational Physics (2007).

[16] B. Cokburn, P. Lefloch, F. Coquel, *An error estimate for finite volume methods for multidimensional conservation laws*, Math. Comp. **vol.63** (1994), pp. 77–103.

[17] B. Crowell, *Conservation laws*, 1998-2009.

[18] L. Evans, *Partial Differential Equations*, vol. 19, American Mathematical society, Graduate Studies in Mathematics, 1997.

[19] P.L. George, *Géneration Automatique de Maillages. Applications aux Méthodes d'élements finis*, Masson (1991).

[20] S.K. Godunov, *Finite Differences Methods for numerical computations of discontinuous solutions of the equations of fluid dynamics*, Mat.Sbornik **vol.47** (1959), pp. 271–306.

[21] B. Haasdonk, C. Rohde, D. Kroener, *Convergence of a staggered Lax-Friedrichs scheme for nonlinear conservation laws on unstructured two dimensional grids*, Numerische Mathematik **vol.88** (2001), pp. 459–484, Preprint No. 07/2000, Mathematsche Fakueltaet, University of Freiburg, Germany, April 2000.

[22] A. Harten, *The artificial Compression Method for computation of shocks and contact discontinuities III, self-adjusting hybrid schemes*, Math.Comput. **vol.32** (1978), pp.363–389.

[23] A. Harten, *High Resolution schemes for hyperbolic conservation laws*, J.Comp. Phys. **vol.49** (1983), no. 3, pp. 357–393.

[24] A. Harten, S.R. Chakravarty, S. Osher, *Uniformly high order accurate essentially non-oscillatory schemes*, JCP. **vol.71** (1987), pp. 231–303.

[25] L. Hörmander, *Lectures on Nonlinear Hyperbolic Differential Equations*, Springer - Verlag Berlin Heidelberg, Mathematiques et applications 26, 1997.

[26] G. Jiang, E. Tadmor, *Non-Oscillatory Central Schemes for muti-dimensional hyperbolic conservation laws*, SIAM J. on Scientific Computing **vol.19** (1998), pp. 1892–1917.

[27] T. Katsapunis, D. Levy, *A modified structured central scheme for 2D hyperbolic conservation laws*, Appl. Math **Lett. 12** (1999), pp. 89–96.

[28] S. Konyagin, O. Trifonov, B. Popov, *On convergence of MinMod-type schemes*, SIAM J.Numer.Anal. **vol. 42** (2005), no. 5, pp. 1978–1997.

[29] D. Kroner, *Numerical Schemes for Conservation Laws*, Wiley - Teubner, Mathematics, 1997.

[30] D. Kröner, M. Rokyta, *Convergence of upwind finite volume schemes for scalar conservation laws in two dimensions*, SIAM J. Numer. Anal. **vol.31** (1994), pp. 324–343.

[31] N. Kruzkov, *First Order Quasilinear Equations in Several Independent Variables*, pp. 60–74, Mat. Sbornik 81, 123 (Russian) and Math, USSR Sbornik 10, 1970.

[32] M. Kuether, *Aprori and aposteriori error estimares for the staggered Lax-Friedrichs scheme in multi-dimensions for scalar nonlinear conservation laws*, Mathematische Fakultaet, Univ. of Freiburg, Germany (2000), Preprint No. 19/2000.

[33] M. Kuether, *Error estimates for the staggered Lax-Friedrichs scheme on unstructured grids*, SIAM J.Numer. Anal. (2001).

[34] A. Kurganov, G. Petrova, B. Popov, *Adaptive Semi-Discrete Central-Upwind Schemes for Nonconvex Hyperbolic Conservation Laws*, SIAM J. Sci. Comput. (2005).

[35] A. Kurganova, G. Petrova, *Central Upwind Schemes on triangular grids for hyperbolic systems of conservation laws*, Numer.Methods Partial Differential Eq. **vol.21** (2005), pp. 536–552.

[36] A. Kurganov and E. Tadmor, *Solution of Two-Dimensional Riemann Problems for Gas Dynamics without Riemann Problem Solvers*, (2002)

[37] P.D. Lax, *Weak solutions of nonlinear hyperbolic equations and their numerical computation*, Comm. Pure and Applied Math **7** (1954), pp. 159–193.

[38] B. Van Leer, *Towards the ultimate conservative difference scheme II. Monotonicity and conservation combined in a second-order scheme*, J.Comp. Phys. **vol.14** (1974), no. 4, pp. 361–370.

[39] B. Van Leer, *Towards the ultimate conservative difference scheme IV. A new approach to numerical convection*, J.Comp. Phys. **vol.23** (1977), no. 3, pp. 276–299.

[40] B. Van Leer, *Towards the ultimate conservative difference scheme V. A second order sequel to Godunov's Method*, J.Comp. Phys. **vol.32** (1979), no. 1, pp. 101–136.

[41] R. LeVeque, *Finite Volume Methods for Hyperbolic Problems*, The press syndicate of the university of Cambridge, 2002.

[42] D. Levy, G. Russo, G. Puppo, *Compact central WENO scheme for multidimensional conservations laws*, SIAM J.Sci. Comput. **vol.22** (2000), pp. 656–672.

[43] K. Michlak, C. Ollivier-Gooch, *Limiters for Unstructured Higher-Order Accurate Solutions of the Euler Equations*, Advanced Numerical Simulation Laboratory (2008), University of British Columbia.

[44] H. Nessyahu, E. Tadmor, *Non-Oscillatory Central Differencing for Hyperbolic Conservation Laws*, Journal of computational physics **vol.87** (1990), 408–463.

[45] J. Von Neumann, R.D. Richtmyer, *Methods for the numerical calculations of hydrodynamical shocks*, J.Math. Phys **vol.21** (1950), p.232.

[46] S. Osher, *Riemann Solvers, the Entropy Conditions and Difference Approximations*, SIAM. J. Numer. Anal. **vol.21** (1984), pp. 217–235.

[47] B. Popov, O. Trifonov, *One-sided stability and convergence of the Nessyahu-Tadmor scheme*, Numerische Mathematik **vol.104** (2006), no. 4, pp. 539 – 559.

[48] R.D. Richtmyer, K.W. Morton, *Difference Methods for Initial Value problems*, Wiley-Interscience (1967).

[49] P.L. Roe, *Approximate Riemann Solvers, parameter vectors and difference schemes*, J.Comp. Phys. **vol.43** (1981), no. 2, pp. 357–372.

[50] F. Sabac, *The optimal convergence rate of monotone finite difference methods for hyperbolic conservation laws*, SIAM J.Num. Anal. **vol.34** (1997), no. 6, pp. 2306–2318.

[51] A. St-Cyr, *Construction de méthodes de volumes finis tridimensionelle sans solveur de Riemann pour les systèms hyperboliques non-linéaires*, Ph.D. thesis, Université de Montréal, Faculté des études supérieures, feb. 2002.

[52] R. Touma, *Central unstaggered finite volume schemes for hyperbolic systems: Applications to unsteady shallow water equations*, Applied Mathematics and Computation **vol. 213** (2009), pp. 47–59.

[53] R. Touma, *Unstaggered central schemes with constrained transport treatment for ideal and shallow water magnetohydrodynamics*, Applied Numerical Mathematics **vol. 60, issue 7** (2010), pp. 752–766.

[54] R. Touma and P. Arminjon, *Central finite volume methods for ideal and shallow water magnetohydrodynamics*, International Journal for Numerical Methods in Fluids **In press** (2010).